UNIVERSITÀ DEGLI STUDI DI MILANO

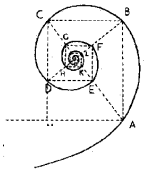

SCUOLA DI DOTTORATO IN MEDICINA MOLECOLARE

CICLO XXVI

Anno Accademico 2012/2013

TESI DI DOTTORATO DI RICERCA

MED/36

Multimodal molecular imaging for HIF-1α non-invasive assessment in a murine glioma model

Dottorando : Alessia LO DICO

Matricola N° R09155

TUTORE: Dott.ssa Luisa OTTOBRINI

DIRETTORE DEL DOTTORATO: Chiar.mo Prof. Mario CLERICI

INDEX

LIST OF ABBREVIATIONS

[^{64}Cu]ATSM: Copper diacetyl-bis (N4-methylthiosemicarbazone)

ATP: Adenosine TriPhosphate

BBB: Blood Brain Barrier

BL: Bioluminescence

BMDC: Bone Marrow Derived Cells

CAIX: Carbonic Anhydrase IX

cCCD: Cooled Charge-Coupled Device

Cdks: Cyclin-Dependent Kinases

CK2: Casein Kinase 2

CNS: Central Nervous System

CoCl2: Cobalt Chloride

CT: Computerized Tomography

D_2R : Dopaminergic type 2 Receptor

DCE-MRI: Dynamic Contrast-Enhanced Magnetic Resonance Imaging

DFX: Deferoxamine

DMOG: DiMethylOxalylGlycine

DNA-PK: DNA-dependent Protein Kinase

EGFR: Epidermal Growth Factor Receptor

[^{18}F]FAZA: 18F-FluoroAzomycin Arabinoside

[^{18}F]FDG: 18F-2-Fluoro-2-DeoxyGlucose

[^{18}F]FLT: 18F-FluoroThymidine

[^{18}F]FMISO: 18F-FluoroMISonidazole

FIH: Factor Inhibiting HIF

FL: Fluorescence

GBM: Glioblastoma Multiforme

GFAP: Glial Fibrillary Acidic Protein

GSK3: Glycogen Synthase Kinase 3

HIF-1: Hypoxia-Inducible Factors

HRE: Hypoxia Responsive Element

HSV1-TK: Herpes Simplex Virus type 1 Thymidine Kinase

LOH: Loss of Heterozygosity

MAPK: Mitogen-Activated Protein Kinase

MDM2: Mouse Double Minute 2 Homolog

MGMT: O-6-MethylGuanine-DNA MethylTransferase

MMR: MisMatch Repair

MRI: Magnetic Resonance Imaging

mTOR: Mammalian Target Of Rapamycin

NMR: Nuclear Magnetic Resonance

ODD: Oxygen-Dependent Degradation

2-OG: 2-OxoGlutarate

PET: Positron Emission Tomography

PHD: Prolyl Hydroxylases

PI3K: PhosphatidylInositol 3-Kinase

PTEN: Phosphatase and Tensin Homolog

RF: RadioFrequency

SPET: Single Photon Emission Tomography

SPIO: SuperParamagnetic Iron Oxide

T/B: Tumour-To-Background

TMZ: Temozolomide

TP53: Tumour Protein 53

US: UltraSound

VEGF: Vascular Endothelial Growth Factor

VHL: Von Hippel-Lindau

WHO: World Health Organization

LIST OF FIGURES

ABSTRACT

SOMMARIO

Introduzione: *L'imaging molecolare è una disciplina emergente nell'ambito della ricerca biomedica che consente di ottenere la rappresentazione visiva, la caratterizzazione precoce e la quantificazione di processi biologici a livello cellulare e subcellulare direttamente in vivo. Le diverse tecniche di imaging sono di grande importanza poiché consentono la traslazione dei dati ottenuti in preclinica direttamente alla clinica. Nel presente progetto di ricerca, l'imaging molecolare è stato applicato allo studio di un modello preclinico di glioma, ed in particolare alla valutazione dell'ipossia intratumorale, come fattore prognostico negativo in quanto principalmente correlata alla resistenza alle terapie, all'aumento dell'invasività e ad una conclusiva prognosi infausta. Per tali ragioni, l'ipossia rappresenta un promettente target terapeutico, sia nel glioblastoma che in altri tipi di tumore, e un interessante marcatore in grado di stimare la prognosi e di predire l'outcome terapeutico. In tale prospettiva, lo studio molecolare dell'ipossia, presentato nel presente progetto di ricerca, è focalizzato principalmente sulla valutazione dell'attività trascrizionale di HIF-1α, che rappresenta il fattore chiave nel processo ipossico.*

Scopo: *Lo scopo principale del progetto di ricerca è lo studio non invasivo dell'attività trascrizionale di HIF-1α in seguito allo sviluppo e alla progressione della malattia neoplastica e dopo trattamenti con inibitori selettivi e farmaci già utilizzati in ambito clinico. In un primo momento gli obiettivi dello studio sono stati volti alla dimostrazione della validità del modello cellulare e animale proposto, successivamente l'attenzione è stata focalizzata sulla comprensione del ruolo rivestito dall'attività trascrizionale mediata da HIF-1α in seguito a trattamenti di diverso genere, al fine di comprendere se tale fattore potesse rivestire il ruolo di biomarcatore prognostico nel modello proposto. I risultati ottenuti potranno essere utilizzati nell'ottica di pianificare trattamenti personalizzati in seguito a stratificazione degli individui sulla base dell'attività di HIF-1α.*

Materiali e metodi: *La linea umana di glioma U251 utilizzata nel corso degli esperimenti è stata opportunamente ingegnerizzata al fine di ottenere tre modelli: nel primo, U251-HRE, il gene reporter della luciferasi è sotto il controllo delle sequenze HRE; nel secondo, U251-pGL3, la luciferasi risulta invece costitutivamente espressa; nel terzo, il modello U251-HRE-mCherry, il gene reporter mCherry viene costitutivamente espresso mentre il gene reporter della luciferasi è di nuovo sotto il controllo delle sequenze HRE. Tali linee sono state dapprima utilizzate in vitro per lo studio di diversi agenti modulanti l'attività trascrizionale di HIF-1α, la cui azione è stata valutata principalmente mediante saggio biochimico per la luciferasi. Successivamente, le stesse cellule sono stata inoculate ortotopicamente in topi nudi e la loro crescita, eventi correlati all'attività trascrizionale di HIF-1α, come l'istaurarsi di uno stato ipossico intratumorale, e la risposta terapeutica, sono stati analizzati mediante diverse tecniche di imaging (BLI, FLI, PET e RM). I dati ottenuti in vitro ed in vivo sono stati inoltre validati ex vivo mediante colorazioni istologiche ed immunoistochimiche.*

Risultati: *Gli studi condotti in vitro hanno mostrato come nel modello U251-HRE l'attività luciferasica possa essere modulata mediante l'utilizzo di farmaci ipossia-mimetici, in relazione all'accumulo nucleare di HIF-1α. Inoltre, esperimenti condotti in vitro hanno consentito di valutare anche il contributo di diversi pathway molecolari sull'attività di HIF-1α: in primis le vie di trasduzione di PI3K/AKT e Ras/MEK/ERK. Come atteso, invece, nella linea U251-pGL3 l'attività luciferasica non è risultata soggetta ad alcuna modulazione e, dopo*

iniezione nel modello animale, il segnale derivante da tali cellule ha mostrato una progressione lineare in relazione alla crescita tumorale. Al contrario, l'andamento del segnale di bioluminescenza relativo all'attività luciferasica in tumori prodotti con cellule U251-HRE ha mostrato un aumento bi-modale con un brusco cambiamento di pendenza all'instaurarsi di aree ipossiche intratumorali, dimostrando come tale modello possa essere utilizzato sia in vitro che in vivo per lo studio della modulazione dell'attività di HIF-1α. Nonostante l'imaging ottico non possa essere, ad oggi, utilizzato nell'uomo, la cross-validazione dei risultati ottenuti con tecniche utilizzate di routine in clinica, come la PET e la RM (che hanno fornito risultati comparabili e complementari a quelli forniti dall'imaging ottico), ha permesso di potenziare il valore dei risultati ottenuti in bioluminescenza e in fluorescenza grazie alla loro trasferibilità clinica. Lo studio preliminare condotto con la TMZ ha mostrato, sia in vitro che in vivo, che precedentemente al manifestarsi dell'effetto citotossico del trattamento è riscontrabile una riduzione precoce dell'attività di HIF-1α. Il meccanismo di azione e il significato di tale riscontro sono comunque da approfondire mediante ulteriori studi.

Conclusione: *Il modello U251, riproponendo le caratteristiche peculiari del GBM umano, risulta essere anche un modello verosimile per lo studio dell'attività trascrizionale di HIF-1α (U251-HRE). In questo contesto, l'imaging ottico risulta essere una tecnica sensibile e versatile nello studio dei processi relativi alla progressione tumorale e all'attività di HIF-1α, ma risulta limitata in quanto non traslabile direttamente all'uomo. Per queste ragioni, risulta estremamente importante la cross-validazione con tecniche di imaging utilizzate nella pratica clinica, tra cui la PET e la RM. Il significato della possibilità di utilizzare l'attività di HIF-1α come marcatore precoce di efficacia dopo trattamento con TMZ dovrà essere valutato in modo più approfondito mediante studi specifici.*

ABSTRACT

Introduction: *Molecular imaging is an emerging discipline in biomedical research that allows the visual representation, the early characterization and quantification of biological processes at the cellular and subcellular level directly in vivo. Imaging techniques are of great importance since they allow the translation of the data obtained in preclinical models directly to the clinic. In this research, molecular imaging has been applied to the study of a preclinical glioma model, to assess intratumoural hypoxia, as a negative prognostic factor, since it has been correlated to chemo and radio-resistance, tumour progression, increase of invasiveness and to a poor prognosis. For these reasons, hypoxia represents a promising therapeutic target, both in GBM but also in other types of cancer, and an interesting marker able to estimate the prognosis and to predict the therapeutic outcome. In this perspective, the molecular study of hypoxia presented herein was focused mainly on the evaluation of the transcriptional activity of HIF-1α , which is a key factor of the hypoxia process.*

Objectives*: The main purpose of this project was to study, in a non invasive manner, HIF-1α transcriptional activity as a result of the development and progression of neoplastic disease and after treatment with selective inhibitors and drugs already used in the clinical setting. The first objectives were the characterization and validation of the proposed cell and animal models and the evaluation of HIF-1α activity after treatments of various inhibitors and drugs, to understand its potential role as a prognostic biomarker. The results obtained could be used in the evaluation of the possibility of performing personalized treatments as a result of stratification of individuals depending on HIF-1α activity.*

Materials and Methods*: The human U251 glioma cell line was used after its appropriatey engineering in order to obtain three models: in the first, U251-HRE, the luciferase reporter gene is under the control of the HRE sequences; in the second, U251-pGL3, the luciferase gene is expressed constitutively, whereas in the third, U251-HRE-mCherry, the mCherry reporter gene is constitutively expressed while the luciferase reporter gene is again under the control of HRE sequences. These lines were first used in vitro for the study of different agents modulating the transcriptional activity of HIF- 1α, whose action has been evaluated primarily by biochemical luciferase assay. Subsequently, the same cells were inoculated orthotopically in nude mice and tumor growth-related events, transcriptional activity of HIF-α, intratumoural hypoxia and therapeutic response, were analyzed using different imaging techniques (BLI, FLI, PET and MRI). The data obtained in vitro and in vivo were also validated ex vivo by histological and immunohistochemical staining.*

Results: *The in vitro studies have shown that in U251-HRE model,the luciferase activity can be modulated through hypoxia mimetic drugs, such DFX, and it was related to HIF-1α nuclear accumulation In addition, in vitro experiments have allowed to evaluate the contribution of different molecular pathways (involving PI3K/Akt and Ras/MEK/ERK) on HIF-1α activity. As expected, in U251-pGL3 model, the luciferase activity was not modulated. In vivo studies, performed after cell injection in murine models receiving U251-pGL3 cells, showed a linear increase of luciferase activity, proportionally to tumour growth. In contrast, in U251-HRE models a bimodal trend was observed, since it was dependent on hypoxia establishment HIF-1α mediated. These results suggested that this model can be used both in vitro and in vivo for the study of the modulation of HIF-1α activity. Although optical imaging cannot be used in humans, cross- validation of the results obtained with techniques routinely used in the clinic, such as PET and MRI (which gave results*

comparable and complementary to those provided by optical imaging), allowed to enhance the value of the results obtained in bioluminescence and fluorescence studies due to the possibility to translate these procedures to the clinical setting. The preliminary study conducted with the TMZ has shown, both in vitro and in vivo, that previously to the onset of the cytotoxic effect of the treatment, an early reduction of HIF-1α activity was detectable. The mechanism of action and the significance of this finding, however, have to be explored by further studies.

Conclusions: *The U251-HRE model, recapitulating GMB features, could be a reliable model for the study of HIF-1α role in tumour progression. In this context, the optical imaging could be considered a sensitive and versatile technique for the study of the processes related to tumour progression especially those mediated by HIF-1α, but it is limited since it is impossible to translate these data into the clinics. For these reasons, it is extremely important the cross-validation with imaging techniques routinely used in the clinical practice, such as PET and MRI. Moreover, HIF-1α activity could be considered as an early efficacy biomarker after treatment with TMZ, although this crucial process has to be studied in depth.*

INTRODUCTION

1. GLIOMA

Human cancer is characterized by several steps accumulating genetic alterations and modifications leading to tumour progression. Stepwise progression of human cancer has been clinically well recognized. The pre-malignant lesions are caused either by genetic alterations which induce monoclonal expansion of the cells, or by environmental factors, which induce polyclonal expansion of the cells. Subsequently, the accumulation of genetic alterations occurs in one (or a few) of the pre-malignant cells, and the cells convert into malignant ones of clonal origin, and produce a primary tumour. However, at the early stage of primary tumour expansion, the cells are not invasive and metastatic. Then, new fully malignant clones with invasiveness and metastatic ability appear as a result of further accumulation of genetic alterations in the cells; however, only a restricted fraction of the cells in a primary tumour are considered to be highly metastatic [1] **(Fig.1).**

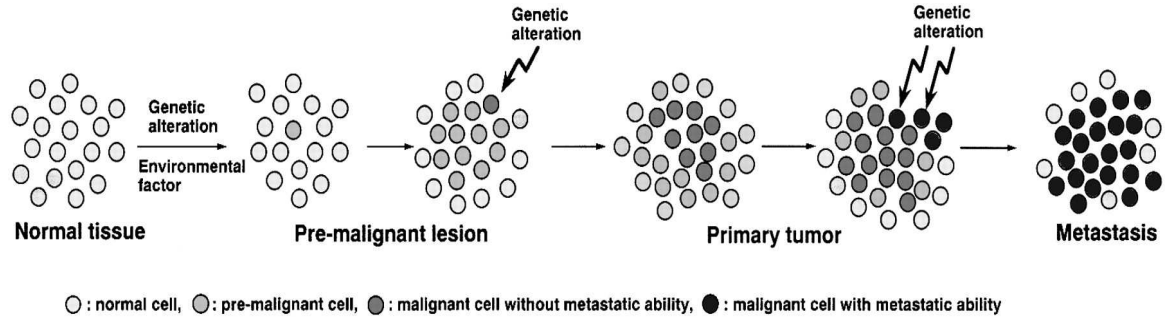

Fig.1: *Malignant progression of tumoural cells: accumulation of genetic alterations resulting in metastatic transformation*

Gliomas represent the most common adult neoplasm of the primary central nervous system (CNS) [2]. The term “Glioma” is generally used to describe any tumour that arises from the glia, the supportive tissue of the brain that provide sustenance and protection to neurons, holding them in place and permitting to function in an optimal way.

Three types of normal glial cells can produce tumours: astrocytes, oligodendrocytes and ependymal cells [3].

Glioma disease could be distinguished by the type of cells it affected:

- **Astrocytoma:** it develops in the connective tissue cells, called astrocytes. The are star-shaped brain cells, also called immortalized astrocytes. This kind of tumour includes juvenile pilocytic astrocytoma, low grade astrocytoma, anaplastic astrocytoma, and glioblastoma (GBM).
- **Ependymoma:** it develops from ependymal cells and its common location is the fourth ventricle.
- **Mixed Glioma (also called Oligoastrocytoma):** these tumours usually contain a high proportion of more than one type of cell, most often astrocytes and oligodendrocytes. The behavior of a mixed glioma appears to depend on the grade of the tumour. It is less clear whether their behavior is based on that of the most abundant cell type.
- **Oligodendroglioma:** it originates from the oligodendrocytes located in the brain or from a glial precursor cell.
- **Optic Glioma:** it develops in or around the optic nerve. It may involve any part of the optic pathway and it has the potential to spread along this pathway. It often occurs in children.
- **Gliomatosis Cerebri:** it is a rare brain tumour characterized by the high presence of glial tumour cells in the brain. This tumour is scattered and widespread, typically involving two or more lobes of the brain. It could be considered a “widespread low-grade glioma” because it does not have the malignant features seen in high-grade tumours.

In 1993, the World Health Organization (WHO) published the classification of neoplasms affecting the CNS, defining an official system of grading system based on the assumption that each type of tumour results from the abnormal growth of a specific cell type. Moreover, this grading system was created using some other features as atypia, mitosis, proliferation and necrosis. These parameters, indeed, reflect invasiveness and malignant potential of tumours.

Since tumour behaviour is related with basic cell type, tumour classification also dictates the choice of therapy and helps the prediction of prognosis. The WHO classification provides a parallel grading system for each type of tumour. In this grading system most named tumours are of a single defined grade.

Concerning the glioma, WHO grading is commonly used for astrocytoma and the most common grading system uses a scale that goes from I to IV. In this case astrocytomas are graded to describe their degree of abnormality [4].

- **Pilocytic astrocytoma (grade I).** Rare tumours, more common in children than in adults. They can be often removed surgically. In absence of surgery, it may remain inactive or be successfully treated with radiation.

- **Low-grade astrocytoma (grade II).** Grade II tumours are slowly-growing tumours that penetrate the surrounding normal brain tissue, making complete surgical removal more difficult. Since these tumours may be growing very slowly, radiation or chemotherapy or both, could be given after surgery. Most Grade II tumours eventually evolve into more-aggressive tumours (grade III or IV), but this process may take many years.
- **Anaplastic astrocytoma (grade III).** Grade III astrocytomas are more aggressive, but not as rapidly growing as grade IV tumours. Treatment involves removing as much of the tumour as possible, followed by radiation therapy and/or chemotherapy.
- **Glioblastoma (grade IV).** GBM is the most common and aggressive astrocytoma. These tumours tend to infiltrate throughout the area of the brain where the tumour is located, making them more difficult to be completely surgically removed. Surgery is generally followed by radiotherapy and chemotherapy. Grade IV tumours tend to recur and are rarely cured.

Finally tumours may be also classified by their growth rate: low grade (slow growth), mid grade (moderate) and high grade (rapid). On that scale, a grade I glioma could be considered benign, because in this case the surgical excision could be considered curative. On the contrary, GBMs are tumours that are usually highly malignant because the cells reproduce quickly and they are supported by a large network of blood vessels.

1.1 GLIOBLASTOMA

Glioblastoma or glioblastoma multiforme ("multiforme" is no longer part of the WHO designation, though glioblastoma is still often abbreviated in "GBM") is the highest grade glioma (grade IV) tumour, is the most malignant form of astrocytoma, and it is synonymous with a grade IV glioma. The histologic features that distinguish glioblastoma from all other grades are the presence of necrosis and the increase of blood vessels around the tumour. Grade IV tumours are always rapidly growing and highly malignant. Moreover, GBMs usually contain a mix of cell types and cystic mineral and calcium deposits formations. Since these tumours come from normal brain cells, it is easy for them to invade and live within normal brain tissue.

There are two types of GBM **(Fig.2):**

- **Primary, or *de novo* GBM**: This term refers to the lack of an identifiable precursor lesion rather than to the assumption that this lesion results from a single-step

malignant transformation. This is the most common form of GBM and the most aggressive one. In fact, these tumours are characterized by a very rapid growth and invasiveness without evidence of a less malignant precursor lesion [5]. Primary GBM accounts for the vast majority of cases (60%) in adults older than 50 years. These tumours manifest *de novo* (i.e., without clinical or histopathologic evidence of a preexisting, less-malignant precursor lesions), after a short clinical history, usually less than 3 months.

- **Secondary GBM:** The secondary GBM has been referred to as progressive form (developing from astrocytic tumours of lower malignancy grade) [6]. These tumours are slower than primary GBM but are still very aggressive (representing about 10% of GBMs) [7,8]. The diagnosis of secondary GBM requires clinical (neuroimaging) or histological (bioptic) evidences deriving from an evolution by a less malignant astrocytoma.

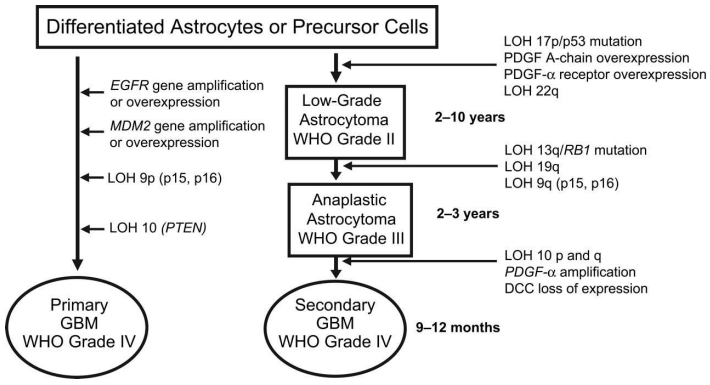

Fig.2 *Classification of GBM: primary or de novo, and secondary with relative genetic alterations occurring during neoplastic transformation.*

Histologic diagnosis of GBM is usually based on two distinctive secondary features rather than on cytologic characteristics. The first feature is vascular proliferation, by which vascular cells divide to produce coiled masses resembling renal glomerulus. Microvascular proliferation is an important feature differentiating GBM from the well differentiated fibrillary astrocytoma and the anaplastic astrocytoma, although a small amount of this proliferation is acceptable within the latter lesion. However, microvascular proliferation is found also in other neoplasms, such as pilocytic

astrocytoma, cerebellar astrocytoma, oligodendroglioma, and medulloblastoma, even if in limited extent. The second diagnostically relevant feature in glioblastoma is necrosis. This feature, with or without associated pseudopalisading neoplastic cells, is a critical parameter distinguishing GBM from anaplastic astrocytoma.

The main biologic properties making GBM fatal are poor response to a series of adjuvant therapies and the infiltrative behaviour that makes the complete surgical resection very difficult. GBM can be difficult to treat because the tumours contain several different cell types: in this view, some cells may respond to specific therapies, while others may not. This is why the GBM treatment plan usually combines several approaches, although the prognosis remains very poor.

1.1.1 CELLULAR COMPOSITION OF GBM

The cellular signaling pathways, important for the genesis of brain tumour, are multiple, with feedback mechanisms that can dramatically affect the efficacy of molecularly targeted therapeutic strategies. The heterogeneous composition of the human GBMs, which consists of tumour stem cells and differentiated tumour cells with varying characteristics, further complicates their susceptibility to treatment. Brain tumours can also evolve within their microenvironment, by adapting to changes altering their intrinsic features and progressing towards a more aggressive phenotype. At the same time, these molecular changes can be used to identify additional targets for therapeutic intervention. Finally, genetic variations between individuals can dictate how tumours initiate, progress, and respond [9].

All GBMs exhibited hypercellularity, nuclear atypia, and pleomorphism, including multinucleated giant cells. Aberrant mitotic figures and anaplastic cells can also be observed as well. Poorly differentiated cells were found in all GBMs, in addition to astrocytic intermediate filaments. With regard to this last feature, considering that there is no specific marker for GBM cells, the expression of proteins in reactive astrocytes has been considered. In the adult brain, astrocytes contain two types of intermediate filaments:

- **Vimentin positive filaments**: although vimentin is expressed also in blood vessels and ependymal cells, in the brain parenchyma vimentin is not expressed in neurons or in any other subclass of glial cell other than reactive astrocytes.
- **GFAP (Glial fibrillary acidic protein) positive filaments**: is variable in human GBMs and depends on the degree of anaplasia. Although vimentin expression is not exclusive for astrocytes, its expression, together with GFAP in these tumours is suggestive of their glial

origin, while usually only cells with astrocytic morphology are positive for GFAP, vimentin staining is more widespread throughout the tumours.

1.1.2 GENETIC OF GBM

It is known that genetic background is crucial for tumour development and progression. Molecular studies have identified some of the genetic changes that underlie the pathologic differences within astrocytic tumours; in fact, the progression of tumour grade is often associated with an ordered accumulation of mutations [10].
Progression from astrocytoma to anaplastic astrocytoma usually involves mutations in tumour suppressor genes including the retinoblastoma gene on chromosome 13q, in addition to other abnormalities such as LOH (Loss of heterozygosity) 10q, TP53 (tumour protein 53) and PTEN (Phosphatase and tensin homolog) mutations, p16INK4a deletion and EGFR (epidermal growth factor receptor) amplification-overexpression [11], which are common in GBMs **(Fig.3).** Below the main mutations are described:

- **p53:** The first genetic alterations identified in astrocytic brain tumours and the most recurring mutations are detected in the p53 gene on chromosome 17p. Alterations of the p53 gene were found in about 30% of benign and anaplastic astrocytomas as well as GBMs. Anaplastic astrocytomas (grade III), found in preexistent low grade astrocytomas or detected *de novo*, have a similar incidence of p53 mutations but, in addition, show a loss of heterozygosity on chromosome 19q in more than 40% of cases [12,13].
- **PTEN:** PTEN mutations are found in ~70% of advanced human GBMs and overexpression of recombinant PTEN in GBMs leads to marked reduction in HIF-1α expression [14]. In fact, normal PTEN is a negative regulator of the phosphatidylinositol 3-kinase PI3K/Akt pathway (by dephosphorylating phosphatidylinositol 3,4,5-triphosphate, the molecular messenger generated by PI3K), and its mutation results in hyperactivation of the PI3K/Akt pathway that may contribute at enhancing the stability, translocation, dimerization and transcriptional activity of hypoxia-inducible factors (HIF-1α), even though this event is context- and cell type-dependent. These genetic aberrations account also for a series of disrupted molecular pathways (i.e. p53/MDM2/p14ARF, p16INK4a/RB1, and EGFR/PTEN/Akt/mTOR pathways) that regulate vital cellular processes, including apoptosis, necrosis, cell proliferation and cell migration [15,16,17].

- **MDM2 (**Mouse double minute 2 homolog): Amplification or overexpression of MDM2 constitutes an alternative mechanism of escaping from p53-regulated control of cell growth by binding to p53 and blunting its activity. Overexpression of MDM2 is the second most common gene mutation in GBMs and is observed in 10-15% of patients. Some studies show that this mutation has been associated with a poor prognosis.

Moreover, in addition to these pathological modifications, the presence of microvascular/endothelial proliferation (i.e., multilayered, mitotically active hyperplasic endothelial cells, smooth muscle cells, and pericytes) is a histopathological hallmark of human GBMs. Endothelial proliferation is usually limited to necrotic areas, where profuse vascularisation is observed. Angiogenesis is the process by which new blood vessels develop from existing vasculature, thereby providing a mechanism for the maintenance of an adequate blood flow in expanding cell populations, including those of tumour tissues [18]. One of the most potent stimulators of angiogenesis is vascular endothelial growth factor (VEGF), which is essential for the proliferation and migration of vascular endothelial cells, thereby enabling the formation of new blood vessels. Production of VEGF is principally driven by hypoxia via transcription activation of the VEGF gene by HIF-1α. The basic importance of hypoxia and especially of HIF-1α in the angiogenic process, has been demonstrated in several experimental and clinical studies [19].

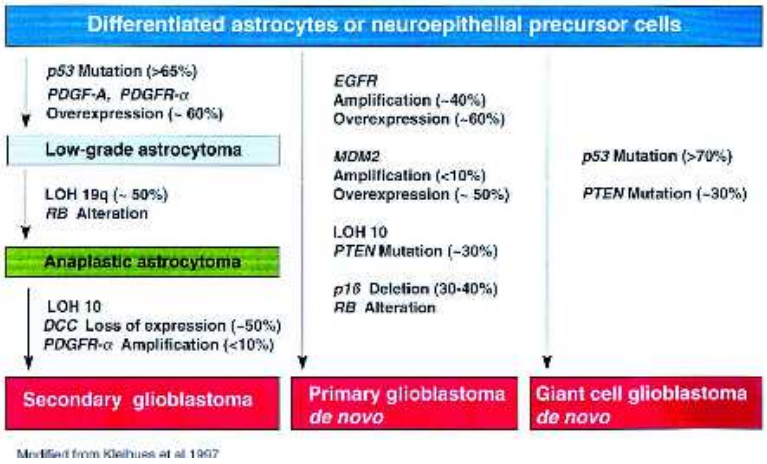

Fig. 3: *Genetic alterations occurring during astrocytes differentiation in primary, secondary or giant cell GBMs.*

2. HYPOXIA

Hypoxia plays a role in many aspects of tumour development and growth. It has been hypothesized that some of the phenotypic changes, fundamental to malignant progression, are mediated by cellular hypoxia being able to induce genomic instability, loss of apoptotic potential, induction of angiogenesis and stem cell genetic instability, finally resulting in an increased metastatic potential and resistance to radio- and chemo-therapy. The process of tumour progression (i.e., proliferation, local invasion, and distant metastasis) is characterized by rapid cellular growth accompanied by alterations of the microenvironment of the tumour cells, firstly, due to an inadequate oxygen (O_2) supply resulting in hypoxia or even anoxia [20].

In detail, developing tumours must form their own vascular network and blood supply, in addition to preexisting host vessels, by forming new microvessels through the influence of tumour angiogenetic factors. However, the newly formed vascular network differs greatly from that found in normal tissues, typically displaying a broad range of structural and functional abnormalities often leading to a diminished delivery of O_2 (and nutrients) to the tumour cells, with the resultant development of hypoxic/anoxic areas. Hypoxia condition is defined as a condition in which oxygen tension (pO_2) is lower than 7 mmHg. Hypoxia can induce changes in the tumour cell proteome , leading to cell growth or to cell death, inducing cell-cycle arrest, apoptosis and necrosis. These changes can also induce the tumour cells to successfully adapt to, or overcome, the O_2- and nutrient-deprived state and to survive or escape from their hostile environment. This conditions can result in the induction of hypoxia-stimulated angiogenesis, glycolysis, inhibition of apoptosis, and upregulation of growth factors (PDGF-B, TGF, IGF-2, EGF**) (Fig.4).**

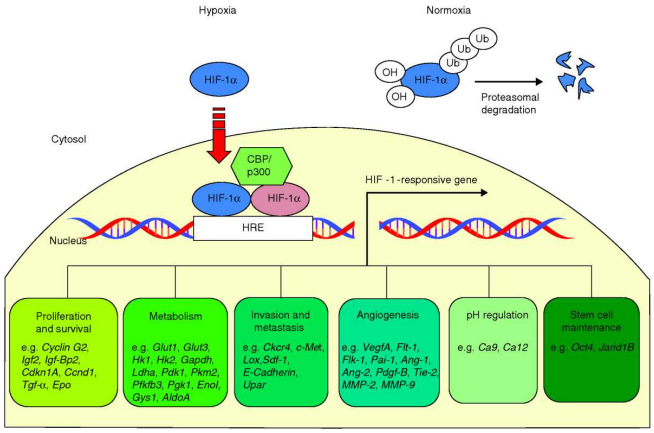

Fig. 4: *Normoxia and hypoxia influence on HIF-1α expression. During hypoxia, HIF-1α regulates several genes involved in proliferation, metabolism, invasion, angiogenesis, ph regulation and stem cell maintenance*

Hypoxia in solid tumours is associated with resistance to radiation therapy and chemotherapy and selection of more invasive and metastatic clones, correlating also with a poor patient prognosis [21,22].

As regards angiogenesis induction, hypoxia and the consequent stabilization of HIFs plays a critical role in fact HIF-1α, directly activates the expression of a number of pro-angiogenic factors that promote neo-angiogenesis and vasculature reorganization, favouring tumour progression and resistance to treatments [23,24,25]**(Fig.5)**.

In particular, hypoxia reduces chemotherapeutic efficacy positively, selecting cells with reduced susceptibility for apoptosis. At the same time, since radio sensitivity is generally due to the presence of molecular oxygen that induces DNA damage through the formation of oxygen free radicals, which occurs primarily after the interaction of radiation with intracellular water, tumour sensitivity to radiation therapy is progressively limited when the O_2 partial pressure in a tumour is less than 25–30 mmHg leading to a significant radio resistance in presence of hypoxia [26].

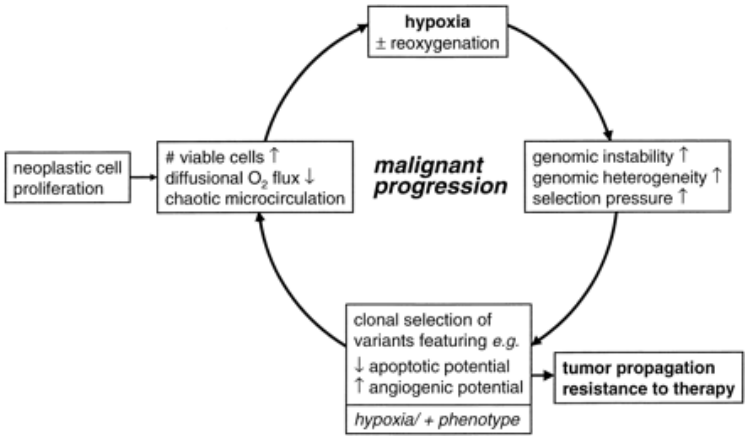

Fig. 5: *Malignant progression in neoplastic cell and hypoxia role: hypoxia induces genomic instability that influences clonal selection of cells.*

2.1 HIF-1α

The best-characterized hypoxia-regulated molecule is HIF-1α, first identified by Semenza and colleagues as a regulator of hypoxia-induced erythropoietin expression and of the expression of more than 30 genes [27] (**Fig.6).** HIF-1 structure is formed by a basic helix-loop-helix PAS (Per-Arnt-Sim) transcription factor composed of two subunits, a constitutively expressed subunit called HIF-1β (or ARNT) and the catalytic and oxygen-dependent subunit, HIF-1α, whose expression is tightly regulated by changes in oxygen concentration.

Overexpression of HIF-1α protein has been reported in several human cancers, where it has been associated with tumour progression, treatment failure, and poor survival [28]. In normoxic condition, in presence of oxygen, the HIF-1α subunit undergoes rapid decay via ubiquitin-proteasome degradation pathway involving the von Hippel-Lindau (VHL) tumour suppressor gene product pVHL. The binding of pVHL to HIF-1α requires the post-translational hydroxylation of proline residues (Pro402 and Pro564) within the HIF-1α oxygen-dependent degradation (ODD) domain by soluble prolyl hydroxylases (PHD). These enzymes are 2-oxoglutarate-dependent dioxygenases that require molecular oxygen as a cosubstrate. In hypoxic condition, this modification is prevented, thus allowing HIF-1α to escape proteolysis, dimerize with HIF-1β, and translocate to the nucleus. A separately controlled, O_2-dependent hydroxylation of asparagine 803 in the HIF-1α C-terminal transactivation domain inhibits HIF-1α interaction with the p300/CBP co-activator, thereby blocking HIF-1α transcriptional activity in the presence of oxygen. Three HIF-1α PHD (PHD 3 to -1, respectively) and one O_2-dependent HIF-1α asparaginyl hydroxylase (HIF inhibiting factor , known as FIH) have been clearly identified. These enzymes are all members of

the 2-oxoglutarate-dependent family of dioxygenases and have an absolute requirement for oxygen, ferrous iron, and 2-oxoglutarate (2-OG) [29].

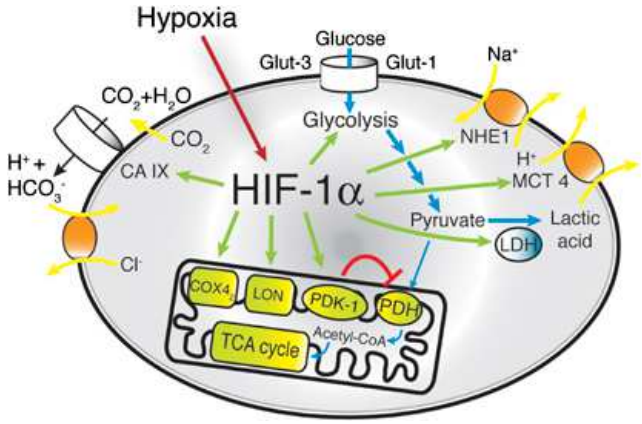

Fig. 6: *HIF-1α pathway in hypoxia. Figure summarizes the metabolic pathways influenced by HIF-1α.*

In addition to the proline hydroxylation of HIF-1α, other regulatory pathways have been reported to be important for the control of HIF-1α protein level by hypoxia such as the PI3K/Akt pathway **(Fig.7).**

Many stimuli are able to activate Akt. In general, phosphatidylinositol 3,4,5-P3 targets Akt in the inner leaflet of the plasma membrane. Akt is phosphorylated on Ser-473 (in the regulatory domain) and Thr-308 (in the catalytic domain) by phosphoinositide-dependent protein kinase, an upstream kinase, resulting in enzymatic activation of Akt. Activated- Akt can phosphorylate various substrates, such as the glycogen synthase kinase 3 (GSK3), an ubiquitous Ser/Thr kinase, that it is one of the well characterized downstream Akt targets. Akt phosphorylates the two isoforms of GSK3 (α and β), respectively on Ser-21 and Ser-9; resulting in an inhibition of its activity. On the other hand, GSK3 activity is up-regulated by Tyr-279/216 phosphorylation, but it is not clear whether a separate kinase regulates the phosphorylation state on this residue or whether this residue is an autophosphorylation site. GSK3 does not seem to be phosphorylated on both sites contemporaneously. GSK3 has been demonstrated to regulate glycogen synthase activity and was first identified as a negative regulator of glycogen synthesis. Now GSK3 is known to phosphorylate and regulate the activation of numerous transcription factors such as c-Myc, AP1 and NF-κB. It is reported that there is a potential consensus site in the HIF-1α oxygen-dependent degradation domain for GSK3 and that this site could play a role in the regulation of HIF-1α protein stability [30].

In GBMs, hypoxia and HIF-1α are contributing factors for the observed increased survival, proliferation rate, invasiveness, new vessels creations, metabolic adaptation and treatment resistance.

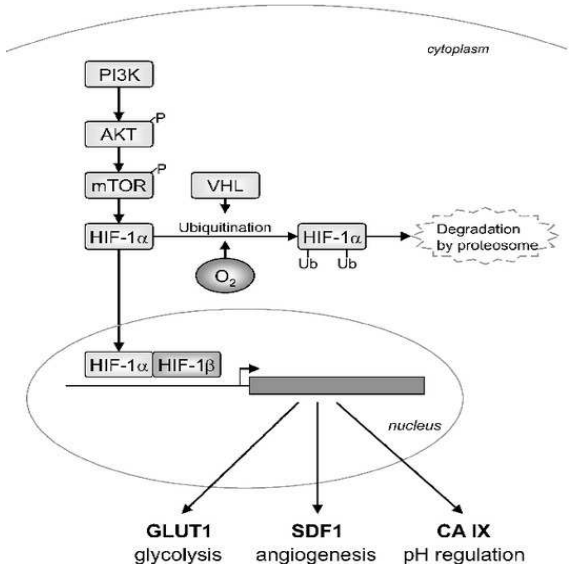

Fig. 7: *PI3/AKT pathway influence on HIF-1* α *accumulation and degradation.*

3. HYPOXIA IN GLIOMA DISEASE

Hypoxia is considered a major driving force for glioma angiogenesis. It is also the main feature of this kind of tumour [31]. Brain tumours, especially the highly aggressive GBM, are characterized by wide necrotic/hypoxic areas within the tumour mass, which correlates with enhanced resistance to therapy, increased invasiveness and a poor prognosis for the patient. Anyway, in oncology, hypoxia is always considered a crucial feature for the treatment planning of many different human cancers, for the outcome and prognosis estimation. This is why *in vivo* hypoxia analysis is increasingly being studied. Among the numerous survival pathways activated by cancer cells, hypoxic cell signalling has attracted significant interest for a number of years. This interest is also based on the assumption that normal tissues do not experience the same extreme variations in oxygen levels present in the tumour microenvironment. Cancer cells are exposed to a gradient of oxygen levels that fluctuates in time and space, triggering the activation of survival pathways that are not usually induced in normal tissues and that can be potentially targeted for therapeutic purposes [32].

Hypoxia is also responsible for the highly invasive behaviour of GBMs, as it induces the migration of GBM cells away from hypoxic areas [33,34]. However, the first clue suggesting the relationship between hypoxia and GBM establishment is the presence of intratumoural necrosis. In fact, the histological diagnosis of GBMs depends on the presence of tumour necrosis surrounded by pseudopalisading cell clusters. Hypoxia, indeed, stimulates pseudopalisading cells to activate HIF-1α leading to overexpression of angiogenetic factors and peritumoural microvascular proliferations [35]. Moreover, all GBM tumours have intratumoural necrosis to a different extent; it does not seem to be related to tumour size, as it is found in both small and large tumours. This suggests that necrosis may not simply be due to inadequate vascular supply but instead may result of intrinsic molecular or genetic changes within the tumour [36]. Indeed, although GBM is a highly vascularised tumour, his microcirculation is functionally very inefficient and may contribute to relative hypoxia and necrosis within the tumour. It is possible that a combination of hypoxia and intrinsic tumour molecular biology are responsible for pseudopalisading necrosis. The direct correlation between tumour grade and HIF-1α expression in GBMs has been shown in several studies, supporting that HIF-1α expression represents an ‘‘angiogenic switch’’ that facilitates the progression of a low grade astrocytoma to a GBM and promotes cell survival in hypoxic conditions by elevating glycolysis and angiogenesis.

With regard to hypoxia-mediated chemo and radio-resistance, evidences in literature [37,38] demonstrated that if inhibiting hypoxia through inhibition of HIF-1α expression, cells become more sensitive to chemoterapeutic treatment, demonstrating the central role of this transcription factor.

For what concerns angiogenesis, GBM is one of the most highly vascularised human tumours, with significant vascular proliferation and angiogenesis. That makes anti-angiogenic therapy, usually in the form of the anti-VEGF antibody therapeutic drug, an attractive treatment option for patients with these tumours. It has been proposed that, in GBMs, hypoxia, caused by vessel regression during the course of antiangiogenic therapy, leads to up-regulation of proangiogenic factors and the recruitment of bone marrow derived cells (BMDCs), able to increase tumour growth through new blood vessel growth [39]. In this case, there is sufficient evidence to suggest that BMDCs are recruited by hypoxia- and HIF-1α-mediated pathways [40,41].

In this scenario, improvements in HIF-1α activity molecular imaging procedures, could be extremely powerful for clinical assessment of treatment response and for the follow-up study.

3.1 GLIOMA MODELS

Preclinical orthotopic and sub-coutaneous murine models are largely used to test novel therapies targeting different GBM features (i.e., angiogenesis, invasion, secretion of immune suppressive molecules and so on). The advantages of the use of these glioma models reside in their highly

efficient gliomagenesis, reproducible growth rates, and the accurate knowledge of the tumour location [42].

In particular, there are some criteria that brain tumour models should follow, to be actually valid models [43-44]:

- they should be derived from glial cells;
- it should be possible to grow and clone them *in vitro* as continuous cell lines and propagate them *in vivo* by serial transplantation;
- tumour growth rates should be predictable and reproducible;
- the tumours should have glioma-like growth characteristics within the brain including neovascularization
- alteration of the blood-brain barrier (BBB), an invasive pattern of growth, and lack of encapsulation;
- host survival time following orthotopic tumour implantations should be of sufficient duration to permit therapy and determination of its efficacy;
- for therapy studies, the tumours should be either non or weakly immunogenic in syngeneic hosts;
- they should not grow into the epidural space or extend beyond the brain;
- their response or lack thereof to conventional treatment should be predictive of the response in human brain tumours

It is important to recognize that no currently available animal tumour model exactly simulates human high grade brain tumours such as GBMs or anaplastic astrocytomas [45]. However, the use of animal models to evaluate, also by means of non-invasive *in vivo* imaging techniques, important variables which are involved in the radiation and chemotherapeutic effect, such as proliferation, cell cycle arrest, apoptosis induction, hypoxia and angiogenesis, as well as diffusion and perfusion, may be helpful in permitting the identification of a biological tumour signature allowing, the estimation of chemo and radio sensitivity and responsivity to treatments [46,47]. Animal models can also be useful in evaluating the efficacy of radio sensitizing therapies designed to improve radio-induced tumour toxicity [48].

One of the most common cell line used *in vitro* and *in vivo* is the U251 human malignant glioma cell line originally established from a 75-year-old male with GBM by Ponten and al [49,50]. This GBM cell line is known to mimic the salient features of human GBMs and received significant

attention over the last four decades in xenogeneic mouse models of cancer [51,52,53]. The U251 cell line has been used both in subcutaneous and orthotopic mouse model of GBM [54,55]. The U251 cell line also displays similarities at the genetic level to human GBMs [56,57,58,59,60] with the identification of non-functional mutant tumour suppressor protein p53 [61] as well as mutant PTEN. Also deletions of p14ARF and p16, two cell cycle suppressor genes coding for critical negative regulators of Cdks (cyclin-dependent kinases), and whose deletion leads to loss of activity of the retinoblastoma protein [62], have been observed in U251 cells [63,64]. Moreover in U251 cells, the PI3K/Akt pathway is up-regulated as a result of high Akt expression. This has been shown to be an important contributing factor of the increased survival, proliferation, migration, angiogenesis and resistance to apoptosis observed in GBMs [65]. Recent studies [66,67] have reported gene expression profile differences between subcutaneous and intracranial tumour models, noting the importance of different *in vivo* growth conditions and the role of the microenvironment in U251 tumour establishment and progression. In summary, it is possible to affirm that since U251 cell line recapitulates the salient histological and immunohistochemical features of human GBMs, it can be considered a very interesting model for GBM translational studies.

4. EFFECT OF DRUG ACTIVITY ON HIF-1α MODULATION

4.1 Hypoxia mimetic: DFX

To study hypoxia processes *in vitro* , a class of drugs, that could be used in culture to mimic hypoxia, have been described. To study the mechanism of hypoxia establishment, hypoxia mimetic drugs could be used to mimic intracellular events related to a mild hypoxia condition, and permitting to study how this condition could modulate cellular pathways. Indeed, hypoxia-mimetic agents artificially mimic hypoxia by blocking for example the degradation of HIF-1α [68]. However, the molecular effects of hypoxia-mimetic agents are comparable to those resulting from reduced atmospheric oxygen levels [69,70,71].

The most common hypoxia mimetic drugs utilized in vitro are cobalt chloride ($CoCl_2$), and the iron chelator deferoxamine (DFX). Both of them are able to block the degradation of HIF-1*α* protein, inducing its accumulation in the cells.

In particular, DFX, by chelating iron, a cofactor necessary to PHD activity, avoid PHD-mediated HIF-1*α* hydroxylation [72,73], thus preventing HIF1*α* binding to VHL protein and inducing his rapid accumulation in the cytoplasm. Also $CoCl_2$ can block the degradation of HIF-1α protein, thereby inducing its accumulation, through a direct action on PHDs. In fact, recent models hypothesized

that cobalt can inactivate PHDs by occupying an enzyme iron-binding site [74]. Whereas $CoCl_2$ is toxic for cells and operator, DFX can be absolutely considered safety [75].

4.2 PI3K pathway inhibitors: LY294002 and BEZ-235

PI3Ks are lipid kinases responsible of the phosphorylation of PIP3. PI3-K plays a central role in cellular proliferation, motility, neovascularization, viability, and senescence. In particular, in cancer development, it has been documented the over-expression of PI3K with recent evidence of oncogenic and probably activating mutations of p110α and loss, or reduction, of the tumour suppressor PIP3 phosphatase PTEN activity [76,77]. Amplification of the gene encoding the p110α subunit is likely an important event in cancer progression. Recently, several studies have focused on the role of PI3K inhibitors as potential tumour suppressor agents.

The flavonoid quercetin derivative, LY294002, is the first synthetic molecule known to inhibit PI3K. LY294002 is a potent PI3K inhibitor: indeed it is a competitive, reversible inhibitor of the ATP binding site of PI3K, consequently preventing cell proliferation and inducing apoptosis. In addition, it was shown that this molecule is able to inhibit not only mTOR (mammalian target of rapamycin) and DNA-PK (DNA-dependent protein kinase) [78-79], but also other protein kinases, such as CK2 (casein kinase 2) and Pim-1 [80]. The effect of LY294002 on cell cycle progression may be extremely fruitful in the studying of the PI3K activation pathway [81].

Previous studies [82,83] indicated that LY294002 is able to completely abolish PI3K activity in several cell types, including neutrophils, endothelial cells, and cancer cells. Two mechanisms may explain the inhibitory effects of LY294002 on cell proliferation. The first one is based on the repression of cell cycle progression by LY294002, inducing specific G_1 arrest, as already described, leading to an inhibition of cell proliferation. Indeed, as suggested in literature, LY294002 prevents cell proliferation by inhibiting G_1 cyclin-dependent kinase activity and the subsequent phosphorylation of retinoblastoma protein, that normally occurs during G_1 progression. These inhibitory effects are, at least in part, a result of induced up-regulation of cyclin-dependent kinase inhibitory p27 [84]. The second possibility is that LY294002 could increase apoptosis. Indeed, a critical role in proliferation pathway is played by Ras, that was found to protect cells from apoptosis through the activation of the protein kinase B/Akt via PI3K. LY294002, by inhibiting PI3-K activity, could block the signal transduction pathway, which in turn may inhibit Ras-mediated protection from apoptosis in different types of cancer cells.

Further optimization for different types of PI3K inhibitors, using a structure-based design approach, led to the identification of NVP-BEZ235, a dual PI3K/mTOR kinase inhibitor. BEZ235 is a synthetic compound, with a small molecular mass, belonging to the class of imidazoquinolines that, at first, potently and reversibly inhibits PI3K catalytic activity by competing for its ATP-binding site.

Secondary, BEZ235 inhibits also mTOR catalytic activity. Indeed, a potential advantage of dual PI3K/mTOR inhibitors, compared with mTOR inhibitors, is the antagonism of rebound Akt activation often found following use of those latter drug. Treatment of U87MG glioma cells with BEZ235 resulted in a high growth arrest in the G1 phase with no apoptosis induction. Several studies [85-86] showed that BEZ235 was more efficient than LY294002 to block Akt activation likely reflecting, once more, the synergistic inhibitory effects on both PI3K and mTOR. For these reasons BEZ235 may represent a useful pharmacological tool for the treatment of advanced cancer, since it displays all the features required for clinical development and has entered phase I clinical trials in cancer patient.

4.3 MEK pathway modulators: TRAMETINIB and PD98059

The members of the mitogen-activated protein kinase (MAPK) family are important for the regulation of cell survival. Indeed, MAPK signaling has an important role in the mitogenic response and in the induction of apoptosis in response to stress [87]. A critical role in the regulation of HIF-1α activity is played by the signaling pathway including the Ras/Raf/ERK1/2 cascade that is also involved in the up-regulation of VEGF expression. In addition, the activation of the Ras/Raf/ERK1/2 pathway may also control tumour growth by regulating HIF-1α-mediated angiogenesis and glucose metabolism [88]. Using the highly selective MEK1/2 inhibitor PD98059, it can be studied how the inhibition of ERK1/2 signaling blocks growth factor-mediated induction of HIF-1α (for example IGF-1 activity). In particular, PD98059 acts as a MEK1/2 inhibitor, by binding to the ERK-specific MAP kinase MEK, thus preventing phosphorylation of ERK1/2 (p44/p42 MAPK) by MEK1/2. It is important to know that PD98059 blocks HIF-1α activity in response to hypoxia by blocking IGF-1 expression, although this drug does not affect directly the HIF-1α accumulation or its localization in the nucleus (also in response to DFX treatment or hypoxic stress) and stability in association with HIF-1β [89].In particular, ERK1 and ERK2, which are members of MAPK family, are thought to be involved in HIF-1α regulation because the activation of ERK1/2 has been shown to induce HIF-1α phosphorylation in vitro . So, this data indicates that kinases, in addition to MEK1/2, are required for HIF-1α activation in response hypoxia. In addition to PD98059, JTP-74057 (commercial name TRAMETINIB) and its dimethyl sulfoxide (DMSO)-solvate form, called GSK1120212, could be used as allosteric inhibitors of MEK1 and MEK2 activity that possess promising clinical activity in melanoma [90]. Indeed, trametinib inhibits activation of MEK by preferentially preventing phosphorylation in serine 217, resulting in a predominantly monophosphorylated protein at serine 221. Although trametinib is not approved by FDA at this time, it showed much more potent antitumour activity than the second generation MEK inhibitors, such as PD098059 [91].

4.4 HIF-1α modulators: FM19G11 and DMOG

FM19G11 is a potent inhibitor of HIF proteins. It was documented that this molecule represses the target genes of both HIF proteins, 1 and 2, in cancer cell lines of various tissues producing decrease in both transcripts and protein levels [92]. FM19G11 causes a reduction of overall histone acetylation with significant repression of p300, a histone acetyltransferase required as a co-factor for HIF-transcription activation, thus influencing transcriptional activity of HIF-1α. Particularly, FM16G11, by promoting pVHL leads to proteasomal degradation of HIF-1α, blocking in this way HIF-1α accumulation and its role in hypoxia pathway.

On the contrary, Dimethyloxalylglycine (DMOG), is a cell-permeable inhibitor of both proline and asparaginyl hydroxylases, which can activate the HIF-1α dependent gene expression both in vitro and in vivo. PHD inhibitors, such as DMOG, have been shown to promote cell survival under hypoxia conditions or growth factor deprivation by elevating HIF-1α levels [93]. Small PHD inhibitors include compounds which are structurally analogs to the 2-oxoglutarate, a co-factor required for these enzymes to function. Indeed, under normoxic conditions HIF-1α is hydroxylated on pro-402 and pro-564 of the α subunit in the ODD-domain by PHD proteins. Proline hydroxylation leads to the HIF-1α recognition by the VHL tumour suppressor and subsequent ubiquitination and proteasomal degradation.

4.5 Temozolomide

Temozolomide (TMZ) was synthesized at Aston University in the early 1980s as one of a series of novel imidazotetrazinones. These agents were structurally unique because they contained three adjacent nitrogen atoms that conferred unique physicochemical properties and much greater antitumour activity than the previously synthesized bicyclic triazenes. The most potent antitumour compound of this class, mitozolomide, showed potent antitumour activity against a large panel of murine tumours. Mitozolomide is a prodrug that spontaneously decomposes to a highly reactive DNA-cross-linking metabolite without any need for metabolic activation. TMZ, a 3-methyl derivative of mitozolomide, is less toxic than mitozolomide and it exhibited comparable antitumour activity against various murine tumours. Indeed, interest in TMZ as an antitumour agent derives from its broad-spectrum of antitumour activity in murine tumour models including glioma, metastatic melanoma, and other difficult-to treat cancers due, among all, to its ability to cross the blood brain barrier, leading to a very important activity in CNS tumours. About its mechanism of action, the methylation of DNA seems to be the main mechanism responsible for the cytotoxicity of TMZ in malignant cells. The spontaneous conversion of TMZ to the reactive methylating agent MTIC is initiated by the effect of water at the highly electropositive C4 position of TMZ. This activity opens the ring, releases CO_2, and generates MTIC that degrades to the methyldiazonium cation, which

transfers the methyl group to DNA and to the final degradation product, AIC, which is excreted via the kidneys. The methyldiazonium cation can also react with RNA and with soluble and cellular proteins. However, the methylation of RNA and the methylation or carbamoylation of proteins do not appear to have any known significant role in the antitumour activity of TMZ. Additional studies are required to clarify the role of these targets in the biochemical mechanism of action of TMZ [94].

Among the lesions produced in DNA after treatment of cells with TMZ, the most common is methylation of guanine in the *N*7 position, followed by methylation of adenine in the *O*3 position and of guanine in the *O*6 position (although both the *N*7-methylguanine and *O*3-methyladenine adducts probably contribute to the antitumour activity of TMZ in some if not all sensitive cells, their role is controversial). The O6-MG adduct (which accounts for 5% of the total adducts formed by TMZ) probably plays a critical role in the antitumour activity of the agent. This is supported by the correlation between the sensitivity of tumour cell lines to TMZ and the activity of the DNA repair protein O-6-methylguanine-DNA methyltransferase (also known as MGMT), which specifically removes alkyl groups at the *O*6 position of guanine. The cytotoxic mechanism of TMZ appears to be related to the failure of the DNA mismatch repair (MMR) system to find a complementary base for methylated guanine. MGMT is capable of counteracting the cytotoxicity induced by *O*6-alkylating agents. In fact, increased MGMT expression (also due to lack of methylation within his promoter region), is well correlated with *in vitro* and *in vivo* glioma resistance to TMZ [95,96]. In this process, MGMT is rapidly degraded via the ubiquitin-proteasome pathway after receiving alkyl groups from DNA and his repletion depends on the resynthesis of the molecule. For these reasons MGMT seems to be a suitable target both for *a priori* assessment of tumour sensitivity to TMZ and for intervention to improve TMZ therapeutic efficacy.

5. IN VIVO IMAGING

In vivo imaging is a rapidly emerging biomedical research discipline that extends observations in living subjects to a more meaningful dimension [97].

In vivo imaging includes both molecular and cellular imaging. It can be defined as a non-invasive repetitive imaging in living organisms, that permits characterization and quantification of biological and cellular processes, at cellular and sub-cellular levels [98]. It is a novel multidisciplinary field, in which the images produced reflect cellular and molecular pathways and *in vivo* mechanisms of disease in the context of physiologically authentic environments.

The term “molecular imaging” implies the convergence of multiple image-capture techniques, basic cell/molecular biology, chemistry, medicine, pharmacology, medical physics, biomathematics, and bioinformatics into a new imaging paradigm. Molecular imaging is becoming a well-established research field based on the use of non-invasive imaging techniques such as positron emission tomography (PET), single photon emission (SPECT), magnetic resonance imaging (MRI), computerized tomography (CT),and ultrasound (US) imaging, that are already used in human studies, and on the use of other procedures initially used for *in vitro* assays, including nuclear magnetic resonance (NMR), bioluminescence (BL) and fluorescence (FL) methods **(Fig.8)** [99]. Some of these clinical techniques have been re-scaled to be used in pre-clinical animal models, increasing their sensitivity and resolution to study smaller organisms (PET/SPET, MRI, CT, US), while other *in vitro* approaches have been up-scaled to be used with small animals but have not the possibility to be used also in the clinics since some physic limitations (BL, FL).

Each approach has its own advantages and disadvantages. MRI, CT, and ultrasonography produce anatomical images of body structures, whereas PET and SPECT can image physiological processes and thus produce functional images.

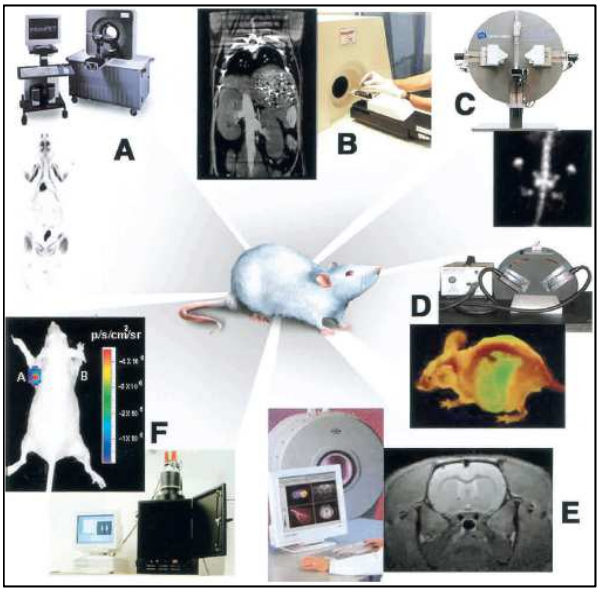

Fig. 8: *In vivo imaging techniques applied on preclinical studies with illustrative examples of the variety of images that can be obtained: (A) microPET, (B) microCT, (C) microSPECT, (D) fluorescence imaging, (E) microMRI, (F) bioluminescence imaging.*

All these technologies differ each other for various aspects: spatial and temporal resolution, energy and penetration depth of the radiation used for the production of the images, need/availability of contrast agents, threshold of detection. The technologies differ also for the type of information, anatomical or functional, that provide. So, each methodology should be used with different efficiency, in relation to the application.

Molecular and cellular imaging progress entails the development of two areas: the one related to detection technologies and the other related to cell labelling strategies, contrast agents, tracers and reporter genes/probes [100].

Several molecular imaging approaches have been described but all can be reported to three categories [101]:

- **Direct imaging**: the image is the result of molecular probe localization at the target, directly and in a single step. The extent of this localization (image intensity) relates directly to the interaction with the target, and each molecular probe is specific to one target.
- **Indirect imaging**: is based on reporter gene expression imaging. The cells or animal are engineered to express a reporter gene coding for a reporter protein, whose expression is easily

detectable and quantifiable through imaging, immunohystochemistry and enzymatic assays. The expression of the reporter is induced following the occurrence of a specific molecular event in study. Once the reporter protein is expressed, a molecular probe (a substrate or a ligand) specific for this protein (an enzyme or receptor) is used to image it. Imaging reporter genes can code for both intracellular (i.e. Luciferase) and membrane associated (i.e. D_2R, that is a dopamine receptor) proteins (enzymes, membrane receptors or membrane transporters).

- **Functional or tissue microenvironment imaging**: is also called 'physiological', 'metabolic' or 'surrogate' imaging. Functional imaging strategies reflect downstream effects of the expression of one or more endogenous genes and/or activation/inhibition of molecular pathways involved in the metabolism, in order to describe the physiologic or pathologic tissues conditions .

Most of current molecular imaging applications, use the principle of 'direct' imaging, mainly because of the longstanding and well established practice of probe development and the extensive use in clinical nuclear medicine, however the development of new specific tracers for new important targets is a long and expensive process involving chemists, physics, biologists and physisicans. For these reasons the use of reporter systems have been proposed to make easier the use of these non-invasive techniques.

New approaches have been proposed related to cell imaging in which specific cell populations are labelled and infused to study their distribution, localization, survival, proliferation and function in the organism. Cells can be labelled with two different procedures **(Fig.9)**.

Direct labelling procedures comprise ex vivo cell labelling with a detectable probe able to bind cell membrane or enter the cell and target intracellular structures, before their reinfusion. In particular, the sample population has to be harvested (1), labeled ex vivo with a radiolabeled molecule, paramagnetic particles or fluorescent probe (2) and reinfused (3). After reinfusion of the labeled population their distribution and behavior in the recipient subject can be visualized by imaging strategies (4).

Indirect imaging entails the genetic modification of the cell population to study, by insertion of reporter genes, whose expression is exploited to monitor genetically modified cells with a specific reporter probe. In this case cells are harvested (1) and transduced ex vivo (2) with an exogenous reporter gene encoding a reporter product. Only after reinfusion of the transduced population (3) and administration of the reporter probe (4), cell distribution and behaviour can be visualized in the recipient subject by imaging techniques (5). Transcription and translation of the reporter gene leads to the production of a reporter product, which can bind or trap a reporter probe within the cell. Direct and indirect labelling protocols have advantages and disadvantages and can be preferentially used for different cell types. The advantages of direct labeling is the easy labelling

protocols respect to the difficulty of cell engineering and the availability of several already clinically approved probes for cell labelling. The great disadvantage of direct imaging is that this approach does not enable long-term monitoring of cell proliferation in the body because the label is lost or diluted owing to apoptosis or mitosis, respectively. The indirect approach is fundamental for imaging of proliferating cells during their migration, activation and division: in fact the transduction of immune and/or stem cells with a reporter gene means that the entire cell progeny can trap the reporter probe, permitting their imaging without loss of signal along generations **(Fig.10)**. Furthermore direct labelling does not enable monitoring of cell viability since probe retention is not dependent from cell functional features and after cell death the probe can be transferred to different cell population such as macrophages, introducing imaging oversight. Indirect labeling procedures comprise stable genetic modification of the cells to monitor their fate and the fate of their progeny expressing the reporter gene inherited from the parental cell in vivo over time, following repeated in vivo probe administrations. In this case only living cells will express the reporter and will produce a specific signal after probe administration, no leakage to other cell population will be possible and it will be possible to study cell viability rate at each observation.However the use of viral vector, exogenous reporter gene and genetic engineering of cells is limiting this approach in the clinics.

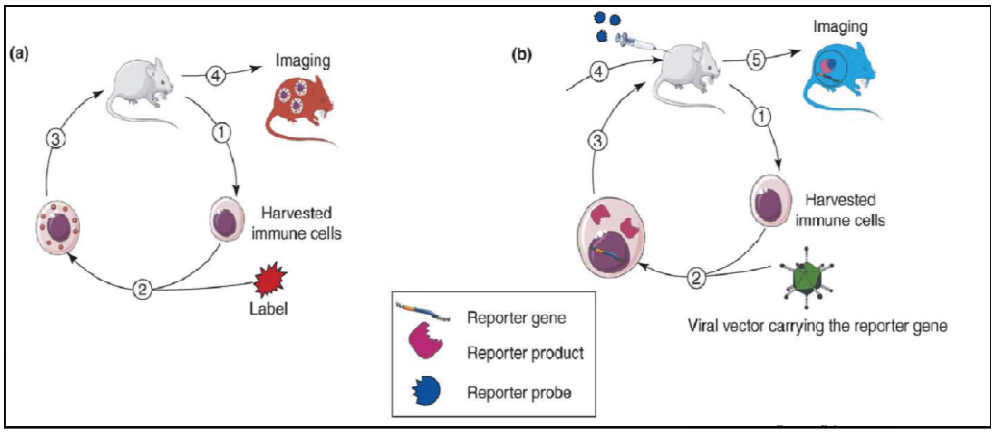

Fig. 9: *Schematic representation of the direct and indirect imaging strategies* a) direct labelling b) indirect labelling.

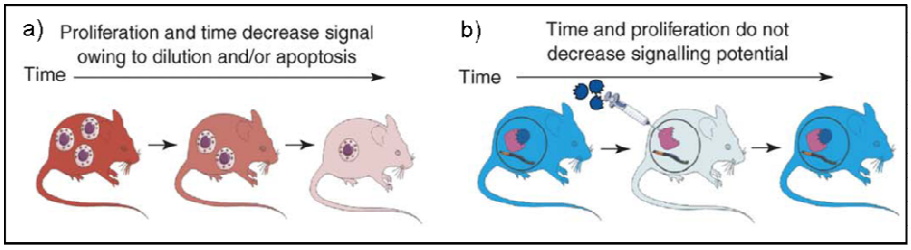

Fig. 10: *Imaging of cell progeny over time*

Molecular imaging in living subjects offers distinct advantages when compared with conventional *in vitro* and cell culture biological research techniques. Although *in vitro* studies in basic biological research have been, and remain, a mainstay for defining biochemical and gene expression pathways, the *in vitro* approach has been less successful in deciphering physiological whole-body contributions of proteins, in which redundancies and differences in regulation can alter the outcome from that initially in vitro predicted [102,103]. Molecular imaging permits both the temporal and the spatial assessment of biological processes to be determined in a more meaningful manner throughout an intact living subject. Visualization of biological functions and molecular events in the entire living subject becomes easier and more realistic in respects to the dynamics of complex biological networks and of complete and holistic biological systems in vitro analyses.

These techniques, especially in oncological studies, allow non-invasive determination of tumour load over time in individual animals. Each animal will be followed up as an individual being, thereby turning the cluster of animal models into an experimental group that can be compared directly with the treatment groups generally enrolled in clinical trials. This approach permits to reduce the numbers of animals needed for each experiment (according to the 3R principle: Refine, Reduce, Replace) and provides information on the various stages of tumour development. Furthermore it allows to increase the statistical power of longitudinal studies, and decrease experimental costs.

5.1 OPTICAL IMAGING

Optical imaging techniques reveal photons at different wavelengths (in visible and infrared ranges), resulting from BL and FL events, by using highly sensitive (cooled) charge-coupled device (cCCD) cameras that are the critica components of the entire acquisition systems. Advancements in the development of these cameras have greatly increased their sensitivity, and this has expanded their utility in a number of applications.

CCD cameras operate by converting light photons, at wavelengths between 400 and 1000 nm, that strike a CCD pixel with an energy of just 2–3 eV into electrons. A CCD contains semiconductors connected so that the output of one serves as the input of the next. In this way, an electrical charge pattern, corresponding to the intensity of incoming photons, is read out by the CCD into an output register and eventually amplified at the edge of the CCD for digitization.

The thermal energy in the CCD chip results in constant electrons release (termed “dark current”), determining formation of background noise. This is dramatically reduced by cooling CCD chip: dark current falls 10 fold every 20° C of temperature de crease (*e.g*. for BL imaging, CCD cameras are usually cooled). Indeed, cooling to absolute - 90^{o}C will allow for maximal sensitivity by maximal suppression of dark current that is essential for sensitivity of detection of bioluminescent signals **(Fig.11).**

In 2D acquisitions, the derived luminescent image is a color image superimposed on a gray-scale photographic image of the small animal obtained by using the image analysis software [104].

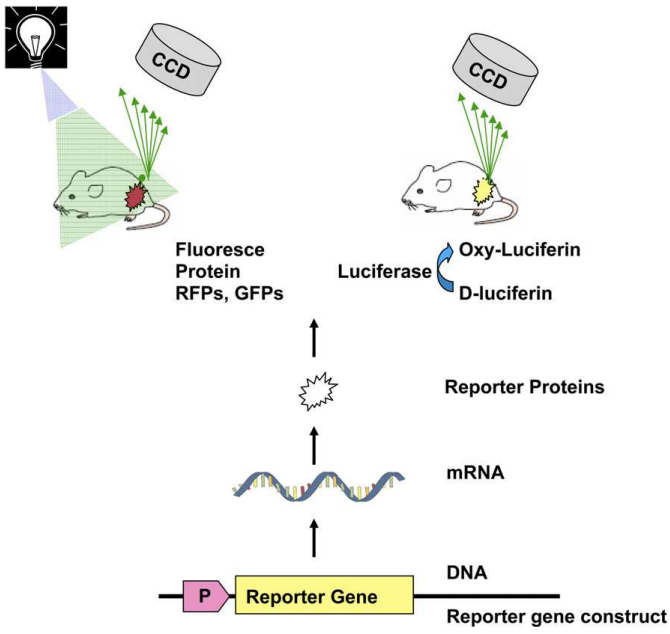

Fig. 11: *Optical imaging in FLI and BLI analyses*

The main advantages of optical imaging modalities, such as fluorescence and bioluminescence imaging, include that they are simpler, cheaper, more convenient, and more user friendly than other imaging modalities. Another advantage, especially for BLI, is its high sensitivity for detecting low levels of gene expression since no bioluminescent background can be found in usually acquired organisms (mice). Various optical reporter genes and constructs, which have been also used *in vitro* , are available for testing the same biologic hypotheses in living animal models.

5.1.1 BIOLUMINESCENCE

BLI is based on the use of reporter genes encoding enzymes able to produce photon emission in the presence of specific substrates and co-factors, in the wavelength range of 485-613 nm.

The most used reporter enzymes are Luciferases. After injection of a substrate, in presence of specific cofactors (*e.g*. Mg^{2+}, oxygen, ATP, etc.), the substrate is oxidized with production of photons. Many luciferases with matching substrates are available. The family of luciferase enzymes, present in certain bacteria, marine crustaceans, fish, and insects, consists of proteins that can generate visible light through the oxidation of an enzyme-specific substrate in the presence of oxygen and, usually, adenosine triphosphate (ATP) as a source of energy. During these reactions, part of the chemical energy is released as visible light.

In particular, firefly luciferase bioluminescence is based on ATP-dependent conversion of luciferin by this enzyme into the product oxyluciferin producing the relative light emission (**Fig.12**).

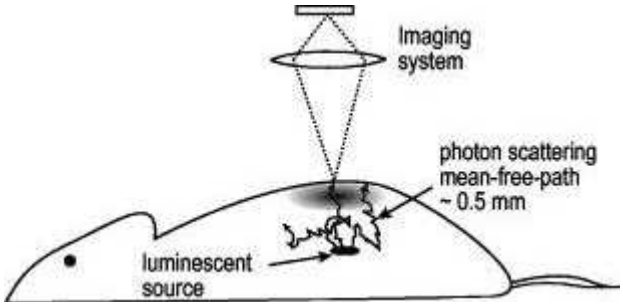

Fig. 12: *BLI imaging process*

The most useful luciferase for molecular imaging is firefly (*Photinus pyralis*) luciferase (and its substrate, D-luciferin). Firefly Luciferase catalyzes the transformation of its substrate D-luciferin into oxyluciferin in an oxygen and ATP-dependent process, leading to the emission of photons with

a peak wavelength at 560 nm, and a wide emission that extends beyond 600 nm, characterized by a sufficient penetrance across small animal tissues. Importantly, the non-immunogenic substrate luciferin, once injected either i.v. or i.p., diffuses within minutes throughout the entire animal body and is rapidly taken up by cells.

However, also Renilla Luciferase, green or red click beetle (*Pyrophorus plagiophthalamus*) Luciferases, and Gaussia Luciferase have been used for *in vivo* imaging approaches. Both Renilla and Gaussia Luciferases emit blue light, which is highly attenuated in living tissue, and possess high bursting activity, therefore requiring care and precision in the readout timing. Moreover, their substrate, coelenterazine, has been shown to be transported by the multidrug resistance transporter Pgp as well as to interact efficiently with superoxide anion and peroxynitrate in light-producing reactions, thereby complicating applications of Renilla and Gaussia Luciferases *in vivo* [105].

BLI imaging is widely used in molecular biology to investigate *in vitro* molecular signaling pathways, protein-protein interaction an so on, but it can also be used for non-invasive and real-time imaging in small animals. It has been shown that BLI can be used to track cells anywhere in the body following the intraperitoneal administration of a saturating dose of luciferin, including potential sanctuary sites like the brain. Moreover, non-invasive BLI is easy to perform and it can be far more sensitive than any of the other noninvasive techniques. Moreover, the formation of bioluminescence is ATP-dependent, and therefore only metabolically active cells contribute to bioluminescence production, and as such, the bioluminescence signal is only derived for example from living cancer cells and not from necrotic areas in tumours neighter it can be produced by apoptotic cells. BLI is also more sensitive than FLI because it does not require an external excitation light source and it does not induce autofluorescent signals. BLI is performed in absolute darkness, thus avoiding the interference with background light, to increase sensitivity and make the measurement of small lesions more reliable. Furthermore contrary to what happens in fluorescence, only the emitted light produced in BLI has to travel through quenching tissue layers. Quenching of the signal by tissue components does occur, but at an acceptable level.

The major limitation to the use of bioluminescent reporters is that the low energy photons emitted are partially absorbed and scattered in the tissue volume encountered on their path from the emission site to the detector system. It has been calculated that about 90% of the BLI signal is attenuated per centimeter of tissue depth. So, the amount of photons detected may not be proportional to the reporter expression or may be insufficient to visualize the enzymatic activity present in the most inner organs of the most common laboratory animals, including mice [106]. However, firefly luciferase emission possesses a broad spectrum with a large component above 600 nm where hemoglobin and melanin (primary light quenchers in tissues) absorb relatively little light and this is the reason for the wide use of this reporter for *in vivo* BLI protocols.

Another downside of BLI is the low spatial resolution and another problem is that cells need to be genetically modified in order to express the luciferase gene, which makes a direct translation of data from animal studies to the clinic impossible.

As regards oncological studies, BLI sensitivity is dependent on various factors, such as luciferase expression levels in the cancer cells, the site of implantation of the tumours, oxygenation and viability of the tumours, and sensitivity and settings of the camera (especially the clustering of pixels, as this determines the signal-to-noise ratio). It has been shown that sensitivity depends from cell localization and density. When tumours are solid masses located close to the surface of the animal, sensitivity is highest. When cancer cells are diffusely present intraperitoneally, sensitivity decreases, whereas intravenous inoculation leads to the lowest sensitivity due to cell high distribution. When cells are inoculated orthotopically, intramuscularly, or intracranially to yield a local tumour mass, the sensitivity resembles that of solid masses as regards cell density by depends on the site of cell injection (mainly depth, vascularization, tissue density). Evidences in literature, comparing the sensitivity of BLI with FLI, showed how BLI was far more sensitive than FLI, due mainly to the much lower background signal.

Despite the ease of use, the low costs and the short acquisition time, BLI depends on pharmacokinetic of the substrate biodistribution, does not provide fully quantitative data and in general offers mainly planar imaging datasets, therefore imposing some positional uncertainty of the attained signal although new instruments have been developed allowing the production of 3D images and a direct superimposition of luminescence map and CT anatomical images.

In summary, BLI is a powerful non-invasive tool for longitudinal assessment of tumour load in small laboratory animals. BLI is easy to perform, yielding a very reasonable throughput and an excellent sensitivity compared with other non-invasive imaging modalities. Cancer cell load can be determined from the moment that cancer cells are inoculated into the animals until their sacrifice. These longitudinal data, provide information about the course of tumour development in asymptomatic animals and can lead to significant differences between experimental groups even using relatively small treatment populations. Although BLI does not provide information on morphology and/or growth patterns of individual tumours or interactions between cancer cells and host tissue, a combined approach of BLI and FLI, CT, ultrasound, or MRI may overcomes this limitation.

5.1.2 FLUORESCENCE

Fluorescent imaging is based on the detection of photons (wavelength range: 442-800 nm) produced by the return to the ground state of electrons excited by laser photostimulation. These photons can be revealed by CCD-cameras by using specific filters to select excitation and

emission band and to reduce background noise. In this technique the influence of tissue scattering and absorption is doubled with respect to bioluminescent probes, because light must cover two-folds the signal-detector distance (excitation and emission pathways).

Examples of fluorescent molecules are green fluorescent protein, red fluorescent protein, rhodamine, indiocyanine, etc. Despite largely used for *in vitro* study, not all these molecules are useful for *in vivo* studies, because of their photon excitation ad emission wavelengths, often under 600 nm. With the introduction of redshifted fluorescent proteins and injectable near-infrared fluorescent probes, the development of highly sensitive photon detection devices and *in vivo* microscopy (confocal and multiphoton), and with the advances in mathematical modeling of photon propagation in tissues, it has been possible to develop innovative macro- and microscopic FLI modalities such as FLI tomography, spectrally resolved whole body FLI imaging, and intravital multiphoton imaging.

There are several strategies to label a protein with a fluorescent tag. In the first, the gene of interest can be fused to or replaced by a reporter gene coding for an intrinsically fluorescent protein, for example a member of the red fluorescent protein family (DsRED). The second one, is performed through the use of reporter genes coding for proteins, such as beta-lactamase or beta-galactosidase, able to activate a specific probe to a differently fluorescent molecule (convert an exogenously added non-fluorescent substrate into a fluorescent derivative, or shift the wavelength of a fluorescent substrate).

Most of fluorescent proteins requires excitation in the blue and green regions of the visible spectrum where tissue absorption of light is particularly high and where autofluorescence from endogenous molecules causes significant background signals.

In 2004 a report appeared describing new fluorescent reporters developed by mutagenesis from already existing ones. These new genes were able to emit photons of several wavelength but with a more consistent set into the red spectrum. These proteins have emission maxima as long as 649 nm, but suffer from low quantum yields and then low brightness that limits their application *in vivo* [107].

In 2007 a brighter red-shifted fluorescent protein was described by Shcherbo *et al* [108]. This protein, named Katushka, is originated from the sea anemone *Entacmaea quadricolor*. Its excitation peak is at 588 mm and the emission peak is at 635 nm, both of which are relatively non-absorbed by tissues and hemoglobin. Katushka has many favorable properties in addition to its absorption and emission peaks, including a rapid maturation time of 20 min, an extinction coefficient of 65 000 $M^{-1}cm^{-1}$ and its quantum yield of 0.34 making Katushka the brightest fluorescent protein with a maximum emission beyond 620 nm. In cells, Katushka forms no visible aggregates or has no other toxic effects.

For what concerns cell labeling for FLI applications, there are commercially available dyes that are trapped by cell membrane, such as PKH26®, VivoTag®, Alexafluor® [109], or fluorescent nanoparticles, such as Quantum Dots [110,111] that can be internalized by cells through phagocytosis or endocytosis in the resence of specific carriers. These molecules offer certain advantages: faster labelling procedures, lower costs no cell genetic perturbation even if disadvantages of these strategies have already been described previously.

Although exciting advances are emerging, FLI imaging still suffers from pitfalls such as, high autofluorescence in the blue-green window resulting in low signal-to-noise ratios, fluorophore photo-bleaching, and high levels of photon attenuation and scattering in living tissues as well as toxicity due to the use of fluorescent dyes. However, imaging of fluorescent proteins (preferably monomeric red-shifted reporters) has an important advantage over other imaging modalities with genetically encoded reporters, *i.e*., no substrate is required, uncoupling the read-out from substrate pharmacokinetic and thereby enabling true real-time imaging. In addition, the use of florescent reporters allows sub-cellular target localization by correlative microscopic analysis.

5.2 NUCLEAR IMAGING

Nuclear-based imaging is centred on the use of selected radiopharmaceuticals and dedicated scanners. It has allowed the *in vivo* study of different biological pathways in living animals and thus the evaluation of several models of disease, such as cancer. It is an analytical technique used to obtain quantitative physiological information about the functionality of a specific organ. Depending on the type of labelled molecule, different information can be obtained. PET and SPECT are both radionuclide-based imaging techniques, yet they differ substantially in the type of radionuclide employed to label the tracer and in the method of data acquisition [112,113]. Both the techniques record high-energy γ-rays emitted from the subject during a physical decay event occurring in instable nuclides **(Fig.13).**

For what concerns PET imaging, natural biological molecules can be labeled with a positron-emitting isotope. The most used isotopes are ^{15}O, ^{13}N, ^{11}C, and ^{18}F; other less commonly used positron emitters include ^{14}O, ^{64}Cu, ^{62}Cu, ^{124}I, ^{76}Br, ^{82}Rb, and ^{68}Ga. Natural decay of these radioisotopes produces emission of a positron from its nucleus, that annihilates with a nearby electron: this interaction is able to produce two 511 keV γ-rays that are emitted simultaneously about 180° apart.

For SPECT, single photon emitting isotopes (*e.g*., ^{99m}Tc, ^{111}In, ^{123}I, ^{131}I) can be used for imaging in living subjects. These radioisotopes are characterized by emitting photons of different energy (*e.g*. ^{111}In decay with emission of two photons of 171 e 245 keV, ^{99m}Tc with one photon of 140keV) [114]

.

Both PET and SPECT imaging are highly dynamic methods permitting the study of biodistribution, localization and elimination of the tracer during time in the whole organism.

Detection of γ-rays is achieved through an array of scintillation crystals able to convert γ-ray energy into visible light, suitable light sensors that convert light into electrons, read-out electronics, and image processing units.

The coincidence detection of both γ-rays in PET within nanoseconds defines the line of response in space and thus the direction of flight helping in the identification of the photons source (electronic collimation) without the need of a physical collimator (used in SPECT) that contribute to decrease sensitivity.

The reconstruction software measures the coincidence events at all angular and linear positions to reconstruct an image that depicts the localization and concentration of the positron-emitting radioisotope within a plane of the scanned organ.

In the SPECT acquisitions, otherwise, to locate the source of an admitted photon, its direction of incidence into the detection system needs to be accurately fixed and its interaction location determined in the position sensitive detector. Lead or tungsten collimators are perforated plates that define the angle of photon incidence and are, therefore, positioned in front of the detector during SPECT acquisition (geometric collimation). Collimator design is a compromise between spatial resolution and sensitivity. In contrast to SPECT, attenuation (quantifiable reduction in events present at the face of the detector due to absorption or scatter through tissues) of the emitted radiation in PET can be corrected precisely because the total length through the body determines the attenuation factor along a coincidence line. By doing so, quantitative information about the tracer distribution can be obtained.

An important principle to note in PET imaging is that because all isotopes used result in two γ-rays of the same energy, if two radiolabelled probes, each with a separate isotope, are injected simultaneously, it would not be possible for the PET detectors to distinguish them. Therefore, to investigate multiple molecular events in PET, radiolabelled probes are usually injected separately, allowing for the decay of one isotope prior to administration of the other. SPECT, on the other hand, does allow simultaneous detection of multiple events owing to the use of multiple isotopes, each with different-energy γ-rays and the identification of energy windows for signal detection.

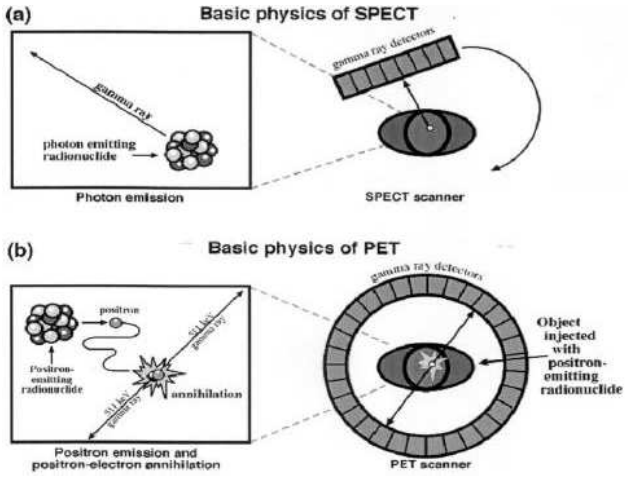

Fig. 13: *Physics of SPECT and PET imaging*

Several reporter gene/reporter probe systems have been developed for nuclear imaging studies. A well-studied strategy is the reporter gene *hsv1-tk* whose proteic product (herpes simplex virus type 1 thymidine kinase [HSV1-TK], an enzyme) can be imaged with the specific radiolabelled substrate (^{18}F-fluoropenciclovir, ^{18}F-FPCV or others) and imaged by PET imaging [115]. However also Iodinated substrates have been developed for the use of this reporter system in SPECT imaging (FIAU, uracil nucleoside derivatives labeled with radioactive iodine) [116].

These radiolabelled reporter probes are transported into cells, and are trapped as a result of phosphorylation by HSV1-TK. When used in non-pharmacological tracer doses, these substrates can serve only for imaging without the well-known toxic suicide effects. More recently, a mutant version of this gene, *HSV1-sr39tk*, was derived using site-directed mutagenesis to obtain an enzyme more effective in phosphorylating ganciclovir (and also less efficient at phosphorylating thymidine) with consequent gain in imaging signal [117].

The Dopaminergic type 2 receptor (D_2R) gene has also been validated for nuclear-based imaging as reporter gene. More recently, a mutant form of D_2R that uncouples the receptor from the signal transduction pathway while maintaining affinity for the ligands has also been reported [118].

^{18}F-fluoroethylspiperone (FESP), a radiolabeled receptor ligand that is an inhibitor of such receptor characterized by high affinity, can be used as reporter probe for PET [119], however also specific SPET tracers have been reported (IBZM) even if characterized by lower sensitivity (and lower receptor affinity). As regards SPECT imaging, Na^+/I- symporter has been largely used as reporter gene. In this case Iodide ($^{123}I^-$) is specifically transported into cells by the ATP-dependent symporter, and accumulated proportionally to the reporter expression level. Once transported into cells, $^{123}I^-$ is not modified and then is free to exit again from the cell. This is a drawback of the use

of this reporter. It has been estimated that 80% of the $^{123}I^-$ transported by the NIS goes out of the cell during the first hour from the tracer administration [120-121].

In the field of cellular imaging, it is possible to label cells for nuclear imaging with indirect protocol using these reporters or using direct labelling strategies by labelling cells with radiolabelled tracers such as 18F-2-fluoro-2-deoxyglucose ([^{18}F]-FDG) [122].

Labelled molecular probes or tracers can be also directly injected into the subject, and then PET or SPET imaging can be used to follow the distribution and concentration of the injected molecules on the base of the specific mechanism of localization (cell methabolism, expression of specific reporter, perfusion, hypoxia and so on).

One of the advantages of PET is that drugs or existing molecules known to interact with a specific target can be modified with a radioisotope while minimally perturbing the parent molecule. These probes serve quite a useful role in monitoring “downstream” changes in pathology, but do not generally serve to characterize early changes in a disease process. Currently, molecular imaging probes with greater specificity and targeting potential can be made by using antibodies, ligands, or substrates that can specifically interact with specific targets such as cells or sub-cellular components.

To study metabolic features, the most used molecule is [^{18}F-FDG] [122]. In the cells, this radioligand is phosphorylayed by hexokinase, providing information about cell metabolism **(Fig.14)**.

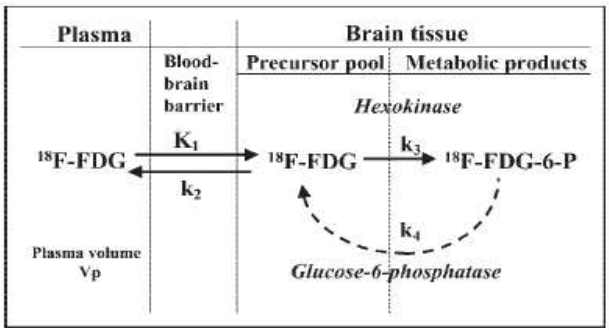

Fig. 14: *[^{18}F]FDG uptake in brain tissue.*

PET with [^{18}F]FDG directly reflects the glucose metabolic activity of tumour cells and is predictive of patient outcome in cancer. However, this radiotracers could be considered not useful for the study of some kind of cancer such as prostatic carcinoma, clear cell renal carcinoma and glioma [123].

Indeed, for example the variability of glucose uptake in recurrent high-grade gliomas and low tumour-to-background ratios due to the high metabolic activity of healthy brain tissue limit the usefulness of ^{18}F-FDG PET.

However, in these cases, a metabolic radiotracer can be changed with a tracer able to report on cell proliferation such as 3′-deoxy-3′-^{18}F-fluorothymidine (^{18}F-FLT), a thymidine analog that has been developed to image tumour cell proliferation. ^{18}F-FLT is a thymidine analog that is transported into tumour cells via nucleoside transporters and is subsequently phosphorylated by thymidine kinase 1 to ^{18}F-FLT 5-phosphate. Though ^{18}F-FLT is not incorporated into DNA, its uptake correlates with tumour tissue proliferation as determined by Ki-67 correlation with antibody staining. ^{18}F-FLT PET has been already used to monitor disease status and to direct treatment in a patient with glioblastoma [124,125].

Another field in which PET study could be applied, is hypoxia *in vivo* study. Indeed, several radiopharmaceuticals designed to target hypoxia have been developed, including the nitroimidazoles ^{18}F-fluoromisonidazole (^{18}F-FMISO) and ^{18}F-fluoroazomycin arabinoside (^{18}F-FAZA) and the copper complexes $^{60/62/64}$Cuethylthiosemicarbazone(Cu-ATSM), and have been evaluated clinically for tumour hypoxia imaging.

5.3 MAGNETIC RESONANCE IMAGING

MRI is widely used for imaging of soft tissues. Nuclei (the most used is ^{1}H due to the water's abundance in the body) placed in a strong magnetic field align their spin to the magnetic field. Radiofrequency (RF) pulses induce some of the magnetically aligned nuclei to alter the alignment of their spins. When the RF pulse is turned off, the nuclei realign with the magnetic field, generating an electromagnetic flux that provides information about the environment of the resonating nuclei

In animal models, the expression of different reporter genes has been studied by MRI. Principal feature of this type of labeling approach is the ability of the reporter to modify the relaxing process of expressing cells. The most used reporter genes are based on enzyme-based strategies [126]:

1) enzyme-based cleavage of functional groups that block water (proton) exchange or protein binding of MR contrast agents, *i.e*. β-galactosidase. This enzyme is able to cleave off galactose to a gadolinium based substrate (EgadMe) and this results in inner sphere relaxation enhancement and increased contrast. A convenience of using β-galactosidase reporter system is the low background contrast, as there is no natural endogenous expression of the enzyme;

2) expression of surface receptors that enable binding of specific MR contrast agents, *i.e*. transferrin receptor. After systemic injection of monocrystalline iron oxide nanoparticles, this agent is retained by the expressed receptor, generating a major contrast;

3) expression of para- and anti-ferromagnetic (metallo)proteins involved with iron metabolism, such as transferrin receptor, ferritin and tyrosinase. For example, the last enzyme is part of the melanin synthesis pathway: it catalyzes the oxidation of tyrosine-yielding dioxyphenylalanine that is converted to melanin at the end of the whole process. It is characterized by a high affinity for iron, allowing its accumulation and generation of a resonance signal [46,127].

To generate contrast in MRI, several contrast agents have been developed, also approved for clinical use. Among these agents T2-weighted iron oxide nanoparticles represent the most sensitive agent used in both animal and human applications. In general, any particle larger than 50 nm is termed superparamagnetic iron oxide nanoparticles (SPIO, as Endorem®), while particles smaller than 50 nm are called ultra small superparamagnetic iron oxide (USPIO). Currently, SPIO is the only t2 contrast agent that have been used in the clinics for MRI, and there are several reasons for its popularity. First, the particles are usually non-toxic for labelled cells, and the particles are biodegradable *in vivo*. Second, it is a negative contrast probe, so it provides clear contrast to the background of the soft tissue, that generally are bright. Third, the particles can remain inside terminally differentiated cells throughout their lifetime, thus allowing long-term studies. Fourth, due to its sensitive signal, SPIO-based imaging requires a much smaller concentration than gadolinium, which makes SPIO more suitable for labeling human cells than other contrast agents.

6. HYPOXIA AND HIF-1α ACTIVITY IMAGING

Small animal molecular imaging is allowing us to increase our knowledge on critical biologic pathways involved in disease progression by non-invasively characterizing biologic processes or tumour properties, analysing their changes after treatments in relation to tumour response and evaluating their modulation following new treatment, helping in identifying new important targets. The use of non-invasive strategies could help also in providing bridges to clinical application, as regards tumour diagnosis, staging, determination of therapeutic targets, monitoring therapy, and in the evaluation of prognosis.

Linking molecular imaging to genetic engineering it could allow real-time assessments of molecular events related to therapeutic efficacy [99,101]. Reporter gene expression imaging of constitutively expressed proteins has first emerged as a useful means for monitoring tumour growth and regression in preclinical models at subcutaneous, orthotopic, or intraperitoneal sites. On the other hand, inducible promoted have been used to monitor their activation by assessing the expression of the reporter gene placed under their control. Several molecular pathways have been studied such as nuclear receptor activation, p53 activation, hypoxia induction and so on with different purposes. Indeed, small animal gene expression imaging techniques can provide a new means for

identifying the expression of drug targets and treatment response biomarkers by accurately selecting the optimal probe or promoter driving reporter gene expression.

In this scenario, since hypoxia is considered a promising target for the treatment of many different human cancers, and its in vivo study could help to predict patient outcome and to estimate prognosis, several procedures have been described to in vivo assess hypoxia extent and activation of molecular pathways involved in hypoxia establishment. Indeed, the ability to survive under hypoxic conditions is one of the fundamental physiological differences between tumour and normal cells.

The noninvasive imaging of hypoxia is of significant importance, given that the onset of hypoxia in malignant

tissues is associated with and influenced by a myriad of complicated physiological processes. Moreover hypoxia has been used as biomarker for the evaluation of tumour progression or estimate tumour response to treatment as well as for the radiotherapy planning in Intesity-modulated radio-therapy protocols. This condition can be also used to stratify patient in order to increase treatment efficacy.

Several protocols have been developed to in vivo assess hypoxia condition and related activation of molecular pathways both in the clinics and in small animal models.

Imaging modalities such MRI, PET and optical imaging have been intensively applied to investigate hypoxia in tumours. Improving molecular imaging in this aspect, could be extremely powerful for clinical treatment evaluation and improvement, for the stratification of patients and for a more accurate follow-up assessment.

For what concerns, MRI, this tecqnique permits to perform non-invasive assessment of tumour microenvironment using dynamic contrast-enhanced magnetic resonance imaging (DCE-MRI). This procedure can be used to measure tumour perfusion and indirectly estimate hypoxia and vascularization. DCE- MRI uses kinetic modeling of tumour contrast uptake and wash-out over time to measure tumour perfusion and vascularity. DCE MRI can be used to determine intratumoural blood flow preoperatively or to predict vascular permeability [128-129]. MRI methods are attractive for the assessment of tumour oxygenation since they avoid the complication of short-lived radioactivity and MRI equipment is widely available.

At the same time, also hypoxia PET imaging with [^{18}F]FMISO, [^{18}F]FAZA and [^{64}Cu]ATMS can be performed [130,131]. Nitroimidazole-based tracers, which are retained in hypoxic cells, allow PET-based assessment of tumour hypoxia, even if current tracers are characterized by slow tracer retention and clearance, resulting in low inter-tissue contrast. Pimonidazole is an immune detectable hypoxia marker widely used for detection of hypoxia in tumour samples. Pimonidazole has excellent chemical properties for hypoxia imaging, but labelling for non-invasive assay has not been attempted [132].

PET imaging of 2-nitroimidazole compounds, such as [^{18}F]FMISO, has been used to identify hypoxic tumours (including gliomas) in human patients [133]. The volume and intensity of hypoxia, measured by [^{18}F]-FMISO PET, in GBM before radiotherapy are strongly associated with poorer time to tumour progression and overall survival. This type of imaging could be integrated into new treatment planning strategies to target hypoxia more aggressively in GBM and could be applied to assess treatment outcome. Limitations of [^{18}F]FMISO PET include a relatively low ratio of hypoxic to normal tissue due to slow blood clearance. [^{18}F]FAZA is a 2-nitroimidazole hypoxia imaging agent with the alkyl side chain in [^{18}F]misonidazole replaced by a polar arabinose sugar in an attempt to increase the overall hydrophilicity of the compound. This tracer displayed a hypoxia-specific uptake mechanism and provided tumour-to-background ratios (T/B ratios) superior to that of the standard hypoxia tracer [^{18}F]FMISO. The predictive value of [^{18}F]FAZA use for hypoxia-directed treatment regimens has been assessed using small animal PET. In these studies [^{18}F]FAZA was cleared more quickly from blood and normal tissues and provided higher tumour-to-muscle ratios in comparison with [^{18}F]FMISO. Similar to [^{18}F]FMISO, [^{18}F]FAZA was found to be useful for imaging hypoxia in various tumours. In patients with GBM, [^{18}F]FAZA yielded remarkably high tumour-to-background ratios due to its selective and presumably hypoxia-specific uptake in tumour reflecting blood–brain barrier disruption. In fact [^{18}F]FAZA does not cross the intact blood–brain barrier because of its hydrophilic nature, producing also a minimal background uptake in normal brain.

An alternative PET agent for hypoxia imaging is based on a metal complex of radioactive copper with ATSM [134]. The ability of the copper thiosemicarbazones to be retained within tumour is largely attributable to the low oxygen tension and subsequent altered redox environment of such tissues, characterized by the presence of increased levels of reduced nicotinamide adenine dinucleotide. Washout of these agents from normoxic tissues is rapid, resulting in high-contrast images. [Cu]ATSM is a non-nitroimidazole compound that is most commonly labeled with [^{60}Cu] (half-life, 24.5 min) or [^{64}Cu](half-life, 12.7 h) for PET imaging of tumour hypoxia. In the presence of hypoxia, Cu-ATSM is trapped intracellularly in the reduced form. It provides high tumour-to-background ratios (≤10.4) in less than 1 h after injection. Clinical studies have shown that Cu-ATSM can predict tumour response to therapy in cervical cancer, non–small cell lung cancer, and, to a lesser extent, rectal cancer. [^{64}Cu]ATSM yielded better-quality images with slightly higher tumour-to-background ratios than did [^{60}Cu]ATSM. Evidences from experimental studies suggest that the hypoxia selectivity of [Cu]ATSM varies among different tumour types and that its uptake in some tumour types at 1–2 h after administration may not truly reflect hypoxia. Indeed preclinical studies with [Cu]ATSM have shown that it is reduced and retained in hypoxic tissues, whereas it is rapidly washed out of normoxic tissues [135,136]. [Cu]ATSM uptake is more rapid than [^{18}F]FMISO uptake, and the reported hypoxic-to-normoxic ratio is greater. This imaging agent shows rapid

delineation of tumour hypoxia (1h) in high tumour-to-background tissue ratios (tumour-to-blood ratios≫2.0). It is apparent that [Cu]ATSM is a clinically relevant PET agent that has enormous value in the imaging of oncological hypoxia. Despite the specificity of the molecular probes exemplified above, background noise can be substantial with this approach. This is because the scanner cannot distinguish the parent tracer from the bound or metabolized tracer, and time is required to allow the parent tracer to be cleared. To circumvent this relative drawback, another category of specific imaging probes consisting in activatable or "smart" probes (also referred to as sensors or beacons) have been proposed. These can only be detected once they have interacted with their target, but have been developed mainly for optical and magnetic resonance imaging applications.

Finally, although *in vivo* optical imaging methods do not yet have a role in human studies of hypoxia, they have played an important role in hypoxia estimation for treatment efficacy in small animal tumour models. Regards to BLI, an genetic engineering approach, several model expressing a reporter gene (Luciferase) under the control of a hypoxia responsive element–luciferase (HRE-Luc) have been used to assess O_2 availability in tumours. In fact, the HRE promoter construct allows Luciferase expression in response to HIF1α transcriptional activity. Even if HIF-1α transcriptional activity is regulated by different molecular pathways, it can be assumed that it is able to report also on Hypoxia extent in the tissue. In this context, tumour cell lines can be transfected to express luciferase reporter gene under the control of HRE promoter, to directly monitor HIF1α activity in different conditions. For example, in our study, the human glioma U251 cell line was engineered to express luciferase reporter gene under control of three copies of the HRE sequences in the U251-HRE cell lines. In this case, U251-HRE cells express luciferase under control of HIF-1α transcription activity, and noninvasive detection of reporter gene expression is an indirect measure of this transcription factor activation due to also intracellular hypoxia. This model expresses low but detectable levels of luciferase in normoxic conditions and this value is significantly increased in hypoxic conditions. The same U251 cell line engineered with a constitutively expressing cassette (U251-pGL3 line) containing the same reporter under the control of a constitutive promoter (Sv40) can be used as control. Indeed, U251-pGL3 cells expresses high luciferase level in normoxic condition, although this level is slightly lowered during hypoxia [28,137].

Moreover, a new promising fluorescent probe has been described to study in a simple and easy way hypoxia in solid tumours by FLI. The HypoxiSense probe, a Carbonic Anhydrase IX (CAIX) specific ligand commercialized by PerkinElmer, is an imaging agent that can be used to image CAIX overexpression in tumours in response to regional tumour hypoxia allowing to non-invasively image and quantitate tumour sub-regions undergoing hypoxia-related changes by assessing its accumulation in tissues. HypoxiSense clears from the bloodstream quickly, with a half-life of

approximately 4 minutes, yet it accumulates within hypoxic regions in tumour tissues with a half-life of 6h. Tumour hypoxia can be detected as early as 3h post-HypoxiSense injection, with optimal signal to noise measured at 12-24h once circulating agent has completely cleared. Binding selectively CAIX, HypoxiSense provides complementary information respect to BLI analyses of HIF-1α mediated luciferase activity showing respectively a late and an early hypoxia biomarker. So, FLI and BLI analyses give different information about the same intratumoural process (cell membrane CAIX expression for FLI and HIF-1α nuclear accumulation and transcriptional activity for BLI) making a complete overview of the hypoxia establishment. Moreover, the cross-validation of BLI and FLI results, permits to overcome limitations of each imaging modality, in term of spatial resolution and sensitivity. Moreover the correlation of BLI and FLI results will allow to have an internal control of hypoxia presence (CAIX) while allowing the study of HIF-1α activity modulation due to different pathways.

In a wider context, involving both optical, nuclear and magnetic imaging, by integrating obtained results from different imaging techniques it could be possible to exploit the advantages of each technology, making negligible the relative disadvantages [106] **(Fig.15)**.

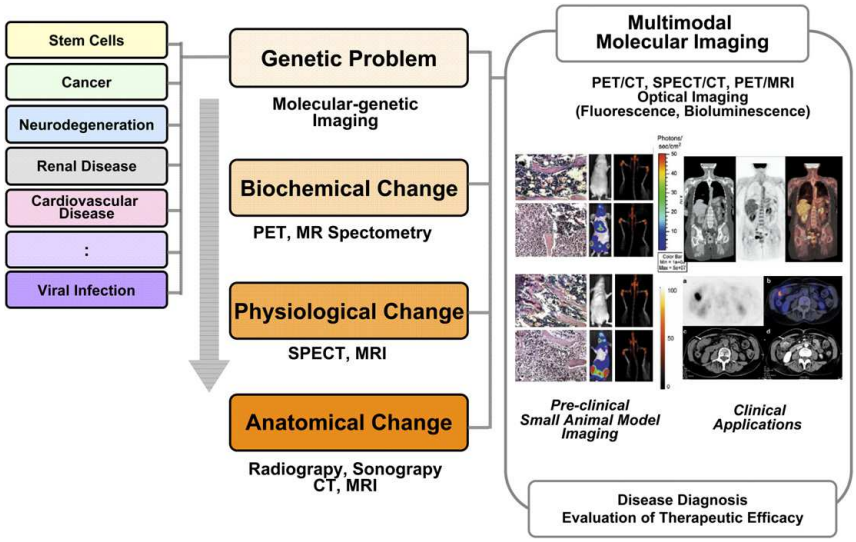

Fig. 15: *Multimodal molecular imaging approaches*

.

AIM OF THE STUDY

The aim of the present project is the study of a preclinical glioma model by using different molecular imaging techniques, focusing the attention on the intratumoral hypoxia establishment.

Brain tumours, especially the highly aggressive glioblastoma (GBM), are characterized by wide necrotic/hypoxic areas within the tumor mass, which correlates with enhanced resistance to therapy, increased invasiveness and a poor prognosis for the patient. In this context, hypoxia is considered a major driving force for GBM development and progression since the metabolic restrictions of hypoxia may allow the progression of lower-grade tumors to GBM. For these reasons, hypoxia is considered a promising target for the treatment of different human cancers, and an important biomarker to predict the treatment outcome and estimate patient prognosis. Hypoxia onset in malignant tissues is associated with and influenced by a myriad of complicated physiological processes finally involving HIF-1α. Several procedures have been described to non-invasively assess intratumoral hypoxia based on the assessment of pO_2, of the overexpression of specific proteins such as CAIX or the assessment of HIF-1α activity. This transcriptional factor, in fact, directly activates the expression of a number of pro-angiogenic factors that, by promoting neo-angiogenesis and vasculature reorganization, tumor invasiveness, loss of apoptotic potential, genomic instability, chemotherapy and radiation resistance, concur to tumor progression.

In this view, due to the main role of HIF-1α transcriptional activity in hypoxia establishment and progression, the first aim of this project was to monitor its activity *in vitro* and *in vivo* at steady state and in presence of different drugs by using an engineered cell model expressing the luciferase reporter gene under control of HRE (Hypoxia Responsive Elements) sequences.

The main purpose was the *in vitro* validation of this cellular model (U251-HRE), by studying the modulation of HIF-1α induced by different molecular pathways and in relation to cytotoxic treatments.

The second aim of this project, was represented by the *in vivo* validation of *in vitro* data, applying molecular imaging techniques. Indeed, molecular imaging allows the early detection of tumors features and the non-invasive quantification of biological processes in the animal model. In this view, improving molecular imaging and understanding the meaning of tumour feature modulation, it could be extremely powerful for clinical evaluation of tumour response to treatment and for the follow-up.

To this aim, orthotopic models were generated to firstly validate *in vitro* results, by using optical imaging modality (BLI and FLI) as preliminary approach. Subsequently, since the impossibility to directly translate optical imaging results into clinical setting, a cross-validation with PET ([^{18}F]FLT and [^{18}F]FAZA) and MRI was performed. Then, molecular imaging modalities were applied in the same models after a cytotoxic treatment (TMZ), with the aim to assess HIF-1α value in estimating

tumour response to treatment. Future studies will be necessary to understand the actual perspectives of the obtained results and to clarify the connections between HIF-1α, TMZ and tumour response also in view of a potential clinical translation of the results for the planning of personalized treatments.

MATERIALS AND METHODS

1. IN VITRO EXPERIMENTS

1.1 Cells lines and reagents

Engineered U251-pGL3 and U251-HRE human glioma cells were kindly provided by Dr Giovanni Melillo, National Cancer Institute, Frederick (MD)**.** U251-pGL3 cells express the luciferase reporter gene under the control of SV40 constitutive promoter and enhancer sequences, (pGL3-control), whereas U251-HRE cells express the luciferase reporter gene under the control of three copies of an HRE sequence, (pGL2-Tk-HRE). We routinely maintained both cell lines in RPMI supplemented with 10% heat-inactivated fetal bovine serum, penicillin and streptomycin (50IU/ml), 2mM glutamine (all Euroclone) and 2 µl/ml G418 (Sigma Aldrich) in a humidified atmosphere of 5% of CO_2 at 37℃.

1.2 U251-HRE infection

To obtain the U251-HRE-mCherry ceullar model, U251-HRE cells were transfected with a lentiviral infection with 5 MOI of PLW lentiviral vector mediated by polybrene (8µg/ml). The pCLL.PGK.Luc.WPRE (PLW) plasmid, containing the Luciferase gene under control of the constitutive promoter PGK, was cloned in our laboratory. The lentiviral vector was produced and the vector copy number (VCN) viral titer (1,72x10^6 TU/ml) was calculated on Hela cell lines through the amplification of the lentiviral specific WPRE region from genomic DNA of Hela infected cells by the use of the Real-Time PCR technique and its comparison to a curve of DNA standards with known VCN.
After infection, the luciferase expression was evaluated after cell lysis, by luminometer through a luciferase biochemical assay.

1.3 Drug preparation for in vitro studies

The hypoxia mimetic agents DFX (Sigma Aldrich) was re-suspended in distilled sterile water and used at a concentration of 100 µM and 1mM, respectively. Cells were incubated with DFX for 30 minutes (min), 1 hour (h), 3h and 6h.
Treatments with LY294002 50mM and FM19G11 1µM (Sigma Aldrich) were carried out to inhibit PI3K and to increase pVHL effects. Both drugs were re-suspended in dimethyl sulfoxide (DMSO) as per data sheet instructions and used with the same scheduling described previously.
Treatments with BEZ235 1µM (NVP-BEZ235) and Trametinib 10µM (GSK1120212 or TRAM, both Aurogene) were performed to evaluate the influence of PI3K/Akt and MAPK pathway on HIF-1α activity. Both drugs were re-suspended in DMSO as per data sheet instructions. Then, BEZ235 was incubated for 48 hours, whereas Trametinib for 72 hours. Finally, treatment with PD98059

10μM (Sigma Aldrich) was also carried out to compare its inhibitory effect on MEK activity respect to those of Trametinib. The drug is re-suspended in DMSO and used for 16h For each set of experiments the control group is represented by untreated cells.

1.4 DFX modulation of luciferase activity

5x10^4 U251-pGL3 or U251-HRE cells/well in 500 μl of complete medium were seeded in 24-wells plates. To induce hypoxia, the day after, the cells were treated with 100μM of DFX at different time points (30min, 1h, 3h, 6h). At the end of the treatment, the medium was removed and a wash with PBS was performed. Cells were then lysated using a 1x lysis buffer (Promega) and after lysing, cells were analyzed on a luminometer (Glomax Multi detection system, Promega). Data were normalized to the amount of proteins through Bradford assay, and expressed as relative luminescence units (RLU = luciferase counts /mg proteins).

1.5 Nuclear HIF-1α detection by immunocytochemistry assay (ICC)

3x10^5 U251-HRE cells were seeded in a chamber slide (Lab tek chamber; VWR International PBI) and treated with DFX 100μM for 30min, 1h,3h and 6 h. At the end of the pharmacological treatment, cells were washed and fixed with cytofix (J.T. Baker).
After a post-fixation in ethanol for 5 minutes at 95℃, the cells were washed in distilled water and then in PBS. Heat-induced antigen retrieval was obtained using a 0,05 M EDTA solution at pH 8.0 in thermostatic bath for 35 minutes at 97.5℃.
The cells were treated according to the manufacturer's recommended protocol with the primary monoclonal anti-HIF-1α antibody (54, BD Transduction Laboratories). Reactions were revealed by a Novolink Max polymer detection system (Leica Biosystems) according to the manufacturer's instructions. The chromogen diaminobenzidine (DAB) was incubated for 8 minutes at room temperature (RT). Cells were finally analyzed by optical microscopy at 20X, 40X, and 63X original magnification (o.m.) (LEICA DMD108 microscope).

1.6 Nuclear HIF-1α detection by Transam kit

An ELISA-based kit was used to detect and quantify HIF-1α nuclear translocation. The 96-well plate was coated with oligonucleotides containing the HRE sequences. Nuclear extracts of U251-HRE cells were prepared using the Nuclear Extract Kit (Vinci-Biochem) and, after quantification, the samples were added to the coated plate and analyzed using the TransAM Kit (Vinci-Biochem). Data were expressed as HIF-1α protein in sample nuclear extract/HIF-1α protein in control nuclear extract (OD 450 nm).

1.7 Effects of LY294002 and FM19G11 on luciferase activity in living and lysated cells

The *in vitro* luciferase activity profile was assessed in living cells and in cell lysates before and after treatment with LY294002 50mM and FM19G11 1µM, alone or in combination, at different time points (30 min, 1h, 3h, 6h).
For living cells, 5x10^3 U251-HRE cells/well in a 96-well plate were seeded. The day after, treatments were performed and, at the end of the treatments, a solution containing luciferin (2mM) was added to the living cells growing in the 96-well plate. Luciferase activity was detected after 5 minutes by cooled charge-coupled device (CCD) camera imaging (IVIS Lumina; PerkinElmer LifeSciences).
For lysates cells, the same study design used for DFX single treatment was applied. Data were expressed as RLU, as described previously.

1.8 Effects of BEZ235 and TRAMETINIB treatment on luciferase activity

To study PI3/Akt pathway and MEK pathway and their involvement in HIF-1α activity, treatment with BEZ235 1µM and Trametinib 10µM were performed.
Once more, 5x10^4 U251-HRE cells/well in 500 µl of complete medium were seeded in 24-wells plates. The day after, the cells were treated with BEZ235 for 48 hours and with Trametinib for 72 hours, alone or in combination.
A parallel experiment was performed treating U251-HRE cells with Trametinib 10µM and PD98059 10µM for 72 and 16 hours, respectively. At the end of the treatment, the medium was removed and the luciferase activity profile was assessed in cell lysates as described previously. All data were expresses as percentage of reduction respect to control (untreated cells).

1.9 In vitro TMZ treatment

To test TMZ effect on luciferase activity, two regimens were tested: a single acute dose of 400µM or a chronic dose of 100µM for 6h, 24h ,48h and 72 h [94-95]. Briefly, 5x10^4 U251-HRE cells/well were seeded in a 24-wells plate. The day after cells were treated as described before. At the end of the treatment, the medium was removed and cells were processed in the same way used previously to assess luciferase activity. Data were expresses as percentage of reduction respect to control (untreated cells).

1.10 MTT assay

5x10^3 U251-pGL3 or U251-HRE cells/well were seeded in 96-wells plate with 100 µl of complete medium. The day after, medium was changed by medium complemented with DFX 100µM, LY294002 50mM, FM19G11 1µM, BEZ235 1µM, Trametinib 10µM, PD98059 10µM , TMZ 100µM or TMZ 400µM for the same incubation time used for luciferase expression assay. At the end of treatment, the medium was removed and Cell Growth Determination Kit, MTT based (Sigma Aldrich) was performed in accordance with the kit manufacturer's instructions. 5mg/mL of MTT solution was added to each well and the cells were incubated for another 3h. Then, 10µl MTT solvent was added to each well. As negative controls three blank wells were considered. After agitation, the optical absorbance (Abs at 570nm) was measured and inhibitory rate (IR) was calculated as follows: IR = (Abs of experimental group/ Abs of negative control group) x100.

2. IN VIVO EXPERIMENTS

2.1 Animal studies

Animal experiments were carried out in compliance with the institutional guidelines for the care and use of experimental animals, which have been notified to the Italian Ministry of Health and approved by the ethics committee of the University of Milan. An orthotopic murine model was obtained by stereotaxic injection (coordinates: 1.5 mm lateral to the bregma as decribed in **fig.16**, 0 mm behind and 3.0 mm ventral to the dura) [138] of 1x10^5 glioma cells (U251-HRE and U251-pGL3) in 2 µl of PBS into 7-8-week-old female nude mice (Harlan Laboratories) at day 0. Cells were aspirated with a 10 µl Hamilton syringe just prior the injection. By pointing to the hole performed with a drill, Z axis was fixed to 0 and the syringe gently inserted into the brain until reaching the correct coordinate (-3 mm depth). Cells were injected at the speed of 1 µl every minute. The syringe was left for additional 5 minutes in the hole before removing it, to avoid cell lift in the path of the needle. The hole was closed using bone wax and the wound was closed with sterile autoclips. Following surgery, mice were monitored for recovery until complete wakening.

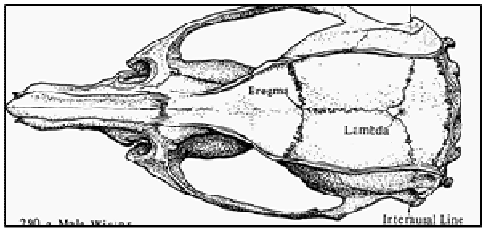

Fig. 16: *Representative image of bregma and lambda coordinates in mouse brain*

2.2 *In vivo* imaging study design

Different groups of animals were monitored by:

- BLI/FLI (n=25; CCD camera, IVIS Lumina and IVIS Spectrum-CT; PerkinElmer LifeSciences);

- PET with 2-deoxy-2-[^{18}F]fluoro-D-glucose ([^{18}F]FDG), 3'-deoxy-3'-[^{18}F]fluorothymidine ([^{18}F]FLT), and [^{18}F]fluoroazomycin-arabinofuranoside ([^{18}F]FAZA) to study glucose metabolism, cell proliferation and tumor hypoxia, respectively (n=6; YAP(S)-PET II; I.S.E. s.r.l.);

- 7T MRI (n=6, Pharmascan; Bruker Biospin).

Starting from cell implantation, BLI scans were performed weekly until the end of the protocol (30 days), while PET and MRI scans were carried out at intermediate (18-20 days) and late (28-30 days) time points

2.3 BLI and FLI studies

Briefly, for the detection of bioluminescence, mice were anesthetized with 4% chloral hydrate v/v (Sigma Aldrich) and then injected intraperitoneally (i.p.) with 150 mg/kg of luciferin (Beetle Luciferin Potassium Salt; Promega). After 20 minutes of biodistribution, mice were placed in the light-tight chamber and the photon emission was then acquired for 10 minutes. Images were analyzed and scaled after completion of all acquisitions, using appropriate computer software (Living Image Software; PerkinElmer LifeSciences). The same region of interest (ROI) was applied on all the bioluminescent tumors. Data were expressed as average radiance(photons/second/cm^2/steradian), which is a calibrated measurement of photon emission. This value was normalized to *in vitro* basal luciferase average radiance measured in both cell lines.

Animals were also acquired by 3D diffuse luminescence imaging tomography (DLIT), performed weekly using the IVIS Spectrum-CT, and by fluorescence imaging tomography (FLIT), performed only at the latest time point (30 days), after administration of the HypoxiSense680 fluorescent probe (PerkinElmer LifeSciences), a carbonic anhydrase IX (CAIX)-targeted fluorescent agent for *in vivo* imaging studies. Both acquisitions were supplemented with an integrated CT scan.

24 h before the acquisition, the animals were intravenously injected with the HypoxiSense680 probe (2 nmol in 100 µl of sterile PBS). The following day they were injected i.p. with 150 mg/kg of luciferin and, after biodistribution, submitted to DLIT and FLIT acquisition. Images were analyzed with Living Image® software (PerkinElmer LifeSciences) using volumetric ROI analysis. Data were expressed as average radiance for DLIT reconstruction and as radiance efficiency for FLIT.

2.4 MRI analysis

MRI was performed on a Bruker Pharmascan system equipped with a 7.0 T horizontal magnet. Scans were acquired at intermediate and later time points after intracranial cell injection.

Animals were anesthetized with gas (2% isofluorane), positioned prone on the animal bed and inserted into the radiofrequency coil (diameter of 38 mm) inside the magnet. Scout transverse and sagittal images were acquired to correct positioning of the ROI. Different MR sequences were used in order to optimize intracranial tumor visualization and contrast.

Anatomical two-dimensional multi-slice turbo spin echo sequences (RARE; field of view, FOV: 2.5x2.5 cm; matrix 256x256; 0.8-mm slice thickness; TR/TE: 4200/14 ms; TEeff: 42 ms; RARE factor: 8; 4 averages; acquisition time: 6' 43'') were run in both transverse and coronal orientations.

Diffusion MRI studies, able to detect necrotic regions in tumors, were performed in the axial orientation with a diffusion-weighted imaging-echo planar imaging (DWI-EPI) sequence [FOV: 2.5x2.5 cm; matrix 128x128; TR/TE: 3000/36 ms; 2 averages; 5A0, 3 directions, 3 b values per direction (b=400, 1100, 1800s/mm2; δ= 7 ms, Δ= 16 ms; acquisition time: 2’48”)].

2.5 PET analysis

After MRI scanning, mice were also evaluated using a YAP-(S)-PET II small-animal scanner with [^{18}F]FDG, [^{18}F]FLT, and [^{18}F]FAZA on consecutive days at intermediate and later time points. [^{18}F]FDG, [^{18}F]FLT and [^{18}F]FAZA were prepared in the same facility for clinical use as indicated in the European Pharmacopeia, VII ed. All the radiopharmaceuticals injected had a radiochemical purity greater than 99%. Animals in fasting condition were injected in a tail vein with 4.41±0.22 MBq of [^{18}F]FDG, 4.28±0.24 MBq of [^{18}F]FLT and 5.72±0.31 MBq of [^{18}F]FAZA. Under light anesthesia with ether, the mice were positioned prone on the tomograph bed with the head centered in the tomograph FOV. The animals were positioned using a special polystyrene support in order to allow co-registration of the images obtained with the three radiotracers. Dynamic acquisitions with [^{18}F]FDG and [^{18}F]FLT started 60 minutes after injection and lasted 30 minutes (6 scans of 5 minutes each), whereas scans with [^{18}F]FAZA started 120 minutes after injection and lasted 15 minutes (3 scans of 5 minutes each). Throughout the scans the animals were kept under gas anesthesia with 2% isoflurane.

PET images were acquired in three-dimensional mode and reconstructed using the expectation-maximization algorithm. All the images were calibrated with a dedicated phantom, corrected for the isotope half-life, and then quantified with PMOD 2.7 software (Zurich, Switzerland). The radiotracer uptake of tumoral and background regions was measured using ROI analysis, as follows: circular ROIs were drawn on the whole tumor mass using the automatic isocontour tool of the PMOD software. Background regions were defined by manually drawing circular ROIs on three

consecutive transaxial slices on a contralateral control region (volume of ROIs: 0.5±0.1 mm^3) for [^{18}F]FDG and on the cerebellum for [^{18}F]FAZA and [^{18}F]FLT (volume of ROIs: 9.7±2.9 mm^3). Radioactivity concentration was calculated as maximum standardized uptake value (SUV_{max}) correcting for injected dose and animal weight, according to the formula: SUV = (region of radioactivity/injected radioactivity)*animal weight. Uptake data were also calculated as tumor-to-background ratio (T/B) dividing the SUV_{max} of the tumor by the SUV_{mean} of the background region. PET images were shown as SUV images after correcting for injected activity and for body weight of animals.

2.6 Immunohistochemistry (IHC)

Following the last acquisition (at 30 days), the animals were sacrificed and their brains were collected, fixed in 10% neutral buffered formalin (Sigma Aldrich) and paraffin-embedded after dehydration with increasing concentrations of ethanol (75%, 85%, 95%, 100% 9 min each) and xylene rinse.

Longitudinal sections (3-4 μm) were cut and stained with hematoxylin and eosin (H&E) for the morphological evaluation. The deparaffinized sections were immunohistochemically assessed using the Genomix i-6000 automated staining system (BioGenex). Heat-induced antigen unmasking was performed using either EDTA (0.05 M, pH8) or citrate (0.01 M pH6) solutions in a thermostatic bath for 35 minutes. After cooling, slides were washed in buffer and then incubated for 1h at RT with the following antibodies: monoclonal anti-HIF-1α antibody (clone 54, dilution 1:200 in EDTA. BD Transduction Laboratories, San Diego, CA); monoclonal anti-CAIX antibody (ab15086, dilution 1:6000 1h in citrate pH6. Abcam); monoclonal mouse anti-human Ki-67 antigen (clone MIB-1, dilution 1:100 in citrate, Dako); anti-firefly luciferase antibody (ab498, Abcam). Reactions were revealed using the Novolink Max polymer detection system (Leica Biosystems), in accordance with the kit manufacturer's instructions, with the polymer for 30 minutes and with DAB for 8 minutes.

2.7 In vivo imaging after temozolomide treatment

The antitumor effects of temozolomide treatment was analyzed in animals bearing U251-HRE-mCherry tumours (n=5) respect to a control group (n=5). Experiments were repeated twice.

The orthotopic model was obtained by the injection of 1x10^5 U251-HRE-mCherry in 2μl of PBS into 7-8-week-old female nude mice (Harlan Laboratories) at day 0, with same procedure described previously. Briefly, in acute regimen TMZ was administered once by oral gavages at the dose of 400mg/Kg at the day 21 after cell injection, whereas for chronic regimen TMZ was administered four times (single dose of 100mg/kg) on alternate days. Accordingly with tumour

bioluminescent signal increase, demonstrating lesion establishment, TMZ treatment began at 21 days after cells injection.

Before and after treatment mice were analyzed by BLI and FLI scan and monitored for the following days until the sacrifice. In addition, HypoxiSense680 and IntegriSense750 fluorescent (PerkinElmer) probe were injected i.v. at day 30 after injection, to in order study CAIX and α3vβ3 integrine expression. Moreover, at day 20 (pre-TMZ administration), at day 23 (intermediate time point) and at day 28 (post-TMZ treatment), [^{18}F]FLT PET scan on control and treated mice were performed, with the same procedure described previously in the longitudinal study. The animals weight was registered every day.

2.8 Statistical analysis

Both *in vitro* and *in vivo* experiments were repeated at least twice giving reproducible results. For *in vivo* analysis, 25 animals for BLI longitudinal analyses, 12 animals for PET and MR imaging and 10 animals for TMZ treatments were considered. Data are presented as mean values ± standard deviation. Statistical analysis was performed using Prism 4 (GraphPad Software Inc., San Diego, CA, USA); one-way ANOVA (non-parametric) was performed, followed by Dunnett's multiple comparison test.

RESULTS AND DISCUSSION

In this study, the GBM U251-HRE cell line properly engineered to express Luciferase reporter gene under control of the HRE sequences has been used. In this cell model, luciferase activity was used as a HIF-1α activity biomarker and, since HIF-1α is the main driver of molecular events induced by hypoxia, in this model luciferase activity has been used also as an indirect hypoxia biomarker.
Firstly, the dependence of luciferase reporter gene expression from HIF-1α activity was demonstrated *in vitro* and *in vivo* by BLI and FLI. In detail, the U251-HRE cell line was characterized *in vitro and in vivo* in relation to the U251-pGL3 control cell line, in term of tumor growth, hypoxia establishment and HIF-1α activity. Subsequently, in order to validate optical imaging technique, preclinical imaging procedures potentially transferable to the clinical setting were used. In particular, *in vivo* studies with MRI and PET imaging were performed.

1. IN VITRO CHARACTERIZATION OF LUCIFERASE ACTIVITY IN RELATION TO HIF-1α MODULATION

In vitro studies were performed both after HIF-1α induction and after pharmacological modulation using two engineered cell lines (chosen as the simplest model for studying HIF-1α activity in GBM): U251-HRE cells, expressing the luciferase reporter gene under the control of the HRE sequences, and U251-pGL3 cells, constitutively expressing the luciferase reporter gene as control [28-137].

1.1 DFX MODULATION OF LUCIFERASE ACTIVITY

To understand the different luciferase expression profile in the two cellular models, luciferase activity was assessed *in vitro* in cell lysates, before and after treatment with the hypoxia mimetic DFX. In particularly, the aim was firstly to investigate the different luciferase response to DFX action and, secondly, to characterize DFX influence on HIF-1α stabilization and on luciferase reporter gene expression in both models. So, the cells were treated with DFX 100μM for 30 min, 1h, 3h and 6h and, at the end of the treatment, Luciferase activity was measured by biochemical assay.
Our results showed that only U251-HRE cells expressed the luciferase reporter gene in relation to the DFX-mediated HIF-1α nuclear accumulation. In detail, the luciferase activity was seen to increase after DFX treatment in U251-HRE cells, showing low luminescent signal at 30 minutes and 1 hour after treatment and, in contrast, an increasing signal between 3 and 6 hours after treatment. Conversely, luciferase activity did not change in U251-pGL3 cells after treatment with DFX, at each time point **(Fig.17)** confirming that in this cell line the hypoxia mimetic treatment did not modulate luciferase profile. So, our preliminary data suggested how, in U251-HRE model,

Luciferase activity can be used to indirectly detect HIF-1α activity also as hypoxia biomarker. On the other hand, U251-pGL3 model can be used as control cell model since Luciferase expression is constitutive and completely independent upon HIF-1α transcriptional activity.

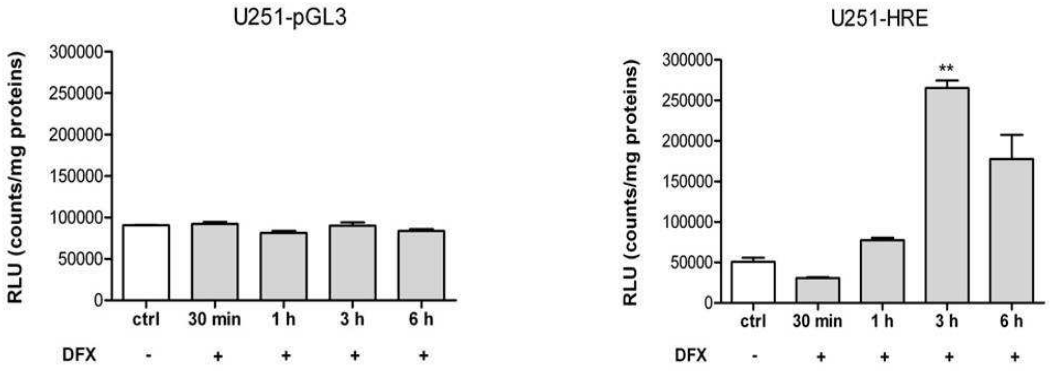

Fig. 17: *In vitro evaluation of luciferase activity in relation to DFX treatment in U251-pGL3 and U251-HRE cell models. All experiments were performed at 30 min, 1h, 3h and 6h after treatment. The control samples were comprised of untreated cells. Data are expressed as RLU (luciferase counts normalized to the amount of proteins quantified by Bradford assay). Data are the mean ± SE of three independent experiments. A p value ≤ 0.01 (**) was considered highly significant: DFX 3h vs control p≤ 0.01 (**).*

Rapisarda *et al*. [28-137]. have already demonstrated that U251-HRE cells show low but detectable levels of luciferase activity in normoxic condition and that these levels increase under hypoxic conditions. On the contrary, U251-pGL3 cells express the same level of luciferase both in normoxic and hypoxic conditions. In accordance with Rapisarda results [28], we confirmed that, after hypoxia mimetic treatment, luciferase activity in U251-pGL3 cells was independent from HIF-1α modulation, in agreement with the presence of a constitutive promoter driving luciferase reporter gene expression. On the other hand**,** in U251-HRE cells a modulation of luciferase activity was observed over time after DFX-mediated induction of the HRE promoter, likely due to the HIF-1α stabilization and nuclear translocation. In detail, a peak of activity was detectable 3h after DFX treatment, followed by a moderate decrease at 6h. In our opinion, this moderate reduction of luciferase activity at 6h after DFX treatment could probably be due to transcription-dependent feedback regulation [139-140]. Indeed, Stiehl *et al* [141] have already demonstrated that HIF-1α mRNA can induce a negative feedback mechanism, decreasing HIF-1α stability, and this

phenomenon was also observed when cells were chronically exposed to hypoxic conditions. In addition, Mottet *et al* [142] suggested, on the basis of *in vitro* studies, that in the presence of prolonged hypoxia the PI3K/Akt pathway activity is reduced, influencing the regulation of glycogen synthase kinase 3 beta (GSK3β) activity on HIF1α. Indeed, reduction of Akt activity reduces the quantity of the regulatory form of GSK3β phosphorylated on Ser-9, and allows the Tyr-216 phosphorylated form of GSK3β, already present in the cell, to reduce the stabilization of HIF-1α and thus its transcriptional activity. Although this process can be observed from 6h after HIF-1α induction, it is stronger at later time points (16h). The data herein reported show that DFX-mediated HIF-1α induction is time-dependent [139,143] and suggest that the greatest effect of HIF-1α is detectable between 3 and 6h after treatment, in line with its transcriptional activity.
Proliferation assay (MTT) confirmed the absence of detectable differences between the two cell lines in terms of DFX toxicity and influence on cell proliferation (data not shown), confirming that the modulation of HIF-1α activity is actually due only to DFX effect.

1.2 NUCLEAR DETECTION OF HIF-1α

Luciferase biochemical assay showed the DFX-mediated modulation of the reporter gene after hypoxia simulation. To understand the influence of hypoxia mimetic treatment on HIF-1α activity, we firstly tested HIF-1α nuclear accumulation after DFX treatment. In detail, both cell lines were incubated with DFX 100 μM and they were analyzed through ICC with HIF-1α-specific antibody. **Fig.18** showed no differences in translocation kinetics between the two cell lines, confirming a peak of nuclear translocation at 3h after DFX treatment and however an high nuclear HIF-1α presence until 6 hours after treatment.

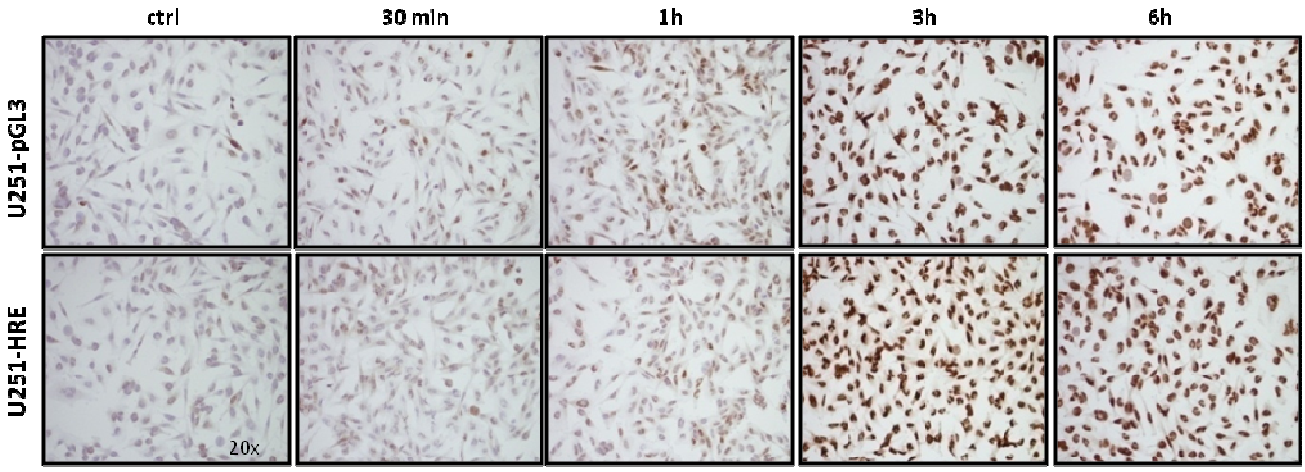

Fig. 18: *ICC for HIF-1α both in U251-pGL3 and in U251-HRE cells, performed after DFX treatment. The cells were analyzed by optical microscopy at 20X original magnification*

These data reflects how the HIF-1α modulation, due to the DFX treatment, is comparable in both cell lines, even if in U251-pGL3 cells Luciferase activity does not change after DFX treatment since its expression is driven by a constitutive promoter, while, in U251-HRE cells, luciferase activity is strongly related to HIF-1α activity, since its expression is driven by a HRE-containing promoter. So, in U251-HRE cells, it can be affirmed that luciferase profile is tightly correlated with HIF-1α transcriptional activity.

Moreover, this last result was also confirmed by a quantitative assay of HIF-1α in nuclear extracts performed in U251-HRE cells. The ELISA-based kit, presenting a specific affinity to HRE sequences, showed that HIF-1α translocates into the nucleus after DFX treatment **(Fig.19)** with the same kinetics already observed in ICC, with a significant increase at 3 hours after treatment, confirming also the luciferase biochemical results. In summary, these results allow to estimate the HIF-1α time course activity and the relative peak between 3 and 6 hours, while after that, the regulatory feedback starts influencing HIF-1α degradation and the relative detectable activity.

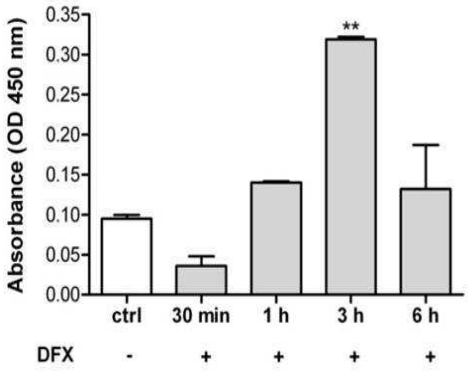

Fig. 19: *Nuclear quantification of HIF-1α using an ELISA-based kit in U251-HRE cells after DFX treatment. Data are expressed as absorbance at 450 nm. Data are the mean ± SE of three independent experiments. DFX 3h vs ctrl **p<0.01.*

1.3 EFFECTS OF LY294002 AND FM19G11 ON LUCIFERASE ACTIVITY

Our results suggested that only in U251-HRE cells, DFX can modulate HIF-1α-mediated Luciferase expression. To investigate in depth hypoxia process and HIF-1α related activity, *in vitro* experiments were performed only in this cellular model with different modulators of molecular pathways regulating HIF-1α activity.

To establish whether luciferase activity can also be modulated by other intracellular pathways influencing HIF-1α activity but different from hypoxia induction, a pharmacological modulation with a PI3K inhibitor (LY294002) or a HIF-1α inhibitor (FM19G11) were performed in U251-HRE cells. There are, in fact, evidences in the literature suggesting that the PI3K/Akt signal transduction pathway plays an important role in hypoxia-induced stabilization of HIF-1α [65,76-79] and could therefore be extremely important as a potential therapeutic target in several tumor types. The effects of PI3K inhibitor (LY294002) and HIF-1α inhibitor (FM19G11), in living and lysated cells, were investigated on the basis of the pathway reconstructed **in Fig.20** [140].

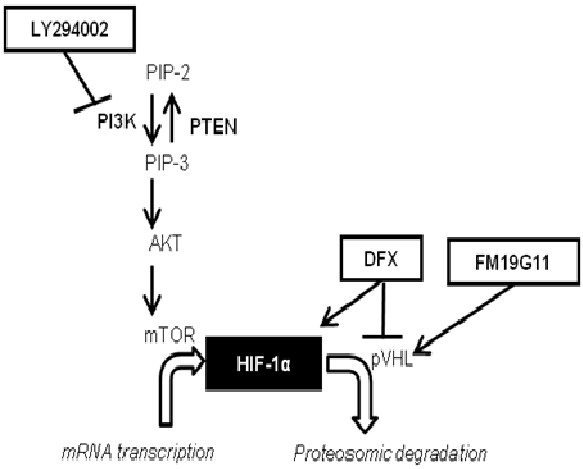

Fig. 20: *Schematic representation of the PI3K/Akt pathway and treatment targets.*

Briefly, LY294002 selectively inhibits PI3K, by blocking therefore Akt pathway and consequently HIF-1α activity, whereas FM19G11 directly represses HIF-1α accumulation by blocking VHL, necessary to promote preoteasomal degradation, and reducing significantly p300, a histone acetyltransferase required as a co-factor for HIF-transcription activation [144].

Figures 21a and **b** show luciferase activity, as a result, of the transcriptional effect mediated by HIF-1α, after treatments with LY294002 and FM19G11, respectively.

a)

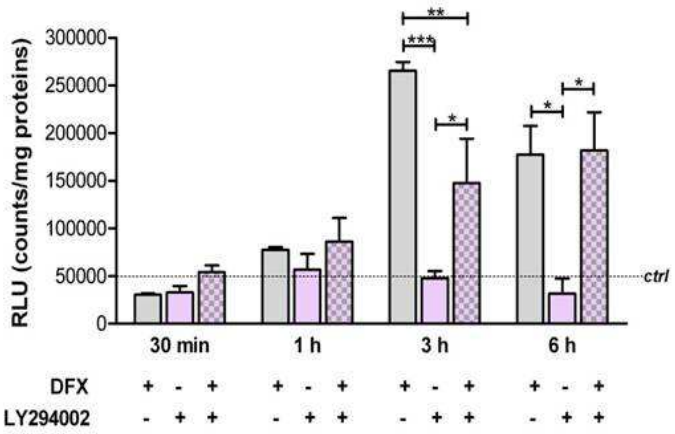

b)

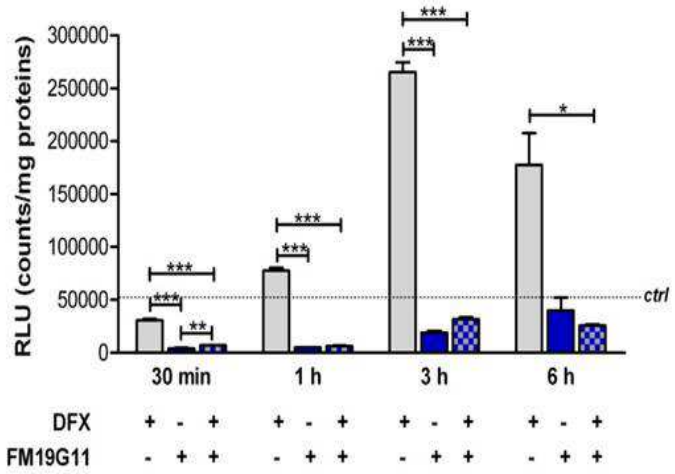

Fig. 21: **a)** *U251-HRE cells underwent both single and double treatments with DFX (100 μM) and/or LY294002 (50 mM), for analysis at the time points previously mentioned. The dashed line indicates luciferase activity in untreated cells (ctrl). Data are expressed as RLU. Data are the mean ± SE of three independent experiments. *p<0.05, **p<0.01, ***p<0.001*. ***b)*** *U251-HRE cells underwent both single and double treatments with DFX (100 μM) and/or FM19G11 (1 μM). The cells were analyzed as previously described. Data are the mean ± SE of three independent experiments.*

We observed that LY294002 treatment had no relevant influence at the early time points (30min and 1h), whereas at 3h, in the presence of DFX, LY294002 treatment was found to counteract hypoxia-mimetic mediated luciferase induction. Indeed, cells concomitantly treated with DFX and the inhibitor, compared with those treated with DFX alone, showed a reduction in luciferase activity. We hypothesize that, in the presence of DFX, LY294002 treatment, was able to reduce Akt-mediated HIF-1α stabilization and thus to produce a decrease in luciferase activity as can be seen at 3h after treatment. On the other hand, at 6h, both treatments (DFX alone and the double treatment) produced comparable luciferase activities. This might be explained by the difference in the timing of the triggering of the negative transcription-dependent pathway in the two different treatments, which depends on the HIF-1α mRNA level, found to be very high at 3h after treatment with DFX alone [139,143].

On the other hand, FM19G11-mediated inhibition completely abolished DFX-mediated luciferase induction, even in the presence of DFX. Indeed, at each time point after FM19G11 treatment, the luciferase expression was strongly reduced both in single and even in the co-treatment FM19G11-DFX. Even though DFX promotes HIF-1α accumulation in the nucleus, FM19G11 completely abrogate its activity, drastically abolishing DFX-mediated luciferase induction. Once more, these

data confirm the relationship between HIF-1α accumulation and luciferase activity. All these results were also obtained by CCD camera imaging of luciferase activity in living cells (**Fig.22**).

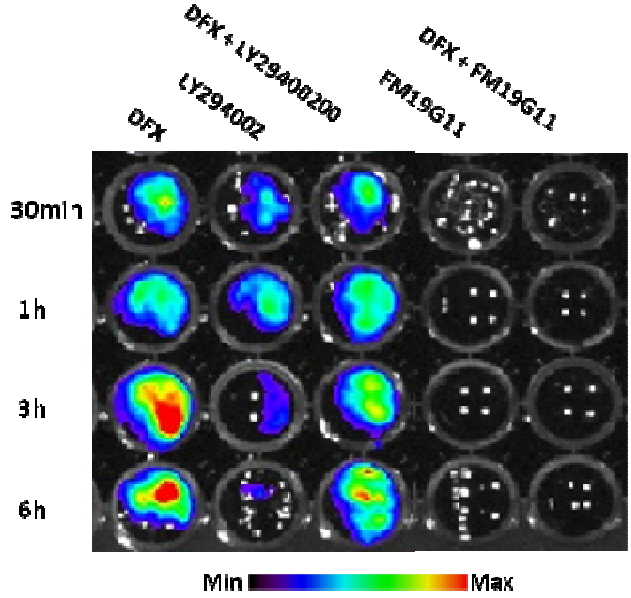

Fig. 22: *Luciferase activity was analyzed in living U251-HRE cells by CCD camera after treatments with DFX (100μM), LY294002 (50mM) and FM19G11 (1μM).*

Indeed, CCD analysis showed the same results visualized through the biochemical assay: as regards LY294002 treatment, only at 3 and 6 hours after co-treatment with DFX, the DFX presence induced the restoration of luciferase activity. On the contrary, FM19G11 treatment completely abrogated DFX effect on luciferase activation both in single and double treatment highlightening the importance of HIF-1α presence for luciferase induction in U251-HRE model and the importance of the degradation pathway on HIF-1α activity. Finally, these results demonstrated that also CCD camera instrument could be used to assess bioluminescence variation due to different treatments also in living cells **(Fig.22)**.

1.4 IN VITRO EVALUATION OF HIF-1α REGULATION BY DIFFERENT DRUGS

Since it was not possible to use LY294002 for *in vivo* experiments, to understand the role and the interaction of PI3K/AKT and RAS/MAPK/MEK pathways on HIF-1α regulation, we tested *in vitro* two different MEKs inhibitors (TRAMETINIB and PD98059), and a dual PI3K/mTOR kinase inhibitor (BEZ235), alone or in combination, to understand their efficacy on our glioma model for

their use also *in vivo* experiments. Since the aim of this study was to analyse HIF-1α activity after treatment, the *in vitro* set of experiments was performed only in the hypoxia responsive model: the U251-HRE cell line. To better understand the different drugs and targets, the **figure 23** summarizes molecular targets of the different drugs used in these experiments.

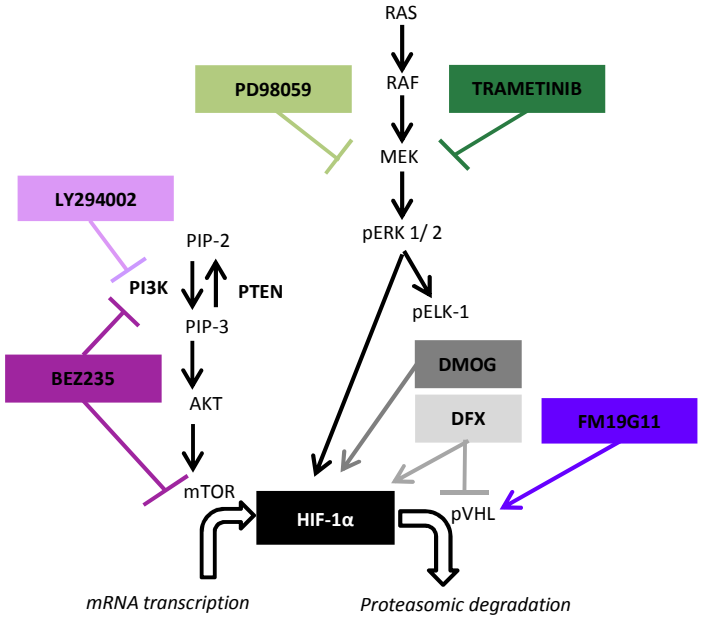

Fig 23: *Schematic representation of drug activity in PI3K/Akt and Ras pathways.*

As regards Ras/MEK/ERK pathway, this molecular pathway was investigated comparing the activity of two different MEK inhibitors such as Trametinib and, one of the first MEK1/2 selective inhibitors, PD98059 [88-89]. Results **(Fig.24a)** showed the higher action of Trametinib on HIF-1α activity, respect to the other one (PD98059) [90-91], in term of percentage of reduction of luciferase expression respect to control group (untreated cells). However MTT showed no cellular cytotoxicity after treatment suggesting that these single treatments were not sufficient to induce a reduction of proliferation **(Fig.24b)**.

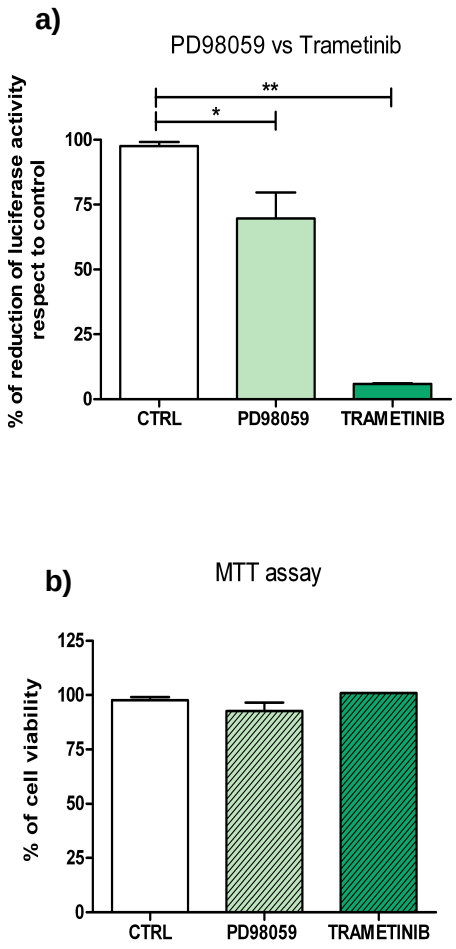

Fig. 24: ***a)*** *PD98059 (10μm) and Trametinib (10μM) treatments were performed on U251-HRE cells. Controls were represented by untreated cells. Results were calculated as RLU and expressed as percentage of fold reduction. Data are the mean ± SE of three independent experiments. PD98059 vs CTRL *p<0.05; Trametinib vs CTRL**p<0.01.*

b) *MTT assay performed in the same conditions of treatment. Data were represented as percentage of cell viability respect to control.*

Since Trametinib provided a stronger effect on HIF-1α mediated luciferase activity, it has been chosen as MEK inhibitor for further experiments. Indeed in the following set of experiments a comparison between Trametinib and the dual PI3K/mTOR kinase inhibitor, BEZ235, was performed.

Figures 25a and **b** showed results obtained after *in vitro* U251-HRE treatment with BEZ235 and Trametinib. As can be observed, both treatments strongly abrogated HIF-1α mediated luciferase activity, respect to untreated cells, in term of percentage of luciferase activity respect to control,

whereas the co-treatment BEZ235-TRAMETINIB completely abolished luciferase activity in U251-HRE cells, suggesting the addictive effect of the two different molecular pathways **(Fig.25a)**.

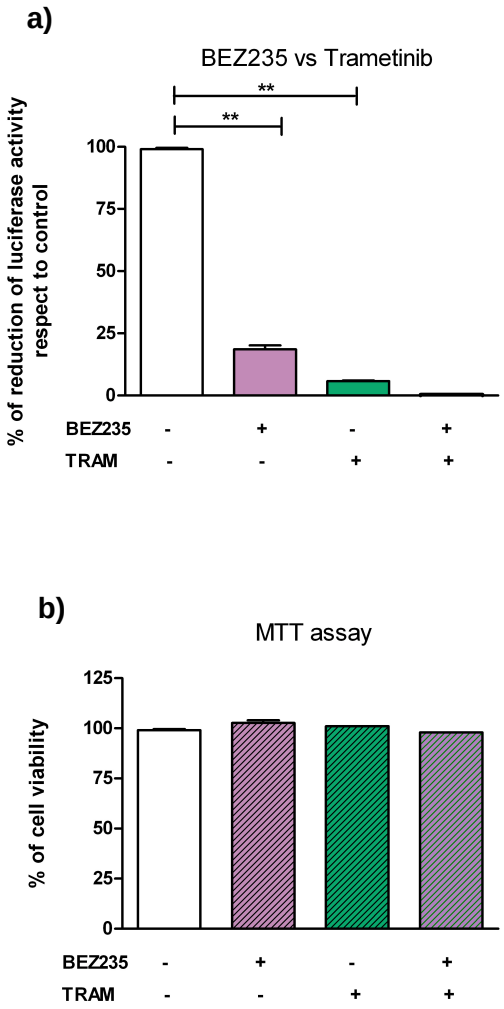

Fig. 25: **a)** *U251-HRE cells underwent single and co-treatment with BEZ235 (1μm) and Trametinib (10μm) Controls were represented by untreated cells. Results were calculated as RLU and expressed as percentage of fold reduction. Data are the mean ± SE of three independent experiments. BEZ235, Trametinib and co-treatment BEZ235-Trametinib vs CTRL **p<0.01*.
b) *MTT assay performed in the same conditions of treatment. Data were represented as percentage of cell viability respect to control*

Figure 25b showed that both the single and the co-treatment BEZ235-TRAMETINIB, did not resulted in a cell cytotoxicity as can be deduced by MTT assay, although HIF-1α mediated

luciferase activity was strongly reduced. Despite the absence of cell citotoxicity, these results suggested that both PI3K/Akt and MEK pathways have a strong influence on HIF-1α activity, as can be seen both in the single and in the co-treatment, highlightening the addictive action between the two molecular pathways, as showed by the co-treatment. In detail, Maira *et al* have demonstrated that the use of BEZ235 [144] induced a robust growth arrest in the G1 phase in U87 cell line with no apoptosis induction suggesting that the inhibition of the PI3K pathway per se is not sufficient to drive cells into apoptosis, at least in these cellular model. This result could be extremely relevant for therapeutic approaches directed to the reduction of hypoxia-mediated molecular events, with the objective to overcome resistance and tumor progression correlated with hypoxia. In detail, using both inhibitors to block the two pathways, it could be possible to completely abrogate HIF-1α activity and hypoxia-correlated pathways since both PI3K/Akt and MEK pathways are often up-regulated in several types of cancer [145].

Indeed, there are some evidences in literature, that suggest the crucial role of the MAPK family for the regulation of tumoral progression, in addition to hypoxia establishment [88-89]. Mutations/amplification or intrinsic mutations of key components of these signaling pathways may occur in cancer cells, which result in the elevated or constitutive activation of various growth factor receptors. Particularly, the Ras/MEK/ERK and PI3K/Akt pathways are often activated by different mutations [89], such as the upstream Ras mutation, occurring in over 20-30% of human cancers [64]. Since Ras/MEK/ERK and PI3K/Akt pathway activity are deeply involved in survival and proliferative pathways, their aberrant regulation can contribute to uncontrolled cell growth and lead to malignant transformation[145].

However the lack of a strong cytotoxicity and the deep reduction of HIF-1α activity after treatments, suggesting that these treatments could provide a better efficacy in combination with other drugs.

1.5 IN VITRO TMZ TREATMENT

Previous treatments have shown how different drugs can block different molecular pathways but producing a deep modulation of a single target. Now we tried to understand if a drug able to induce a significant cytotoxicity in glioma, could have any effect on HIF-1α activity. To this end, an anti-neoplastic drug widely used for glioma treatment was evaluated in U251-HRE cell model. To estimate drug efficacy in U251-HRE model, since responsiveness to TMZ depends on the methylation of MGMT promoter, involved in DNA reparation after TMZ-induced mutation [94-96], a pyrosequencing analysis was performed to describe the methylation profile of MGMT promoter in our tumor model. This test showed that MGMT promoter results to be sufficiently methylated to produce a silencing of the MGMT gene expression (data not shown**)** [94].In this view, TMZ treatment on this cellular line has been performed since this model showed a relative sensitivity to treatment.

Once confirmed U251-HRE sensitivity to TMZ treatment, acute and chronic TMZ regimen were tested. In the first one, the cells were treated with TMZ at the acute dose of 400 μM in a single dose, whereas in the chronic regimen cells were treated with a lower dose of 100 μM of TMZ repeated each day for a total of four doses. At the end of the treatment, the cells were lysated and analyzed for luciferase activity by luminometer to understand if TMZ treatment could modulate luciferase expression, at the same time cytotoxicity was tested through MTT assay in the same treatment conditions.

Results obtained by luminometer were shown in **figure 26**. As can be observed, both in the acute and in the chronic regimen, already 6 hours after TMZ addiction, a reduction of luciferase activity respect to control group was observe. Luciferase activity continued to decrease over time until 72 hours of treatment **(Fig.26 a.1- b.1)**. To avert that luciferase reduction was due to a decrease of growth, we compared luciferase biochemical assay with MTT assay. MTT assay **(Fig.26 a.3- b.3)** registered no cytotoxicity after 6 and 24 hours of treatment, whereas after 72 hours a relative cytotoxicity of the drug was registered (65%). This result was extremely important because showed that TMZ treatment influenced HIF-1α-mediated luciferase activity at least *in vitro* despite it did not influenced proliferation rate, as described by MTT. Indeed, HIF-1α mediated luciferase activity was reduced after treatments at each time points, even in acute and in chronic regimen, although cells remains viable, as confirmed by TMZ treatment and by MTT assay performed in the U251-pGL3 control cell line **(fig.26 a.2-a.4** and **b.2-b.4,** respectively**)**.

Summarizing, after TMZ treatment we observed an earlier HIF-1α reduction respect to the cytotoxic effect. For these reasons we supposed that HIF-1α activity could be used as early marker of therapeutic efficacy, but due to the manifold background of the anti-neoplastic treatment mediated events and HIF-1α activity regulation, this data have to be better investigated.

a)

1.

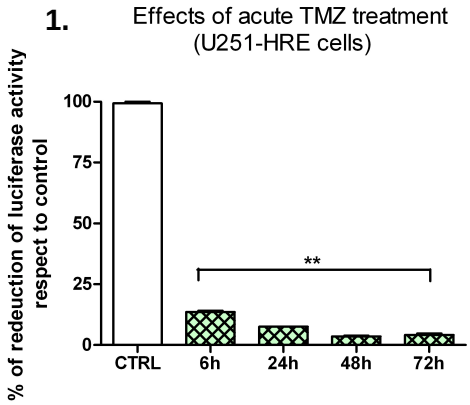
Effects of acute TMZ treatment
(U251-HRE cells)
% of redeuction of luciferase activity respect to control
100
75
50
25
0
**
CTRL
6h
24h
48h
72h

2.

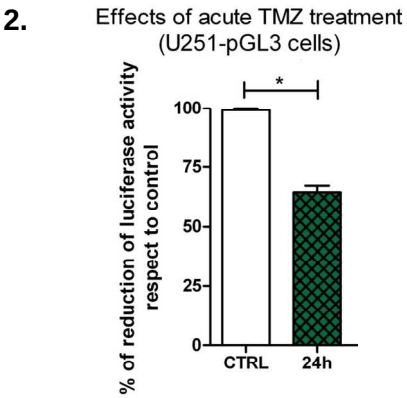
Effects of acute TMZ treatment
(U251-pGL3 cells)
% of reduction of luciferase activity respect to control
100
75
50
25
0
*
CTRL
24h

3.

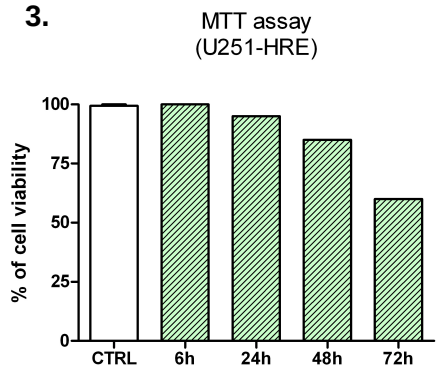
MTT assay
(U251-HRE)
% of cell viability
100
75
50
25
0
CTRL
6h
24h
48h
72h

4.

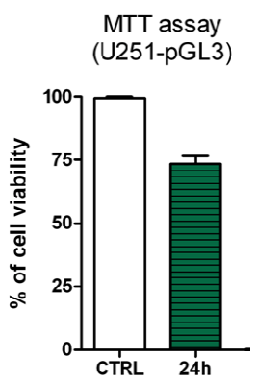
MTT assay
(U251-pGL3)
% of cell viability
100
75
50
25
0
CTRL
24h

b)

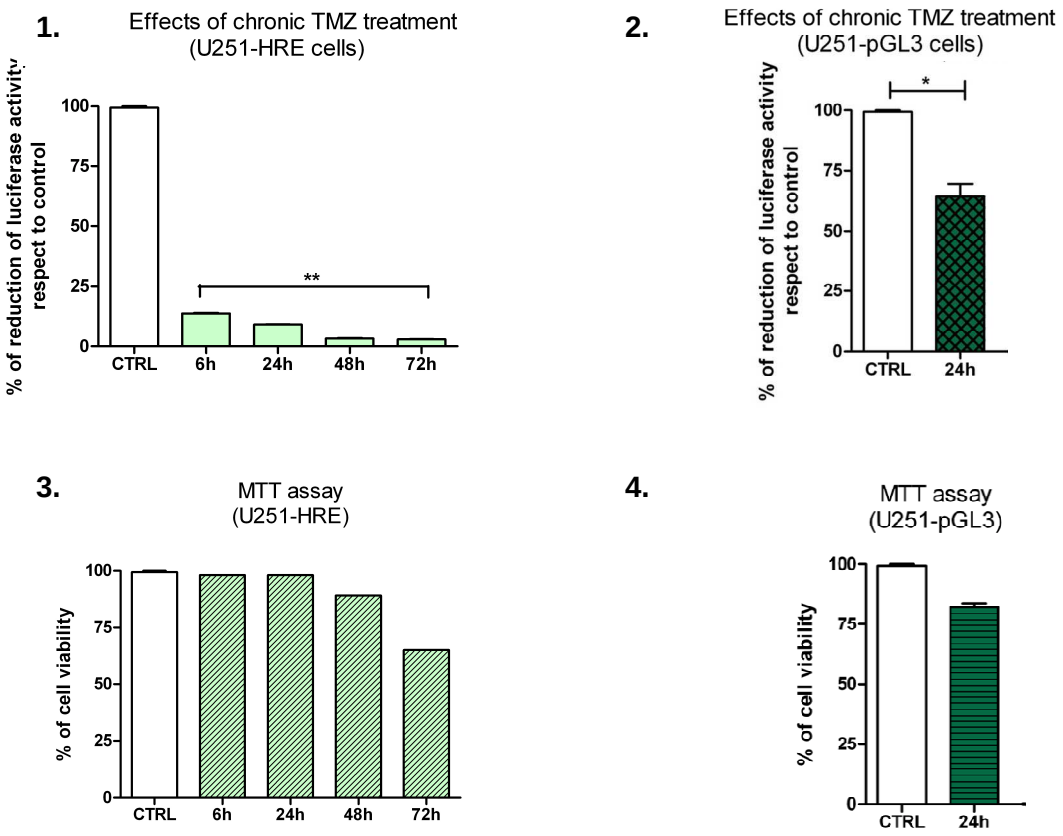

Fig. 26: a.1) *Acute (TMZ 400μM once) and* ***b.1)*** *chronic (TMZ 100μM administered four times) treatment regimens were tested on U251-HRE cells at different time points (6,24,48 and 72hours). On the right, acute* ***(a.2)*** *and chronic* ***(b.2)*** *TMZ administration on U251-pGL3 cells for 24h were showed, respectively. After treatment, cells were analyzed by luminometer. Data were expressed as percentage of luciferase activity reduction respect to untreated cells (CTRL). Data are the mean ± SE of three independent experiments. **p<0.01 U251-HRE treated cells vs control. *p<0.05 U251-pGL3 treated cells vs control*

Graphs below luciferase assay showed MTT assay performed after treatment on U251-HRE ***(a.3-b.3)*** *and U251-pGL3 cells (****a.4-b.4****), respectively. Data were expressed as percentage of cell viability respect to control.*

2. *IN VIVO* STUDY OF LUCIFERASE ACTIVITY IN RELATION TO INTRATUMORAL HYPOXIA

In vitro studies showed that luciferase activity reflects HIF-1α accumulation in U251-HRE model, whereas in U251-pGL3 cells this activity was not influenced from HIF-1α transcription activity. In this context, to investigate if the same reporter induction could be visualized also *in vivo*, we performed experiments in orthotopic murine models obtained using both U251-HRE and U251-pGL3 cells. The aim of these experiments was to compare the U251-HRE and U251-pGL3 models *in vivo* in a longitudinal study by optical imaging to assess luciferase activity modulation during tumor growth and in relation to HIF-1α activity, in particular during hypoxia establishment. Obtained data were, then, cross-validated with data obtained with different imaging modalities, such as PET and MRI, as described in **figure 27.**

2.1 BLI ANALYSIS

For BLI acquisition, each mouse was imaged once a week to monitor bioluminescence signal over time in order to understand the different luciferase behaviour in the two models. In orthotopic U251-pGL3 model, luciferase activity was found to be detectable immediately after injection and to progressively increase over time in relation to tumor growth, showing a linear trend for the entire period of observation. On the contrary, in U251-HRE orthotopic model, the luciferase activity linearity was not maintained to the late time point. Indeed, luciferase activity was very weak during the first days after cell injection, respect to U251-pGL3, whereas starting from day 18, luciferase activity showed a sudden increase, changing the slope of the expected linear progression **(Fig.28-29)**.

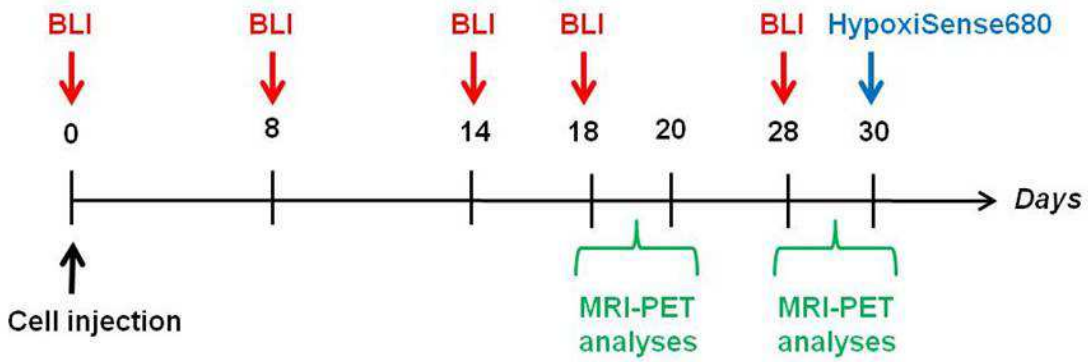

Fig. 27: *Time line of the study design: in red are described BLI analyses, performed once a week to monitor bioluminescence signal over time. In green are described MRI and PET analyses performed at intermediate time point (18-20 days) and at late time point (28-30 days). At day 30 after cell injection FLI scan with HypoxiSense probe (in blue) was performed.*

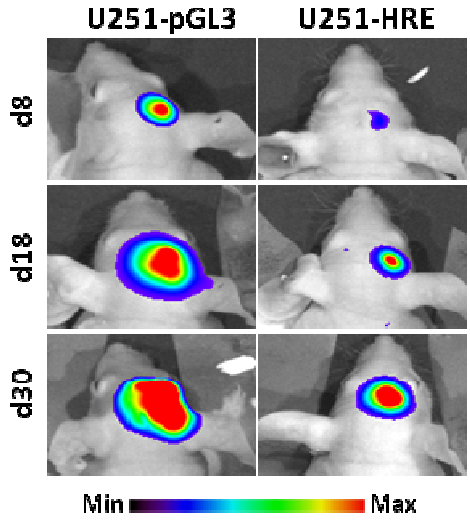

Fig. 28: 2D BLI images in U251-pGL3 and U251-HRE tumour models analyzed at 8, 18 and 30 days after cell injection. Images are presented with the same scale bar.

Analyzing these results it was hypothesized that the two cell lines had different luciferase linearity windows due to the different meaning of luciferase expression in the two cell lines. U251-pGL3 cells showed an increase of luciferase activity proportional to cell proliferation while U251-HRE cells showed a bi-modal trend of luciferase expression where from day 18 (that is after hypoxia establishment), luciferase basal activity was found to be enhanced due to hypoxia induced HIF-1α transcriptional activity **(Fig.28-29)**. In summary, also *in vivo* the different meaning of luciferase expression can be observed in these two cell lines: it was related to cell proliferation in U251-pGL3 cells and to HIF-1α activity in U251-HRE cells, suggesting that this latter model could be used for the *in vivo* study of HIF-1α mediated and hypoxia-related processes, and hypoxia-targeted treatments.

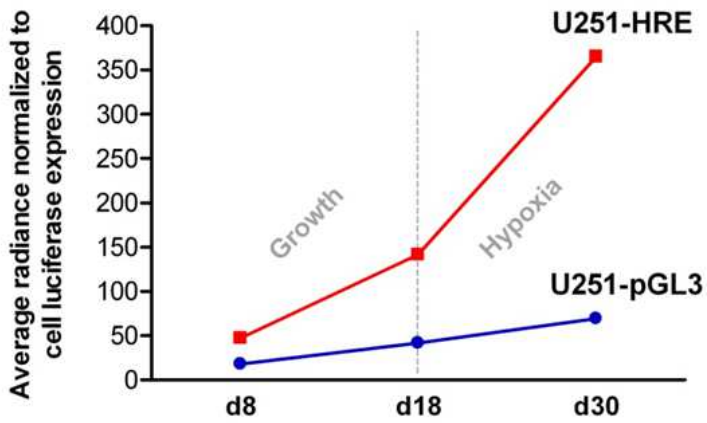

Fig. 29: *Graphical representation of luciferase activity over time in the two orthotopic models. ROIs were drawn on 2D images and the resulting luciferase activities, expressed as average radiance (p/s/cm^2/sr), were normalized to basal luciferase activity for each cell line*

The suitability of U251-HRE cells for long-term study of hypoxia has also been confirmed in literature [137,139]. In fact it has been demonstrated that U251-HRE cells are able to maintain stable hypoxia-mediated luciferase activity for long periods of time, making this model suitable for HIF-1α activity investigation.

Indeed, even though MRI showed slower growth kinetics in U251-HRE than in U251-pGL3-derived tumors (data not shown), in the U251-HRE models the trend line reporting the bioluminescent single quantification of luciferase activity over time showed a steep increase with respect to the linear signal observed in U251-pGL3 **(Fig.29)**, probably due to hypoxia establishment within the implanted tumor. In view of these findings and since the objective of this study was to investigate intratumoral hypoxia, subsequent studies were concentrated on U251-HRE cells.

2.2 FLI VALIDATION OF BLI RESULTS

BLI analyses suggested that the luciferase activity in U251-HRE was regulated by hypoxia establishment and mediated by HIF-1α activity. To demonstrate this hypothesis, hypoxia establishment was investigated also through FLI analysis by using in detail the accumulation of the hypoxia probe HypoxiSense to demonstrate the correlation between Luciferase signal and specific-probe accumulation (reporting hypoxia extent) in U251-HRE cells. Indeed, HypoxiSense, by binding selectively to CAIX, that is overexpressed in hypoxic tumor regions, provides specific information about regional tumor hypoxia.

After HypoxiSense biodistribution, mice were acquired for FLI (FLIT) and BLI (DLIT) using a 3D modality with a CCD camera with an integrated CT system. Volumetric region of interest (ROI) analysis of the DLIT images allowed tumor location and dimension to be determined (mean volume = 11.97mm^3 ± 3.1, depth = 2.3mm ± 0.1). The FLIT acquisition showed an extensive hypoxic area co-localizing with the bioluminescent signal (mean volume = 9.34mm^3 ± 2.8), confirming that in U251-HRE cells luciferase activity was able to report on hypoxia extent, since it is driven by HIF-1α activity **(Fig.30).**

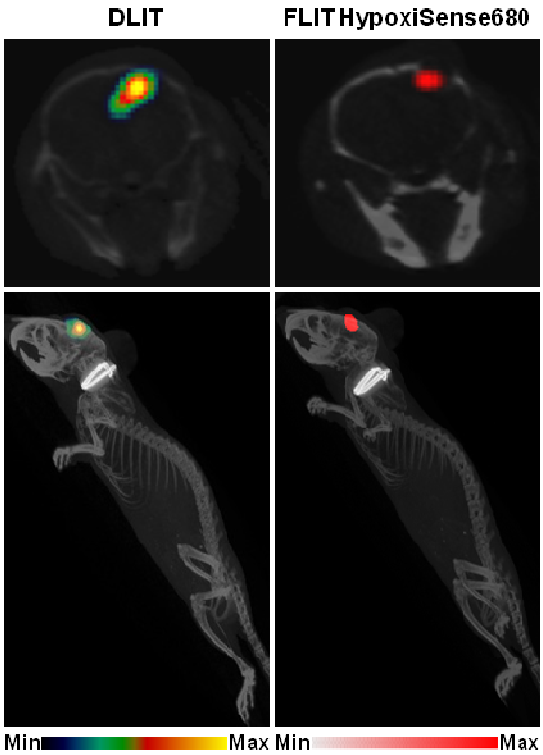

Fig. 30: *3D and axial comparison of luciferase activity and HypoxiSense680 fluorescent probe uptake in a representative U251-HRE orthotopic mouse model. Scans were performed at day 30*.

Summarizing, by using HypoxiSense fluorescence imaging and luciferase bioluminescence imaging technologies, it is possible to image and quantify tumor sub-regions undergoing hypoxia-related changes in a non-invasively manner. Moreover, we demonstrated that optical imaging, by using U251-HRE model, can provide a complete view of hypoxia establishment and progression in preclinical models.

2.3. IN VIVO STUDY OF TUMOR FEATURES BY MRI AND NUCLEAR-BASED IMAGING (PET)

Although the promising results obtained through optical imaging, actually this method does not yet have a role in human studies, so it is necessary to cross-validate optical imaging data with those obtained with MRI and PET, used routinely in the clinical practice.

In this context, MRI provided high-resolution images for assessing tumor localization and features (volume, perfusion, presence of necrotic areas). Particularly, 30 days after cell injection, anatomical and diffusion MRI were performed in the biggest tumors, revealing internal tumor necrosis, a structural modification subsequent to hypoxia establishment. On anatomical RARE images **(Fig.31)**, U251-HRE tumors were delineated from normal brain tissue as isointense or slightly hyperintense, poorly demarcated and irregularly rounded areas.

MRI diffusion experiments were performed to analyze the relative diffusion coefficient in necrotic and non-necrotic tumor regions. **Figure 31** shows some examples of color-coded diffusion maps (DWI-EPI) (1-3) and the corresponding anatomical RARE images (2-4). At 20 days very few areas of internal necrosis were found and diffusion maps appeared mostly homogeneous (1-2); at 30 days, the biggest tumors started showing internal necrotic regions, characterized by a higher diffusion coefficient (3-4).

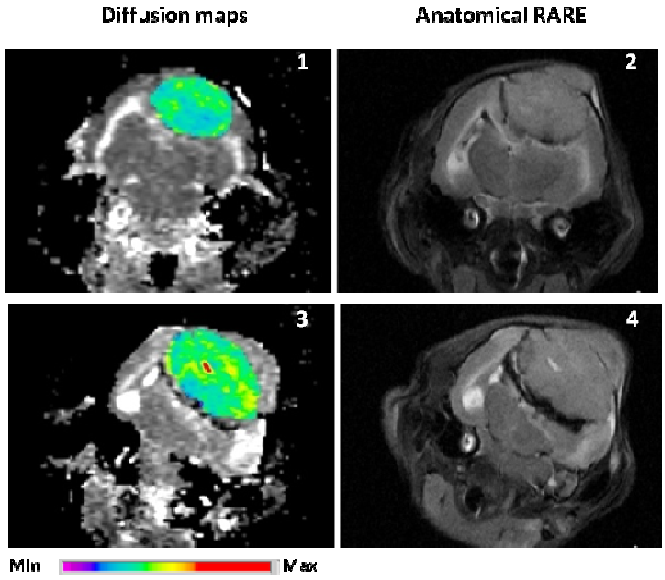

Fig. 31: *Color-coded MRI diffusion maps (1,3) with corresponding anatomical RARE images (2,4) at 20 (1,2) and 30 days (3,4): tumors are encircled by white dotted lines on RARE images. Higher diffusion coefficient values are depicted as yellow or red areas.*

To complete *in vivo* studies of U251-HRE models and to better characterize glucose metabolic profile, hypoxia and tumour growth three radiolabelled tracers were used for PET imaging studies at 18-20 and 28-30 days after cell implantation: [^{18}F]FDG for metabolic profile, [^{18}F]FAZA for tissue hypoxia and [^{18}F]FLT for cell proliferation .

[^{18}F]FDG PET studies revealed no significant increase in uptake either at intermediate (T/B = 1.27 ± 0.17) or at late time points (1.08 ± 0.06) **(Fig.32)**. On the contrary, U251-HRE animal models showed poorly hypoxic ([^{18}F]FAZA T/B = 1.01 ± 0.09) but highly proliferative tumors ([^{18}F]FLT T/B = 1.33 ± 0.14) on the intermediate PET studies (18-20 days). At 30 days after cell injection, tumours showed hypoxic areas as indicated by [^{18}F]FAZA uptake (T/B ratio: 1.38 ± 0.09) and the [^{18}F]FLT T/B ratio increased significantly to 2.38 ± 0.15 (a 1.78-fold increase, p = 0.003). In U251-HRE injected mice, [^{18}F]FAZA uptake within tumor lesions was detectable only in the acquisitions performed 30 days after cell injection **(Fig.33)**. The results were very similar to those obtained with FLI analysis, and therefore contributed to validate this cell model for the study of hypoxia establishment and progression also by PET.

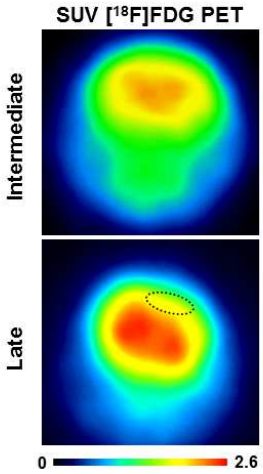

Fig. 32: *Glucose metabolism in U251-HRE animal models by PET. Representative images of [^{18}F]FDG uptake at intermediate and late time points in a U251-HRE mouse. Tumour uptake is the same as background. The tumour is delineated by white dotted lines.*

Unlike what was reported in rats using U251 cells [125], [^{18}F]FDG uptake was found to be close to normal brain tissue levels **(Fig.32)**. This difference may be due to the limited spatial resolution of YAP-(S)PET, used for PET experiments, in detecting mouse brain lesions using tracers that, similarly to [^{18}F]FDG, show high background uptake in the brain.

For what concerns hypoxia study, only at the late time point [^{18}F]FAZA PET uptake was detectable contrary to what was observed in bioluminescence hypoxia signal **(Fig.33)**[146]. This was due mainly to the different mechanism of action of optical and nuclear-based imaging. Indeed, the entrapping mechanism of [^{18}F]FAZA radiotracer is dependent by pO2 in the cellular microenvironment. In normoxic conditions, [^{18}F]FAZA diffuses along cell membrane, whereas only in hypoxia and when O_2 is not available, [^{18}F]FAZA is not re-oxidated and so remains accumulated into the cells. A different reasoning need to be done for bioluminescence, indeed its mechanism of hypoxia detection is based on HIF-1α binding to HRE sequences. Indeed, comparing bioluminescence and PET imaging, we could affirm that bioluminescence hypoxia signal was detected earlier than [^{18}F]FAZA, probably because it detected an earlier hypoxia event, that is HIF-1α nuclear accumulation and its transcription activity. [^{18}F]FAZA uptake, instead, was regulated by pO_2 intracellular level and by relative redox reaction, that probably constitutes a more late event in hypoxia establishment, since it depends only on intracellular pO2 [147].

Moreover, it is important to consider the different resolution of the two imaging techniques. Indeed, probably PET imaging had a lower resolution not sufficient to detect small regions of intratumoural hypoxia.

As regards [^{18}F]FLT uptake, since it reflects tumoural proliferation, showing a very low background signal, it was clearly detectable from the early time point and increased over time, as also demonstrated by *ex vivo* correlation with the Ki67 marker [148].

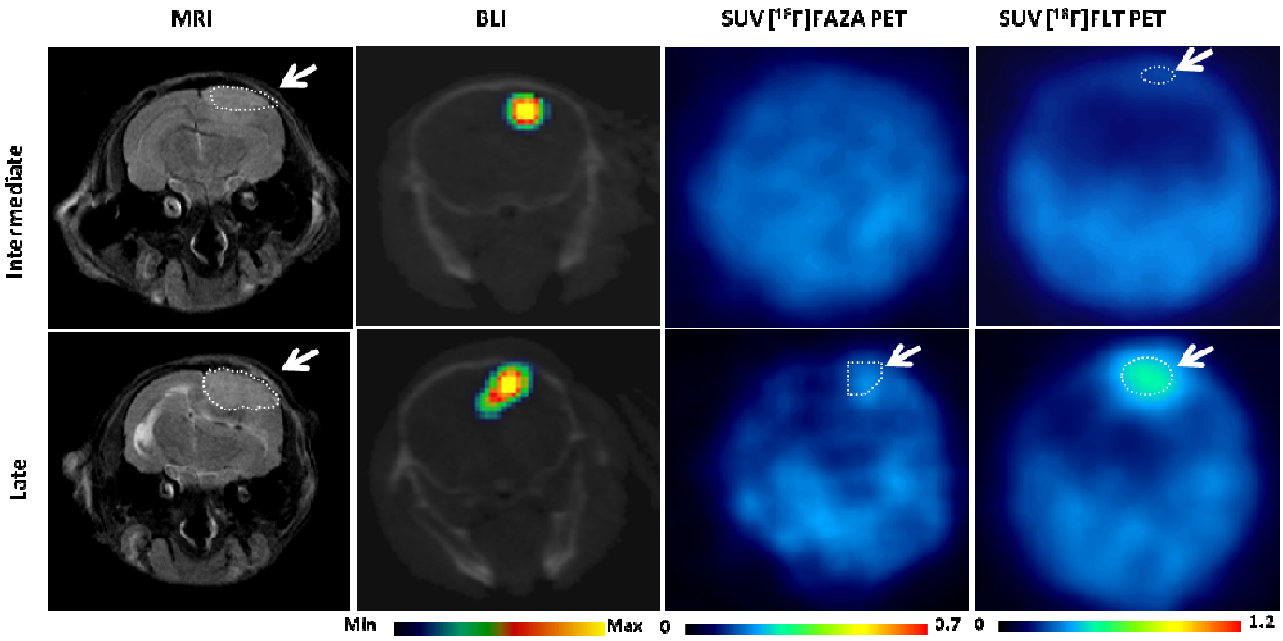

Fig. 33: *Representative axial MRI, BLI and PET images in U251-HRE animal models performed at intermediate (18-20 days) and late (28-30 days) time points. White arrows indicate tumors. Tumours are delineated by white dotted lines.*

3. EX VIVO VALIDATION

3.1. MORPHOLOGICAL AND IMMUNOHISTOCHEMICAL ANALYSES

After *in vitro* and *in vivo* model characterization, to validate GBM features and imaging data, morphological and immunohistochemical analyses (IHC) were performed on explanted brains. *Ex vivo* H&E staining showed distinctive features of high-grade glioma (i.e. GBM), namely, markedly hypercellular proliferation of spindle and/or fusiform cells, with atypical and pleomorphic nuclei, high mitotic activity, prominent microvascular proliferation, and necrosis. Moreover, the U251-HRE cells showed an infiltrative pattern of invasion into normal brain parenchyma, illustrating the aggressiveness of these tumor cells [53]**(Fig.34)**.

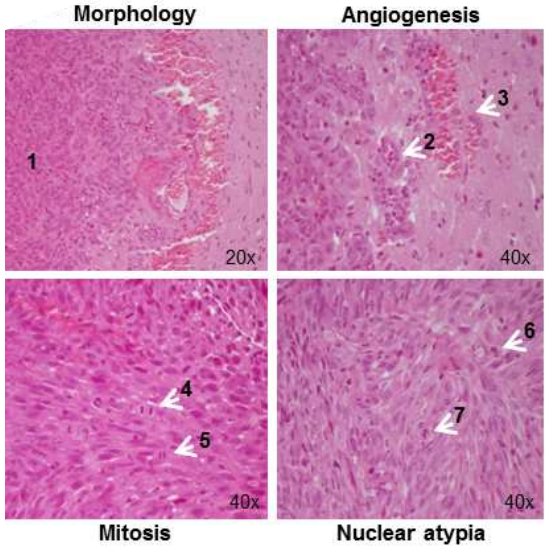

Fig. 34: *H&E staining and IHC validation on ex vivo brain sections. a Ex vivo H&E staining shows hypercellular neoplastic tissue (1), infiltrating the brain parenchyma. Tumors are characterized by "glomeruloid capillaries" (2) and prominent microvascular proliferation (3); brisk mitotic activity (4-5); nuclear atypia (6) and abnormal mitoses (7).*

IHC showed a strong positivity for hypoxia markers: nuclear HIF-1α and membrane carbonic anhydrase IX (CAIX) were observed, in keeping with the presence of hypoxia in the tumors. IHC showed a zonal pattern of HIF-1α and CAIX positive cells in U251-HRE cells, accordingly with the presence of hypoxia within the tumour: in fact HIF-1α and CAIX resulted differentially expressed at the micro-regional level, with a high level of the two hypoxia marker in deeper regions of the tumour respect to more superficial areas **(Fig.35)**. For what concerns the proliferation marker Ki67,

IHC staining before treatment was strongly positive, reflecting the high proliferation index of tumor lesions. Finally, IHC for luciferase expression supported the results of the *in vivo* bioluminescence analysis. Indeed, positive cytoplasmic staining of luciferase was found to co-localize with HIF-1α nuclear positivity in adjacent sections **(Fig.35)**.

These findings demonstrate *in vivo* imaging data as already reported. Indeed, Ki67 staining confirms the high proliferation index showed by [^{18}F]FLT PET, confirming the aggressiveness and infiltrative pattern of this kind of tumors [148]. For what concerns hypoxia establishment, hypoxia markers, such as HIF-1α and CAIX, confirm [^{18}F]FAZA PET results, underlying how hypoxia is a crucial features of GBM and how this feaature can be non-invasively studied by different imaging modalities.

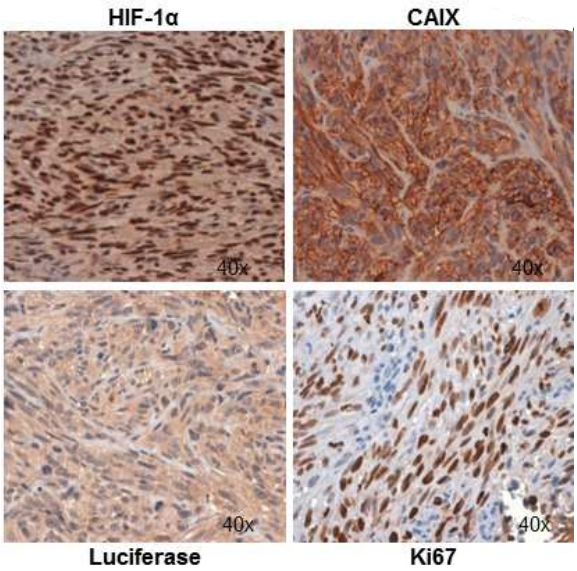

Fig. 35: *IHC staining for hypoxia markers (HIF-1α and CAIX), for proliferation marker (Ki67), and for luciferase expression.*

4. IN VIVO TEMOZOLOMIDE TREATMENT

Once evaluated *in vitro* the effect of TMZ treatments on HIF-1α activity and cell toxicity, TMZ action was assessed also *in vivo* in mice bearing U251-HRE-mCherry orthotopic tumours. Mice were treated with acute or chronic TMZ, starting at 21 days after cells injection (after tumour growth and hypoxia establishment) in accordance to what observed in longitudinal BLI experiments described previously. The aim was to analyze by BLI the TMZ effect on HIF-1α activity, in relation to cell viability assessed by FLI (m-Cherry expression). Once more, two different TMZ treatments were

used: an acute single administration (400mg/kg) and a chronic treatment (4 doses of 100mg/kg) as described in **figure 36**.

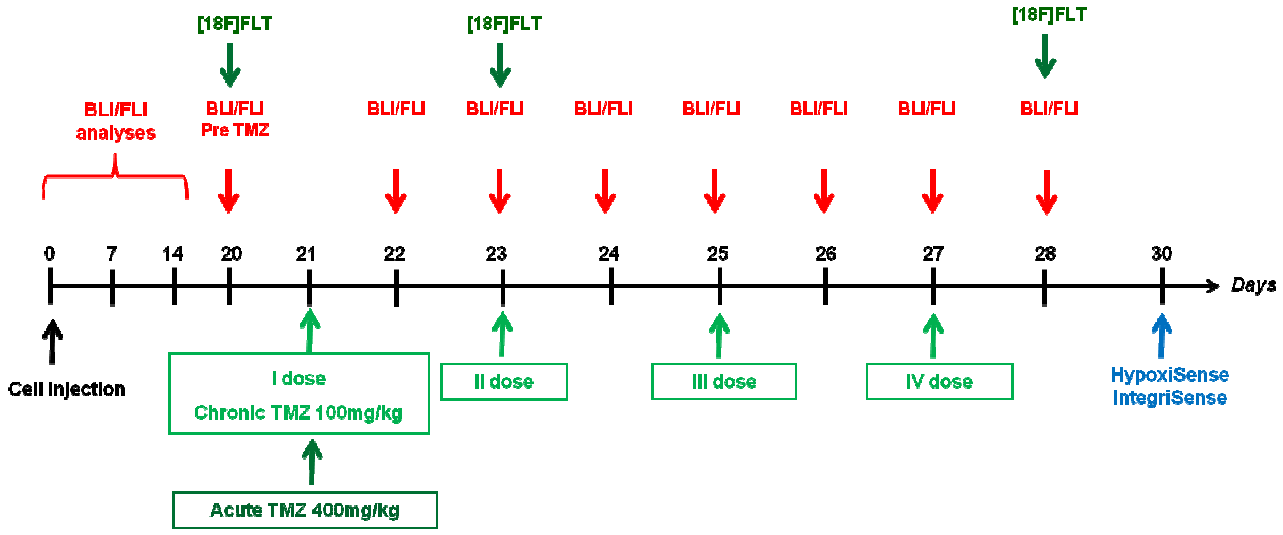

Fig. 36: *Time line describing the BLI and FLI acquisitions (red), [^{18}F]FLT PET (dark green)and HypoxiSense and IntegriSense (light blue) in relation to TMZ administration. In light and dark green chronic and acute TMZ administration were showed, respectively.*

Imaging data **(Fig.37a)** showed the bioluminescent and fluorescent signal at three different time points from cell injection: *1)* Pre-TMZ (day 20), *2)* 2 days after TMZ first administration (day 23) and *3)* 7 days after TMZ administration (day 28). Before TMZ administration, both the bioluminescent and the fluorescent signal were high, as expected because of the hypoxia establishment (HIF-1α transcription activity) and the high proliferation rate, respectively. Two days after TMZ treatment (at the end of acute treatment and after the first two doses of the chronic treatment), a significant reduction of the bioluminescence was observed, in particular as regards the acute treatment group, while m-Cherry fluorescence remained comparable to controls.

On the contrary, a week after the beginning of the TMZ treatment, corresponding also to the end of the chronic treatment schedule, in both regimens, a strong reduction of bioluminescent signal as well as of the fluorescent m-Cherry signal was observed in comparison to the controls. Bioluminescent and fluorescent signal quantification also demonstrated these observations

(Fig.37b). The different treatment scheduling and doses could account for the differences in bioluminescence reported for the two therapeutic regimens.

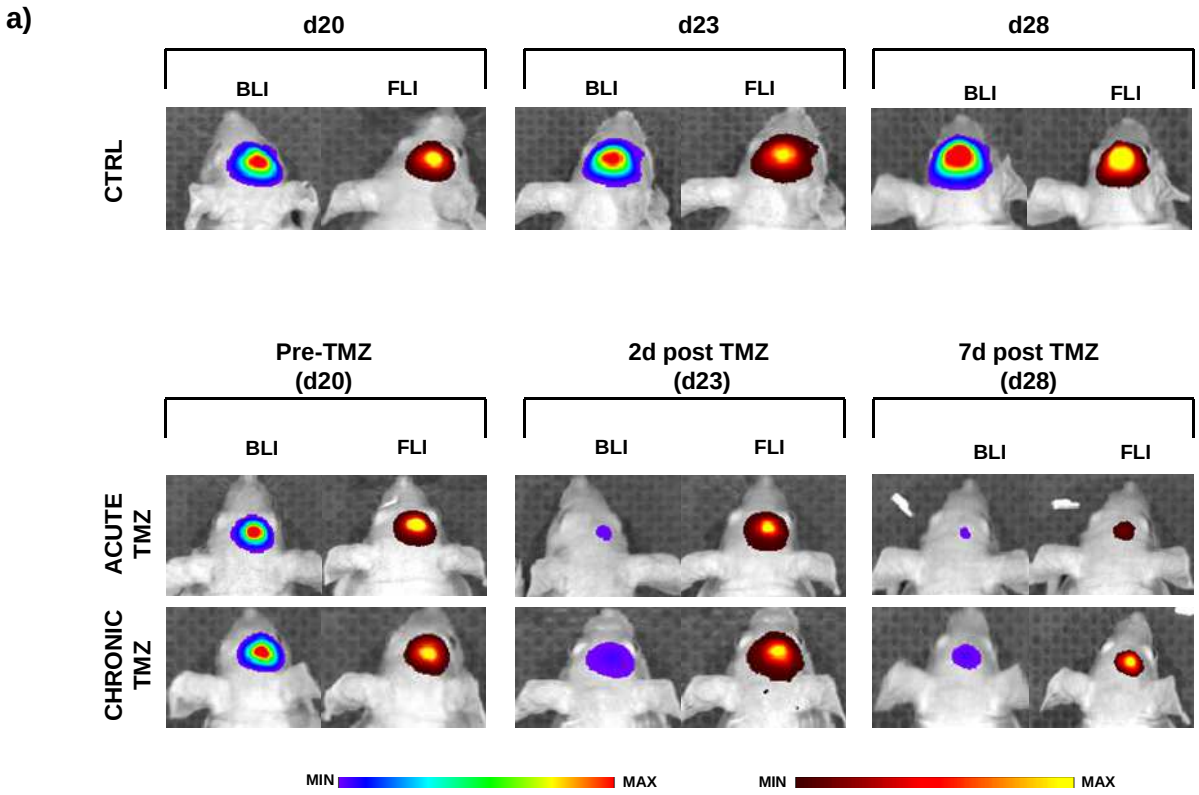

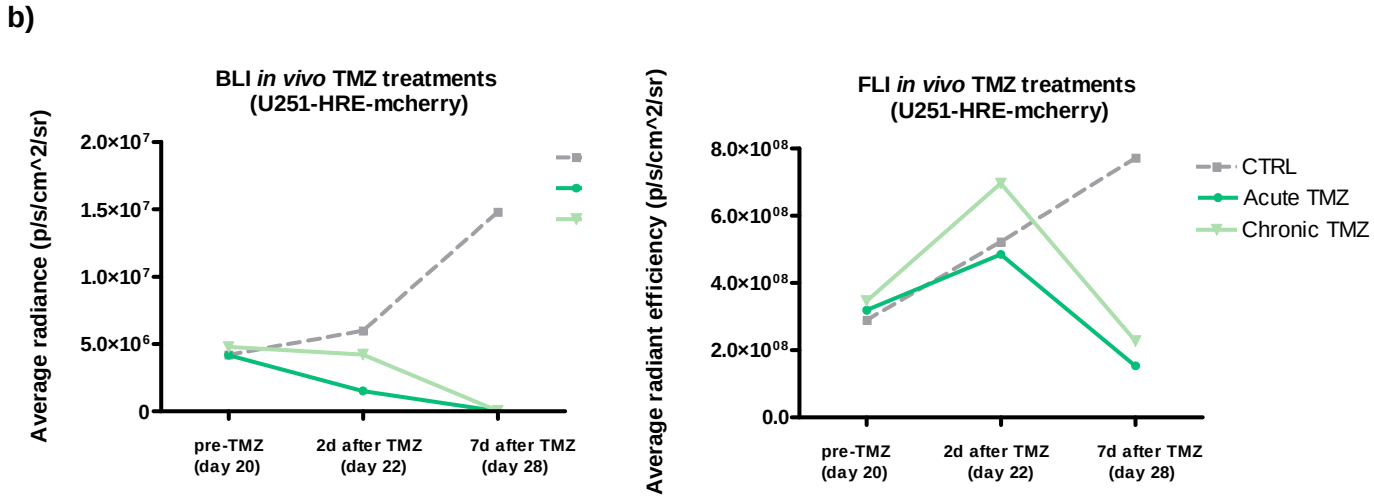

Fig. 37: a) *BLI (luciferase activity) and FLI (mCherry expression) in U251-HRE-mcherry tumour bearing mice non treated (first row), treated with acute TMZ regimen (second row) or with chronic TMZ regimen (third row). Images showed results obtained before treatment and two or seven days after TMZ administration. Images were represented with the same scale bar.* ***b)*** *Images quantification of luciferase and mCherry activity over time in a representative mouse for each group , treated with acute or chronic TMZ. ROIs were drawn on 2D images to obtain resulting luciferase activity, expressed as average radiance (p/s/cm^2/sr), and mCherry activity, expressed as average radiant efficiency (p/s/cm^2/sr).*

A PET study performed on the same animals at the same time points reported in the **figure 38**, showed that tumor proliferation was not reduced until mCherry signal started decreasing, corroborating our hypothesis about the role of HIF-1α activity as early biomarker of tumor response to TMZ treatment.

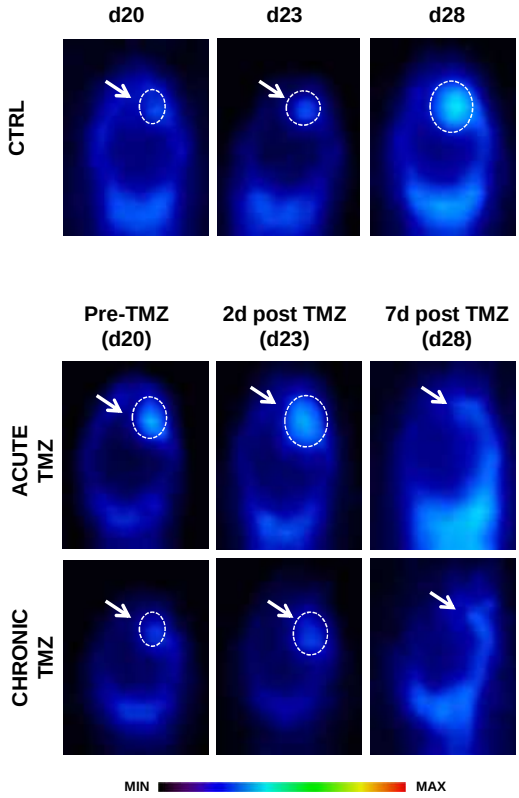

Fig. 38: *Images showed three representative mice injected with [^{18}F]FLT proliferation radiotracer before and 2days and 7 days after TMZ treatment. A control and two treated mice were showed. Images were showed with the same scale bar.*

At the end of all treatments, mice underwent also a scan with two different fluorescent probes **(Fig.39)**: HypoxiSense and IntegriSense to assess hypoxia extent and tumour angiogenesis, respectively. In both acutely and chronically treated mice, fluorescence analysis showed only a modest HypoxiSense uptake, respect to controls, indicating the presence of only limited intratumoral hypoxic areas in treated-mice. At the same time, also IntegriSense showed a low accumulation in treated mice respect to controls, indicating a reduction of tumour angiogenesis following both acute and chronic treatment regimens.

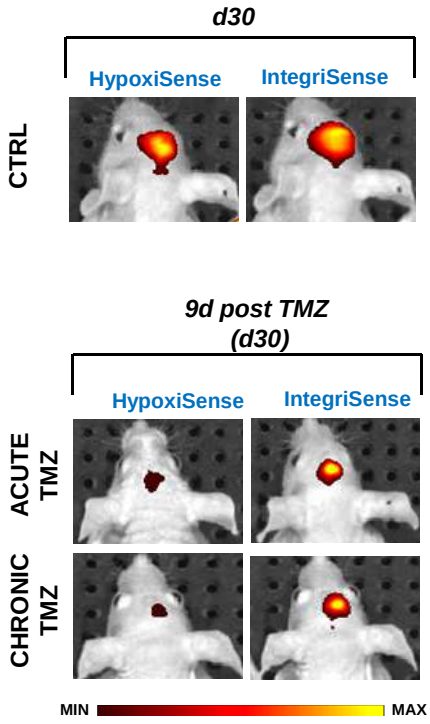

Fig. 39*: Images showed three representative mice injected with HypoxiSense and IntegriSense at later time points (day 30).*

These results were extremely significant showing the consequences of the treatment also in relation to HIF-1α modulation: firstly, TMZ treatment produced, an early reduction of bioluminescent signal regulated by HIF-1α activity. Secondly, mCherry signal, due to tumor cell viability, decreased only at later times, suggesting that as already described *in vitro*, the cytotoxic effect of TMZ treatment was detectable only some days after the administration. Finally, the reduction of HypoxiSense and IngetriSense uptake, demonstrated treatment efficacy. Moreover, the accumulation of the fluorescent probes showed that HypoxiSense uptake co-localizes with the IntegriSense probe, indicating that hypoxia was present in the inner portion of tumor. A more detailed study will be performed to assess by FLI hypoxia and angiogenesis, before and during TMZ treatment to validate their use as response biomarkers for TMZ treatment.

TMZ treatment by inducing the formation of methylated nucleotides, could concurs to induce their degradation by increasing proteasome activity, resulting also in a faster HIF-1α degradation [94-95]. In this scenario by reducing this transcription factor, Luciferase expression (in U251-HRE-mCherry cells) and transcription of all the gene driven by HRE sequences would be reduced resulting in a decrease in angiogenesis (see Integrisense uptake results). Furthermore this mechanism could be the reason for the synergic effect of TMZ with other anti-angiogenic drugs such as bevacizumab acting on downstream targets respect to HIF-1α activity [125,149]. This is only an hypothesis, however future studies will be necessary to demonstrate this theory.

In this view, HIF-1α, and its modulation after TMZ administration, could be used as early biomarker of TMZ efficacy after only 2 doses in the chronic regimen although a cytotoxic effect would not be detectable until after a week of treatment.

Despite further studies have to be performed to understand in depth the mechanism of action of TMZ, the *in vitro* and *in vivo* results presented herein are in accordance reporting an early reduction of HIF-1α activity before the induction of a real cell toxicity. The dual bioluminescent-fluorescent model U251-HRE-mCherry was very useful, showing a strong reduction of luciferase signal yet 48h after treatment, whereas m-Cherry fluorescent signal decreased only after a week. Since luciferase reporter gene is under control of HRE sequences (HIF-1α modulated), whereas fluorescent signal is under a constitutive promoter, we can hypothesise that TMZ, beyond its well known capacity of interfering with DNA replication, could have an indirect effect on HIF-1α activity, while fluorescence signal reported only on cell viability.

The use of the two specific fluorescent probes (HypoxiSense and IntegriSense) constitutes only a first pilot evaluation of the possibility to use these variables as response biomarkers after TMZ treatment with a sensitive and highthroughput technique before its validation with translational imaging tecniques such as PET and MRI.

In conclusion, this preliminary result, is extremely important because it opens the way to new hypothesis about TMZ mechanism of action, endorsing HIF-1α transcriptional factor as early

biomarker of TMZ efficacy, despite the molecular mechanism is not clear at the moment. Further studies need to be performed to understand the complete mechanism of action of TMZ.

CONCLUSIONS

This study suggests that the U251-HRE model, with luciferase activity as biomarker, can be used to evaluate HIF-1α activity in both *in vitro* and *in vivo* longitudinal studies geared at improving therapeutic approaches. Indeed, the objectives of the *in vitro* studies were the comprehension of molecular pathway influence in regulating hypoxia establishment using different modulators, and the relationship between HIF-1α induction and luciferase expression. In this view, our results showed that HIF-1α accumulation can be inducted by using hypoxia mimetic agents, such as DFX, and that this modulation was detectable only in U251-HRE cells [28,137,139] validating the use of this cell line for hypoxia studies and luciferase activity as a reliable HIF-1α specific biomarker in these cells.

Moreover, our results showed the involvement of PI3K/Akt and MAPK pathways on HIF-1α activity, resulting in luciferase expression modulation and underlying, once more, the importance of these processes as potential therapeutic targets [30,64,65,84].

Firstly, PI3K/Akt pathway was studied through LY294002 and BEZ235 treatment that acting on PI3K and mTOR were able to modulate Akt action and HIF-1α activity. The use of the inhibitors resulted in a reduction of HIF-1α-mediated luciferase activity in U251-HRE cells, suggesting an important role of this pathway on HIF-1α activity. Secondly, MEKs inhibitors such as TRAMETINIB and PD98059 were used to investigate the contribution of the Raf/MEK/ERK pathway in influencing HIF-1α activity. Different inhibitors were tested both as single treatments and as co-treatments to evaluate potential additive effects also of the two molecular pathways. Finally, a downstream regulator of HIF-1α, FM19G11, was used to understand the influence of degradation pathway on HIF-1α accumulation into the nucleus and transcriptional activity.

These studies allowed to conclude that U251-HRE cells can be used to assess HIF-1α activity after treatments by Luciferase activity assessment.

For what concerns *in vivo* studies, our results showed that our preclinical model, and the powerful imaging strategy proposed herein, can be useful for the early identification of hypoxic tumor regions and for the validation of specific treatments, accelerating the translation of preclinical data into clinical applications. Indeed, this study demonstrates that the U251-HRE orthotopic murine model may be proposed as a predictive and reliable tool to evaluate HIF-1α dependent processes in preclinical glioma models by BLI and FLI. Indeed, post-mortem analyses confirmed that the U251-HRE model recapitulates the salient features of human GBM in term of aggressiveness, high proliferation index and hypoxia and that Luciferase expression actually correlates with HIF-1α nuclear accumulation and CAIX expression in hypoxic regions.

In particular, although optical imaging methods do not yet have a role in human studies, cross-validating imaging results obtained with PET and MRI studies, have improved bioluminescence and fluorescence results. Indeed, optical imaging modality offered the possibility to indirectly study HIF-1α induction by monitoring luciferase activity. In addition, fluorescence scan for HypoxiSense

probe, confirmed the intratumoural hypoxia, validating BLI results. Supplementary, MRI showed the morphological features of tumours and diffusion studies gave information about the hypoxia microenvironment. On the other hand, PET provided information about glucose metabolism ([^{18}F]FDG) and proliferation ([^{18}F]FLT), while hypoxia ([^{18}F]FAZA) study confirmed BLI results in term of tumor hypoxia extent.

By combining information obtained with different modalities, it is possible to understand, in a complete view, the tumoral features, progression potential and the instauration of intratumoral hypoxia as well as the response to different treatments, identifying also potential response biomarkers.

In addition, a preliminary study with Temozolomide drug was performed on mice bearing U251-HRE-mCherry orthotopic tumours. The use of the tumour expressing the two reporters showed the different timing in HIF-α activity reduction and cell toxicity due to the treatment, allowing the identification of HIF-1α activity as potential biomarker of tumour response to TMZ and the suggestion of a new indirect mechanism of action of this drug. For all these reasons, the development of non-invasive procedure for the study of HIF-1α activity in hypoxia microenvironment could be extremely important to improve therapeutic approaches and, maybe in the future, to stratify glioma patients basing on intratumoral hypoxia level to maximize toxic effects of the antineoplastic treatment on tumors also in multi-drug regimens.

In conclusion, our data suggest that the U251-HRE model can be used to evaluate tumour hypoxia with multiple imaging modalities, with a view to opening up new avenues for the planning of personalized treatments. Translational molecular imaging modalities, indeed, offer the possibility of cross-validating preclinical optical imaging data with small-animal PET and MRI results, as a preliminary approach that may facilitate the transfer of the obtained results and of specific imaging procedures into the clinical setting [97,100,106].

FUTURE PERSPECTIVE

In the near future, *in vitro* experiments will be focused at the clarification of the mechanisms and significance of HIF-1α regulation, after treatment with different inhibitors and drugs acting on PI3K/Akt and MAPK pathways and proteasome activity, both *in vitro* and *in vivo*.

In this view, the U251-HRE-mCherry model will be used to evaluate the *in vivo* effect of TMZ treatment in association with other drugs acting for example in the blockage of angiogenesis at different levels, to better understand the molecular background influencing HIF-1α-mediated hypoxia establishment and tumour response. In addition, it will be necessary to *in vitro* understand the TMZ effect on HIF-1α regulation in term of molecular mechanism and cytotoxicity by assessing proteasome activity and the induction of different transduction pathways.

Furthermore it will be assessed if a stratification of the individuals in term of HIF-1α activity level, could help in improving therapeutic protocols, with a view to opening up new avenues for the planning of personalized treatments.

Finally, a cross-validation with different molecular imaging techniques will be performed with PET ([^{18}F]FLT and [^{18}F]FAZA) in order to study proliferation and/or hypoxia before and after pharmacological treatments and with MRI (diffusion and perfusion studies). These studies will explore tumor vasculature and will be aimed at comparing the different imaging procedures in the characterization of tumors in relation to treatment and in view of a clinical translation of the obtained results.

BIBLIOGRAPHY

[1] Yokota J, “Tumour progression and metastasis”, *Carcinogenesis*, 2000;,21(3):497-503

[2] Lonn S, Klaeboe L, Hall p *et al*, “Incidence trend of adult primary intracerebral tumours in four Nordic countries”, *International Journal of Cancer*, 2004, 108(3):450-5.

[3] Russell D, Rubinstein LJ, “Pathology of tumours of the nervous system”, 5th edn, 1989 Arnold, London

[4] WORLD HEALTH ORGANIZATION.”International Statistical Classification of Diseases and Related Health Problems” 10th revision, 1992, Vol. I, Geneva

[5] Ohgaki H. and Kleihues P, “Genetic pathways to primary and secondary glioblastoma”, *Am J Pathol,* 2007, 170(5):1445-53.

[6] Newcomb EW, Cohen H, Lee SR *et al*. “Survival of patients with glioblastoma multiforme is not influenced by altered expression of p16, p53, EGFR, MDM2 or Bcl-2 genes”, *Brain Pathol,*1998, 8(4):655-67

[7] Mischel PS, Nelson SF, Cloughesy TF, “Molecular analysis of glioblastoma: pathway profiling and its implications for patient therapy”, *Cancer Biol Ther*, 2003, 2(3):242-7, Review

[8] Brat DJ, Van Meir EG, “Vaso-occlusive and prothrombotic mechanisms associated with tumour hypoxia, necrosis, and accelerated growth in glioblastoma”, *Lab Invest,* 2004, 84(4):397-405, Review

[9] Kaur B, Tan C, Brat DJ, Post DE, Van Meir EG, “Genetic and hypoxic regulation of angiogenesis in gliomas”, *J Neurooncol*, 2004, 70(2):229-43, Review

[10] Von Deimling A, Louis DN, Wiestler OD, “Molecular pathways in the formation of gliomas”, *Glia*, 1995, 15(3):328-38

[11] Chakravarti A, Chakladar A, Delaney MA, Latham DE, Loeffler JS, “The epidermal growth factor receptor pathway mediates resistance to sequential administration of radiation and chemotherapy in primary human glioblastoma cells in a RAS-dependent manner”, *Cancer Research*, 2002, 62(15):4307-15

[12] Alderson LM, Castleberg RL, Harsh GR, Louis DN, Henson JW, “Human gliomas with wild-type p53 express bcl-2”, *Cancer Research*, 1995, 55(5):999-1001

[13] Nakamura M, Yang F, Fujisawa H, Yonekawa Y, Kleihues P, Ohgaki H, “Loss of Heterozygosity on Chromosome 19 in Secondary Glioblastomas”, *J Neuropathol Exp Neurol,* 2000, 59(6):539-43

[14] Zundel W, Schindler C, Haas-Kogan D et al, “Loss of PTEN facilitates HIF-1-mediated gene expression”, *Genes Dev*, 2000, 14(4):391-6

[15] Mills GB, Lu Y, Fang X, Wang H et al, “The role of genetic abnormalities of PTEN and the phosphatidylinositol 3-kinase pathway in breast and ovarian tumourigenesis, prognosis, and therapy”, *Semin Oncol*, 2001, 28(5 Suppl 16):125-41

[16] Lu Y, Lin YZ, LaPushin R et al, “The PTEN/MMAC1/TEP tumour suppressor gene decreases cell growth and induces apoptosis and anoikis in breast cancer cells”, *Oncogene,* 1999, 18(50):7034-45

[17] McCubrey JA, Steelman LS, Abrams S et al, “Roles of the RAF/MEK/ERK and PI3K/PTEN/AKT pathways in malignant transformation and drug resistance”, *Adv Enzyme Regul,* 2006, 46:249-79

[18] Vajkoczy P, Menger MD, “Vascular microenvironment in gliomas”, *Cancer Treat Res*, 2004, 117: 249-262

[19] Vaupel P, “The role of hypoxia-induced factors in tumour progression” *The Oncologist,* 2004, 9(suppl 5):10-17

[20] Vaupel P, Harrison L, “Tumour hypoxia: causative factors, compensatory mechanisms, and cellular response”, *The Oncologist,* 2004, 9 Suppl 5:4-9.

[21] Semenza GL, “Defining the role of hypoxia-inducible factor 1 in cancer biology and therapeutics”, *Oncogene*, 2010, 29(5):625-34, Review

[22] Vaupel P, “Hypoxia and aggressive tumour phenotype: implications for therapy and prognosis”, *The Oncologist*, 2008, 13 Suppl 3:21-6, Review

[23] Semenza G, “Signal transduction to hypoxia-inducible factor 1”, *Biochem Pharmacol*, 2002, 64:993–998

[24] Ivan M, Kondo K, Yang H et al, “HIFalpha targeted for VHL-mediated destruction by proline hydroxylation: implications for O2 sensing”, *Science*, 2001, 292:464–468

[25] Höckel M, Vaupel P, “ Biological consequences of tumour hypoxia”, *Semin Oncol*, 2001, 28(2 Suppl 8):36-41

[26] Vaupel P, Kelleher DK, Höckel M, “Oxygen status of malignant tumours: pathogenesis of hypoxia and significance for tumour therapy”, *Semin Oncol,* 2001, 28(2 Suppl 8):29-35

[27] Semenza GL, Koury ST, Nejfelt MK, “Cell-type-specific and hypoxia-inducible expression of the human erythropoietin gene in transgenic mice”, *Proc Natl Acad Sci U S A*,1991, 88(19):8725-9

[28] Rapisarda A, Zalek J, Hollingshead M et al, “Schedule-dependent inhibition of hypoxia-inducible factor-1alpha protein accumulation, angiogenesis, and tumour growth by topotecan in U251-HRE glioblastoma xenografts”, *Cancer Res*, 2004, 64(19):6845-8

[29] Lu H, Dalgard CL, Mohyeldin A et al, “Reversible inactivation of HIF-1 prolyl hydroxylases allows cell metabolism to control basal HIF-1”, *J Biol Chem*, 2005, 280(51):41928-39

[30] Flügel D, Görlach A, Michiels C and and Kietzmann T, “Glycogen Synthase Kinase 3 Phosphorylates Hypoxia-Inducible Factor 1α and Mediates Its Destabilization in a VHL-Independent Manner”, *Mol Cell Biol,* 2007, 27(9): 3253–3265

[31] Jensen RL, “Hypoxia in the tumourigenesis of gliomas and as a potential target for therapeutic measures”, *Neurosurg Focus,* 2006, 20(4):E24

[32] Osinsky S, Zavelevich M, Vaupel P, “ Tumour hypoxia and malignant progression”, *Exp Oncol*, 2009, 31(2):80-6

[33] Pennacchietti S, Michieli P, Galluzzo M et al, “Hypoxia promotes invasive growth by transcriptional activation of the met protooncogene” *Cancer Cel,* 2003, 3(4):347-61

[34] Brat DJ, Castellano-Sanchez AA, Hunter SB, et a, “Pseudopalisades in glioblastoma are hypoxic, express extracellular matrix proteases, and are formed by an actively migrating cell population”, *Cancer Res*, 2004, 64(3):920-7

[35] Brat DJ, Castellano-Sanchez A, Kaur B, Van Meir EG “Genetic and biologic progression in astrocytomas and their relation to angiogenic dysregulation”, *Adv Anat Pathol*, 2002, 9(1):24-36

[36] Raza SM, Lang FF, Aggarwal BB et al, “Necrosis and glioblastoma: a friend or a foe? A review and a hypothesis”, *Neurosurgery*, 2002, 51:2–12

[37] Chen Z, Htay A, Dos Santos W, et al, “In vitro angiogenesis by human umbilical vein endothelial cells (HUVEC) induced by three-dimensional co-culture with glioblastoma cells”, *J Neurooncol*, 2009, 92(2):121-8

[38] Merighi S, Benini A, Mirandola P et al, “Hypoxia inhibits paclitaxel-induced apoptosis through adenosine-mediated phosphorylation of bad in glioblastoma cells”, *Mol Pharmacol*, 2007, 72(1):162–172

[39] Bergers G, Hanahan D, “Models of resistance to anti-angiogenic therapy” *Nat Rev Cancer*, 2008, 8(8):592-603

[40] Ceradini DJ, Kulkarni AR, Callaghan MJ et al “Progenitor cell trafficking is regulated by hypoxic gradients through HIF-1 induction of SDF-1”, *Nat Med,* 2004, 10(8):858-64

[41] De Falco E, Porcelli D, Torella AR, et al “SDF-1 involvement in endothelial phenotype and ischemia-induced recruitment of bone marrow progenitor cells”, *Blood*, 2004, 104(12):3472-82

[42] Candolfi M, Curtin JF, Nichols WS et al, “Intracranial glioblastoma models in preclinical neuro-oncology: neuropathological characterization and tumour progression”, *J Neurooncol,* 2007, 85(2):133-48

[43] Barth RF, “Rat brain tumour models in experimental neuro-oncology: the 9L, C6, T9, F98, RG2 (D74), RT-2 and CNS-1 gliomas”, *J Neurooncol*, 1998, 36(1):91-102

[44] Singh M, Murriel CL, and Johnson L, “Genetically Engineered Mouse Models: Closing the Gap between Preclinical Data and Trial Outcomes”, *Cancer Res,* 2012, *72; 2695*

[45] Kruse CA, Molleston MC, Parks EP, “A rat glioma model, CNS-1, with invasive characteristics similar to those of human gliomas: a comparison to 9L gliosarcoma”, *J Neurooncol*, 1994, 22(3):191-200

[46] Martelli C, Libani I, Lui R, Ottobrini L, “Imaging in drug development with reporter mice”, *Minerva Biotec*, 2009, 21:53-66

[47] Kapoor GS, Gocke TA, Chawla S et al, “Magnetic resonance perfusion-weighted imaging defines angiogenic subtypes of oligodendroglioma according to 1p19q and EGFR status”, *J Neurooncol,* 2009, 92(3):373-86

[48] Yu M, Han J, Dai M, “Influence of PEG-conjugated hemoglobin on tumour oxygenation and response to chemotherapy”, *Artif Cells Blood Substit Immobil Biotechnol*, 2008, 36(6):551-61

[49] Ponten J, “Neoplastic human glia cells in culture*”, Human Tumour Cells* in Vitro*,* 1975, 175–206

[50] Houchens DP, Ovejera AA, Riblet SM, Slagel DE, “Human brain tumour xenografts in nude mice as a chemotherapy model”, *Eur J Cancer Clin Oncol*, 1983, 19:799–805

[51] Husain SR, Behari N, Kreitman RJ, Pastan I, Puri RK, “Complete regression of established human glioblastoma tumour xenograft by interleukin-4 toxin therapy*”, Cancer Res*, 1998, 58:3649–3653

[52] De Vries NA, Beijnen JH, van Tellingen O, “High-grade glioma mouse models and their applicability for preclinical testing”, *Cancer Treat Rev*, 2009, 35:714–723

[53] Radaelli E, Ceruti R, Patton V, Russo M, Degrassi A, Croci V, Caprera F, Stortini G, Scanziani E, Pesenti E, Alzani R “Immunohistopathological and neuroimaging characterization of murine orthotopic xenograft models of glioblastoma multiforme recapitulating the most salient features of human disease”, *Histol Histopathol,* 2009, 24:879–891

[54] Camphausen K, Purow B, Sproull M, Scott T, Ozawa T, Deen DF, Tofilon PJ,”Influence of *in vivo* growth on human glioma cell line gene expression: convergent profiles under orthotopic conditions”, *Proc Natl Acad Sci USA*, 2005, 102:8287–8292

[55] Valdes PA, Samkoe K, O'Hara JA, Roberts DW, Paulsen KD, Pogue BW, “Deferoxamine iron chelation increases delta-aminolevulinic acid induced protoporphyrin IX in xenograft glioma model” *Photochem Photobio*l, 2010, 86:471–5

[56] Louis DN, “The p53 gene and protein in human brain tumours”, *J Neuropathol Exp Neurol,* 1994, 53:11–21

[57] Louis DN, Holland EC, Cairncross JG, “Glioma classification: a molecular reappraisal”, *Am J Pathol,* 2001, 159:779–786

[58] Furnari FB, Fenton T, Bachoo RM, Mukasa A, Stommel JM, Stegh A, Hahn WC, Ligon KL, Louis DN, Brennan C, Chin L, DePinho RA, Cavenee WK, “Malignant astrocytic glioma: genetics, biology, and paths to treatment”, *Genes Dev,* 2007, 21:2683–2710

[59] Krakstad C, Chekenya M, “Survival signalling and apoptosis resistance in glioblastomas: opportunities for targeted therapeutics”, *Mol Cancer,* 2010, 9:135

[60] Van Meir EG, Hadjipanayis CG, Norden AD, Shu HK, Wen PY, Olson JJ, “Exciting new advances in neuro-oncology: the avenue to a cure for malignant glioma”, *CA Cancer J Clin.* 2010;60:166–193.

[61] Radaelli E, Rustighi A, Scanziani E, “ Giant cell tumor of bonelike lesion in a Trp53 mutant mouse”, *Toxicol Pathol,* 2012, 40(4):675-81

[62] Ju He, Jeffrey J. Olson, and C. David James, “Lack of $p16^{INK4}$ or Retinoblastoma Protein (pRb), or Amplification-associated Overexpression of cdk4 Is Observed in Distinct Subsets of Malignant Glial Tumours and Cell Lines, *Cancer Res,* 1995, *55: 4833-4836*

[63] Fueyo J, Gomez-Manzano C, Yung WK, Clayman GL, Liu TJ, Bruner J, Levin VA, Kyritsis AP, “Adenovirus-mediated p16/CDKN2 gene transfer induces growth arrest and modifies the transformed phenotype of glioma cells”, *Oncogene*, 1996, 12:103–110

[64] Ishii N, Maier D, Merlo A, Tada M, Sawamura Y, Diserens AC, Van Meir EG, “Frequent co-alterations of TP53, p16/CDKN2A, $p14^{ARF}$, PTEN tumour suppressor genes in human glioma cell lines”, *Brain Pathol*, 1999, 9:469–479

[65] Jiang H, Shang X, Wu H, Gautam SC, “Resveratrol downregulates PI3K/Akt/mTOR signaling pathways in human U251 glioma cells”, *J Exp Ther Oncol,* 2009, 8(1):25-33

[66] Valerie L Jacobs, Pablo A Valdes, William F Hickey, Joyce A De Leo, “Current review of *in vivo* GBM rodent models: emphasis on the CNS-1 tumour model”, *ASN Neurol*, 2011, 3(3):e00063. doi: 10.1042/AN20110014.

[67] Shankavaram UM, Bredel M, Burgan WE et al, “Molecular Profiling Indicates Orthotopic Xenograft of Glioma Cell Lines Simulate a Subclass of Human Glioblastoma”, *J Cell Mol Med,* 2012, 16(3): 545–554

[68] Hui-Lan Zeng, Qi Zhong, Yong-Liang Qin, “Hypoxia-mimetic agents inhibit proliferation and alter the morphology of human umbilical cord- derived mesenchymal stem cells”, *BMC Cell Biology*, 2011, 12:32

[69] Hirsilä M, Koivunen P, Xu L, Seeley T, Kivirikko KI, Myllyharju J, “Effect of desferrioxamine and metals on the hydroxylases in the oxygen sensing pathway”, *FASEB J,* 2005*;*19:1308–10

[70] Jung JY, Kim WJ, “Involvement of mitochondrial- and Fas-mediated dual mechanism in CoCl2-induced apoptosis of rat PC12 cells2”, *Neurosci Lett* 2004, 23:85-90

[71] An WG, Kanekal M, Simon MC, Maltepe E, Blagosklonny MV, Neckers LM, “Stabilization of wild-type p53 by hypoxia-inducible factor 1 α”, *Nature*, 1998, 392:405-8

[72] Mircea I, Keiichi K, Haifeng Y et al, “HIFα Targeted for VHL-Mediated Destruction by Proline Hydroxylation: Implications for O_2 Sensing”, *Science,* 2001, *292(5516): 464-468*

[73] Jaakkola P, Mole DR, Tian YM et al, “Targeting of HIF-alpha to the von Hippel-Lindau ubiquitylation complex by O2-regulated prolyl hydroxylation”, *Science*, 2001, 292(5516):468-72

[74] Yuan Y, Hilliard G, Ferguson T, Millhorn DE, “Cobalt Inhibits the Interaction between Hypoxia-inducible Factor-α and von Hippel-Lindau Protein by Direct Binding to Hypoxia-inducible Factor-α*”, J Biol Chem*, 2003, 278 (18): 15911–15916

[75] Wang GL, Semenza GL, “Desferrioxamine induces erythropoietin gene expression and hypoxia-inducible factor 1 DNA-binding activity: implications for models of hypoxia signal transduction”, *Blood,* 1993, 82(12):3610-5

[76] Engelman JA, Luo J. and Cantley LC, “The evolution of phosphatidylinositol 3-kinases as regulators of growth and metabolism”, *Nat Rev Genet*, 2006, 7: 606–619

[77] Hennessy BT, Smith DL, Ram PT, Lu Y and Mills GB, “Exploiting the PI3K/AKT pathway for cancer drug discovery”, *Nat Rev Drug Disco,* 2005, 4: 988–1004

[78] lahos CJ, Matter WF, Hui KY, Brown RF, “A specific inhibitor of phosphatidylinositol 3-kinase, 2-(4-morpholinyl)-8-phenyl-4H-1-benzopyran-4-one (LY294002)”, *J. Biol. Chem*, 1994, 269:5241-5248

[79] Brunn GJ, Williams J, Sabers C, Wiederrecht G, Lawrence Jr JC and Abraham RT, “Direct inhibition of the signaling functions of the mammalian target of rapamycin by the phosphoinositide 3-kinase inhibitors, wortmannin and LY294002”, *EMBO J,* 1996, 15:5256–5267

[80] Jacobs MD, Black J, Futer O, Swenson L, Hare B, Fleming M and Saxena, K., “PIM-1 ligand-bound structures reveal the mechanism of serine/threonine kinase inhibition by LY294002”. J*. Biol. Che,* 2005*,* 280: 13728–13734

[81] Hu L, Zaloudek C, Mills GB, Gray J, Jaffe RB, “In vivo and in vitro ovarian carcinoma growth inhibition by a phosphatidylinositol 3-kinase inhibitor (LY294002)” *Clin Cancer Res*, 2000,6(3):880-6

[82] Gharbi SI, Zvelebil MJ, Shuttleworth SJ, “Exploring the specificity of the PI3K family inhibitor LY294002”, *Biochem J* , 2007, 404:15–21

[83] Chen L, Han L, Shi Z et a., “LY294002 enhances cytotoxicity of TMZ in glioma by down-regulation of the PI3K/Akt pathway”, *Mol Med Rep*, 2012 Feb;5(2):575-9.

[84] Casagrande F, Bacqueville D, Pillaire MJ, et al, “G_1 phase arrest by the phosphatidylinositol 3-kinase inhibitor LY294002 is correlated to up-regulation of p27Kip1 and inhibition of G_1 CDKs in choroidal melanoma cells”, *FEBS Lett*, 1998, *422*:*385*-390

[85] Maira SM, Stauffer F, Brueggen J, et al, “Identification andcharacterization of NVP-BEZ235, a new orally available dual phosphatidylinositol 3-kinase/mammalian target of rapamycin inhibitor with potent in vivo antitumour activity”, *Mol Cancer Ther*, 2008, 7(7):1851–63

[86] Kim A, Park S, Lee JE et al, “The dual PI3K and mTOR inhibitor NVP-BEZ235 exhibits anti-proliferative activity and overcomes bortezomib resistance in mantle cell lymphoma cells”, *Leuk Res*, 2012, 36: 912– 920

[87] Kim BM, Chung HW, “Desferrioxamine (DFX) induces apoptosis through the p38-caspase8-Bid-Bax pathway in PHA-stimulated human lymphocytes”, *Toxicol Appl Pharmacol,* 2008: 228(1):24-31

[88] Minet E, Arnould T, Michel G *et al*, “ERK activation upon hypoxia: involvement in HIF-1 activation”, *FEBS Lett* , 2000, 1: 53–58

[89] Sutton KM, Hayat S, Chau NM et al. “Selective inhibition of MEK1/2 reveals a differential requirement for ERK1/2 signalling in the regulation of HIF-1 in response to hypoxia and IGF-1. *Oncogene*, 2007, 26(27):3920-9.

[90] Salama AK, Kim KB. “Trametinib (GSK1120212) in the treatment of melanoma” Expert Opin Pharmacother. 2013, 14(5):619-27

[91] Yamaguchi T, Kakefuda R, Tanimoto A, Watanabe Y, Tajima N “Suppressive effect of an orally active MEK1/2 inhibitor in two different animal models for rheumatoid arthritis: a comparison with leflunomide”, *Inflamm Res*, 2012, 61(5):445-54

[92] Moreno-Manzano V, Rodríguez-Jiménez FJ, Aceña-Bonilla JL et al. “FM19G11, a new hypoxia-inducible factor (HIF) modulator, affects stem cell differentiation status”, *J Biol Chem*, 2010, 285(2):1333-42

[93] Zhong H, Chiles K, Feldser D et al. “Modulation of hypoxia-inducible factor 1alpha expression by the epidermal growth factor/phosphatidylinositol 3-kinase/PTEN/AKT/FRAP pathway in human prostate cancer cells: implications for tumour angiogenesis and therapeutics”, *Cancer Res*, 2000, 60(6):1541-5.

[94] D. M. Kokkinakis, D. B. Bocangel, S. C. Schold, R. C. Moschel, and A. E. Pegg, “Thresholds of O6-alkylguanine-DNA alkyltransferase which significant resistance of human glial tumour xenografts to treatment with 1,3-bis(2-chloroethyl)-1-nitrosourea or TMZ” Clin Cancer Res, 2001, 7(2), pp. 421–428

[95] Fruehauf JP, Brem H, Brem S et al, “In vitro drug response and molecular markers associated with drug resistance in malignant gliomas”, *Clin Cancer Res*, 2006, 12(15):4523-32

[96] Ma J, Murphy M, O'Dwyer PJ, Berman E, Reed K, Gallo JM, “Biochemical changes associated with a multidrug-resistant phenotype of a human glioma cell line with TMZ-acquired resistance,” *Biochem Pharmacol,* 2002, 63(7):1219-28

[97] Massoud TK, Gambhir SS, “Molecular imaging in living subjects: seeing fundamental biological processes in a new light”, *Genes Dev*, 2003, 17(5):545-80

[98] Bulte JW, Kraitchman DL, “Iron oxide MR contrast agents for molecular and cellular imaging”, *NMR Biomed*, 2004, 17(7):484-99

[99] Lewis JS, Achilefu S, Garbow JR, Laforest R, Welch MJ., “Small animal imaging. Current technology and perspectives for oncological imaging”, *Eur J Cancer*, 2002, 38(16):2173-88

[100] Lucignani G, Ottobrini L, Martelli C, Rescigno M, Clerici M, “Molecular imaging of cell-mediated cancer immunotherapy”, *Trends Biotechnol*, 2006, 24(9):410-8

[101] Massoud TF, Gambhir SS, “Integrating noninvasive molecular imaging into molecular medicine: an evolving paradigm”, *Trends Mol Med*, 2007, 13(5):183-91

[102] Livingston JN, “Genetically engineered mice in drug development”, *J Intern Med*, 1999, 245(6):627-35

[103] Gassmann M, Hennet T, “From genetically altered mice to integrative physiology”, *News Physiol Sci,* 1998, 13:53-57

[104] Spibey CA, Jackson P, Herick K, “A unique charge-coupled device/xenon arc lamp based imaging system for the accurate detection and quantitation of multicolour fluorescence”, *Electrophoresis*, 2001, 22(5):829-36

[105] Gross S, Piwnica-Worms D, “Spying on cancer: molecular imaging in vivo with genetically encoded reporters”, *Cancer Cel*, 2005,n 7(1):5-15

[106] Ottobrini L, Ciana P, Biserni A, Lucignani G, Maggi A, “Molecular imaging: A new way to study molecular processes in vivo”, *Mol Cell Endocrinol*, 2006, 246(1-2):69-75

[107] Shaner NC, Campbell RE, Steinbach PA, Giepmans BNG, Palmer AE, Tsien RY, “Improved monomeric red orange and yellow fluorescent proteins derived from *Discosoma sp*. red fluorescent protein”, *Nat Biotechnol,* 2004, 22(12):1567-72

[108] Shcherbo D, Merzlyak EM, Chepurnykh TV et al “Bright far-red fluorescent protein for whole-body imaging”, *Nat Methods*, 2007, 4(9):741-6

[109] Swirski Swirski FK, Berger CR, Figueiredo JL, et al “A Near-Infrared Cell Tracker Reagent for Multiscopic In vivo Imaging and Quantification of Leukocyte Immune Responses”, *PLoS One*, 2007, 2(10):e1075

[110] Noh YW, Lim YT, Chung BH “Noninvasive imaging of dendritic cell migration into lymph nodes using nearinfrared fluorescent semiconductor nanocrystals”, *FASEB J*, 2008, 22(11):3908-18

[111] Sen D, Deerinck TJ, Ellisman MH, Parker I, Cahalan MD, “Quantum Dots for Tracking Dendritic Cells and Priming an Immune Response In vitro and In vivo”, *PLOS ONE*, 2008, 3(9):1-13

[112] Phelps ME. “Positron emission tomography provides molecular imaging of biological process”. *Proc Natl Acad Sci U S A*, 2000, 97(16):9226-33

[113] Lecchi M, Ottobrini L, Martelli C, Del Sole A, Lucignani G, “Instrumentation and probes for molecular and cellular imaging”, *Q J Nucl Med and Molecular Imaging*, 2007, 51(2): 111-26

[114] Rosenthal MS, Cullom J, Hawkins W, Moore SC, Tsui BM, Yester M, “Quantitative SPECT imaging: A review and recommendations by the Focus Committee of the Society of Nuclear Medicine Computer and Instrumentation Council”, *J Nucl Med*, 1995, 36(8): 1489-513

[115] Iyer M, Barrio JR, Namavari M, Bauer E et al “8-[F-18]fluoropenciclovir: An improved reporter probe for imaging HSV1-tk reporter gene expression in vivo using PET”, J *Nucl Med2001,* 42(1): 96-105.

[116] Tjuvajev JG, Finn R, Watanabe K et al, “Noninvasive imaging of herpes virus thymidine kinase gene transfer and expression: A potential method for monitoring clinical gene therapy”, *Cancer Res*, 1996 , 56818): 4087-95

[117] Gambhir SS, Bauer E, Black ME et al “A mutant herpes simplex virus type 1 thymidine kinase reporter gene shows improved sensitivity for imaging reporter gene expression with positron emission tomography”, *Proc Natl Acad Sci USA*, 2000, 97(6): 2785-90

[118] Liang Q, Satyamurthy N, Barrio JR et al, “Non-invasive, quantitative imaging in living animals of a mutant dopamine D2 receptor reporter gene in which ligand binding is uncoupled from signal transduction”, *Gene Ther,* 2001, 8(19):1490-8.

[119] MacLaren DC, Gambhir SS, Satyamurthy N et al, “Repetitive, non-invasive imaging of the dopamine D2 receptor as a reporter gene in living animals”, *Gene Ther*, 1999, 6(5):785-91.

[120] Haberkorn U, Henze M, Altmann A et al, “Transfer of the human Na/I symporter gene enhances iodide uptake in hepatoma cells”, *J Nucl Med*, 2001, 42(2):317-25

[121] Cho JY, Xing S, Liu X et al “Expression and activity of human Na^+/I^- symporter in human glioma cells by adenovirus-mediated gene delivery”, *Gene Ther*, 2000, 7(9): 740-9.

[122] Ido T, Wan CN, Casella V et al, “Labelled 2-deoxy-D-glucose analogs. 18F-labelled 2-deoxy-2-fluoro-D-glucose, 2-deoxy-2-fluoro-D-mannose and 11C-2-deoxy-2-fluoro-D-glucose”, *J Label Comp Radiopharm*, 1978, 14(2):175-83

[123] Bar-shalom R, Valdivia AJ, Blaufox MD, “PET imaging in oncology”. Semin Nucl Med, 2000, 30(3):150-85

[124] Chen W, Cloughesy T, Kamdar N et al, “Imaging proliferation in brain tumours with 18F-FLT PET: comparison with 18F-FDG”, *J Nucl Med*, 2005, 46(6):945-52

[125] Corroyer-Dulmont A, Peres EA, Petit E. et al, “Detection of glioblastoma response to TMZ combined with bevacizumab based on {micro}MRI and {micro}PET imaging reveals [18F]-fluoro-L-thymidine as an early and robust predictive marker for treatment efficacy” Neuroncology 15(1): 41-56

[126] Gilad AA, Winnard PT Jr, van Zijl PCM, Bulte JWM, “Developing MR reporter genes: promises and pitfalls”, *NMR in Biomedicine*, 2007, 20(3): 275-90

[127] Ahn BC “ Application of molecular imaging in drud discovery and development process”, *Curr Pharm Biotechnol*, 2011, 12(4):459-68

[128] Daldrup H, Shames DM, Wendland M et al “Correlation of dynamic contrast-enhanced MR imaging with histologic tumour grade: comparison of macromolecular and small-molecular contrast media”, *AJR Am J Roentgenol*, 1998, 171(4):941-9

[129] Gossmann A, Okuhata Y, Shames DM, et al, “Prostate cancer tumour grade differentiation with dynamic contrast-enhanced MR imaging in the rat: comparison of macromolecular and small-molecular contrast media--preliminary experience”. *Radiology,*1999, 213:265–272

[130] Krause BJ, Beck R, Souvatzoglou M, Piert M, “PET and PET/CT studies of tumour tissue oxygenation”. *Q J Nucl Med Mol Imaging*, 2006, 50(1):28-43

[131] Carmen S. Dence, Datta E. et al, “Autoradiographic and small-animal PET comparisons between 18F-FMISO, 18F-FDG, 18F-FLT and the hypoxic selective 64Cu-ATSM in a rodent model of cancer”, *Nucl Med Biol*, 2008, 35: 713–720

[132] Busk M, Jakobsen S, Horsman MR et al. “PET imaging of tumour hypoxia using 18F-labeled pimonidazole*”, Acta Oncol,* 2013, 52(7):1300-7

[133] Bentzen L, Keiding S, Nordsmark M et al “Tumour oxygenation assessed by 18F-fluoromisonidazole PET and polarographic needle electrodes in human soft tissue tumours”, *Radiother Oncol*, 2003, 67(3):339-44

[134] Padhani AR, Krohn KA, Lewis JS, Alber M “Imaging oxygenation of human tumours”, *Eur Radiol*, 2007, 17(4):861-72

[135] Fujibayashi Y, Taniuchi H, Yonekura Y, Ohtani H, Konishi J, Yokoyama A. “Copper-62-ATSM: a new hypoxia imaging agent with high membrane permeability and low redox potential”, *J Nucl Med*, 1997, 38(7):1155-60

[136] Vāvere AL, Lewis JS " Cu-ATSM: a radiopharmaceutical for the PET imaging of hypoxia", *Dalton Trans*, 2007, (43):4893-902

[137] Rapisarda A, Uranchimeg B, Scudiero D "Identification of small molecule inhibitors of hypoxia-inducible factor 1 transcriptional activation pathway", *Cancer Res*, 2002; 62(15):4316-24

[138] Maes W, Deroose C, Reumers V et al. "In vivo bioluminescence imaging in an experimental mouse model for dendritic cell based immunotherapy against malignant glioma", *J Neurooncol*, 2009; 91:127–139

[139] Demidenko ZN, Rapisarda A, Garayoa M et al "Accumulation of hypoxia-inducible factor 1α is limited by transcription-dependent depletion", *Oncogene*, 2005, 30:4829–4838

[140] Arsham AM, Plas DR, Thompson CB, Simon MC "Phosphatidylinositol 3-kinase/Akt signaling is neither required for hypoxic stabilization of HIF-1 alpha nor sufficient for HIF-1-dependent target gene transcription" *J Biol Chem,* 2002; 277:15162–15170

[141] Stiehl DP, Wirthner R, Köditz J et al "Increased prolyl 4-hydroxylase domain proteins compensate for decreased oxygen levels: evidence for an autoregulatory oxygen-sensing system", *J Biol Chem,* 2006, 281(33):23482–23491

[142] Mottet D, Dumont V, Deccache Y et al " Regulation of hypoxiainducible factor-1alpha protein level during hypoxic conditions by the phosphatidylinositol 3-kinase/Akt/glycogen synthase kinase 3beta pathway in HepG2 cells", *J Biol Chem 2003*; 278(33):31277–31285

[143] Görlach A "Regulation of HIF-1alpha at the transcriptional level", *Curr Pharm Des,* 2009 15(33):3844–52, Review

[144] Maira SM, Stauffer F, Brueggen J et al." Identification and characterization of NVP-BEZ235, a new orally available dual phosphatidylinositol 3-kinase/mammalian target of rapamycin inhibitor with potent in vivo antitumor activity", *Mol Cancer Ther,* 2008;7(7):1851-1863

[145] Steelman LS, Chappell WH, Abrams SL et al "Roles of the Raf/MEK/ERK and PI3K/PTEN/Akt/mTOR pathways in controlling growth and sensitivity to therapy-implications for cancer and aging", *Aging* 2011; 3(3): 192–222

[146] Valtorta S, Belloli S, Sanvito F et al. "Comparison of 18Ffluoroazomycin-rabinofuranoside and 64Cu-diacetyl-bis(N4-methylthiosemicarbazone) in preclinical models of cancer", *J Nucl Med*, 2013, 54(7):1006–12.

[147] Reischl G, Dorow DS, Cullinane C et al “Imaging of tumor hypoxia with [124I]IAZA in comparison with [18F]FMISO and [18F]FAZA-first small animal PET results”, *J Pharm Pharm Sci*, 2007, 1082):203–211

[148] Chen W, Cloughesy T, Kamdar N et al “ Imaging proliferation in brain tumors with 18F-FLT PET: comparison with 18F-FDG" *J Nucl Med*, 2005; 46(6):945–952

[149] Mathieu V, De Nève N, Le Mercie M et al “Combining Bevacizumab with Temozolomide Increases the Antitumor Efficacy of Temozolomide in a Human Glioblastoma Orthotopic Xenograft Model”, *Neoplasia* 2008; 10(12): 1383–1392

SCIENTIFIC PRODUCTS

Publication:

"**VALIDATION OF AN ENGINEERED CELL MODEL FOR *IN VITRO* AND *IN VIVO* HIF-1 EVALUATION BY DIFFERENT IMAGING MODALITIES**"

Lo Dico A., Valtorta S., Martelli C., Belloli S., Gianelli U., Tosi D., Bosari S. Degrassi A., Russo M., Raccagni I., Lucignani G., Moresco R.M and Ottobrini L.

Molecular Imaging & Biology (2013) DOI: 10.1007/s11307-013-0669-0

Abstract:

"**MULTIMODAL HYPOXIA IMAGING IN A PRECLINICAL GLIOMA MODEL**"

Lo Dico A., Martelli C., Belloli S Degrassi A., Russo M., Valtorta S., Gianelli U., Tosi D., Todde S., Monterisi C., Lucignani G., Ottobrini L. and Moresco R.M.

Eur J Nucl Med Mol Imaging (2012) 39 (Suppl 2):S498–S611. DOI 10.1007/s00259-012-2225-6

Poster:

***"*MOLECULAR IMAGING APPLIED ON HYPOXIA EVALUATION: COMPARISON OF BLI, FLI AND PET IMAGING"**

Lo Dico A., Martelli C., Belloli S., Valtorta S., Gianelli U. , Tosi D., Todde S., Monterisi C., Lucignani G., Moresco R.M and Ottobrini L.

European Molecular Imaging Meeting (EMIM), Torino 2013

"MULTIMODAL HYPOXIA IMAGING IN A PRECLINICAL GLIOMA MODEL"

Lo Dico A., Martelli C., Belloli S Degrassi A., Russo M., Valtorta S., Gianelli U., Tosi D., Todde S., Monterisi C., Lucignani G., Ottobrini L. and Moresco R.M.

European Association of Nuclear Medicine (EAMN) and World Molecular Imaging Congress (WMIC), Milano and Dublin 2012

GRANTS

We thank the IRCCS Cà Granda Foundation for allowing the use of the imaging system IVIS Spectrum/CT. This work was supported in part by FP7 funded INSERT project (HEALTH-2012- INNOVATION-1, GA305311).